SIEMENS

MReadings: MR in RT

Contributions from our MAGNETOM users

siemens.com/magnetom-world-rt

Not for distribution in the US

Second Extended Edition

Dear Reader,

Trends in modern radiation therapy point towards hypofractionated and highly precise treatments. Curative intent is becoming the goal of more and more treatments. These advancements drive the need for more advanced imaging. Indeed, according to a US survey conducted in 2014 [1], every fourth treatment plan used PET images and every fifth plan involved MR images – a four-fold increase in only seven years.

Following the rapid adoption of MRI in radiation therapy, Siemens has developed tailored solutions that also address those departments that have traditionally used CT imaging alone. This issue of the MReadings, aims to increase the peer-to-peer exchange of practices and to demonstrate how MAGNETOM users around the world are tackling the challenges posed by the introduction of MRI in the radiotherapy routine.

Practical implementation of MRI in the workflow

Even in the past, institutions such as the Liverpool Cancer Therapy Centre in Sydney, Australia, relied heavily on local radiology scanners to access MR images for RT planning. In the first article of this issue, Liney et al. describe their initial experience with a dedicated installation of a 3T MAGNETOM Skyra for exclusive use in radiotherapy, and how they implemented MR-based planning into their clinical practice.

A prerequisite for the proper integration of MR into RT workflows is the ability to generate MR scans in the treatment position. In the second article, Koch et al. give hands-on guidance on how to set up patients with support devices, such as an MR compatible flat indexed tabletop and coils suitable for imaging in the treatment position.

In addition to these hardware components, Siemens Healthcare recently introduced a dedicated imaging workflow for Radiation Therapy (RT), the RT Dot Engine, which is described by my colleagues Thoermer and Requardt in the third article. Both the accessories for patient positioning as well as the RT Dot Engine are included in our dedicated MAGNETOM RT Pro edition for the MAGNETOM Aera 1.5T and the MAGNETOM Skyra 3T.

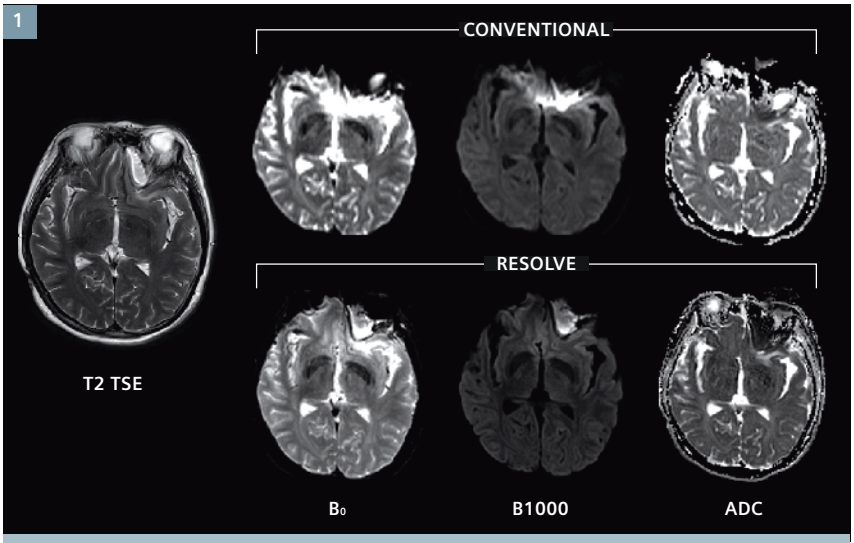

1 While spatial integrity of the conventionally acquired DWI scans often is compromised by susceptibility artifacts (caused by dental metal implants* in the case shown here), images acquired with the readout segmented DWI technique result in significantly reduced artifacts and superior spatial integrity.
Images courtesy of Tongji Hospital, Wuhan, China.

Clinical application in external beam radiotherapy

The requirements of MR images for external beam RT differ significantly from those of the diagnostic world. Sohlin et al. from the Sahlgrenska University Hospital in Gothenburg, Sweden have identified a significant benefit of optimized 3D SPACE sequences in their clinical practice and describe their application in head and neck cancer patients.

In treatment planning and therapy monitoring, functional techniques such as diffusion-weighted imaging (DWI) can provide additional valuable information. Schmidt et al. from the Royal Marsden, Sutton, UK, elegantly summarize that "the ultimate aim of functional imaging techniques is to identify radio-resistant disease and thus provide a biological target volume for dose boosting." However, standard DWI techniques "in regions adjacent to air-tissue interfaces are known to suffer from poor geometric integrity". They further describe how applications like the Siemens-unique RESOLVE technique (Figure 1) help "to ensure that the MRI examinations undertaken for RT planning purposes achieve the required geometric accuracy."

Further evidence has been published in the scientific literature [2, 3].

Another advanced imaging technique is Diffusion Tensor Imaging (DTI). Histopathological examinations have revealed that tumor cell dissemination in glioblastoma predominantly occurs along white matter tracts and brain

*The MRI restrictions (if any) of the metal implant must be considered prior to patient undergoing MRI exam. MR imaging of patients with metallic implants brings specific risks. However, certain implants are approved by the governing regulatory bodies to be MR conditionally safe. For such implants, the previously mentioned warning may not be applicable. Please contact the implant manufacturer for the specific conditional information. The conditions for MR safety are the responsibility of the implant manufacturer, not of Siemens.

2

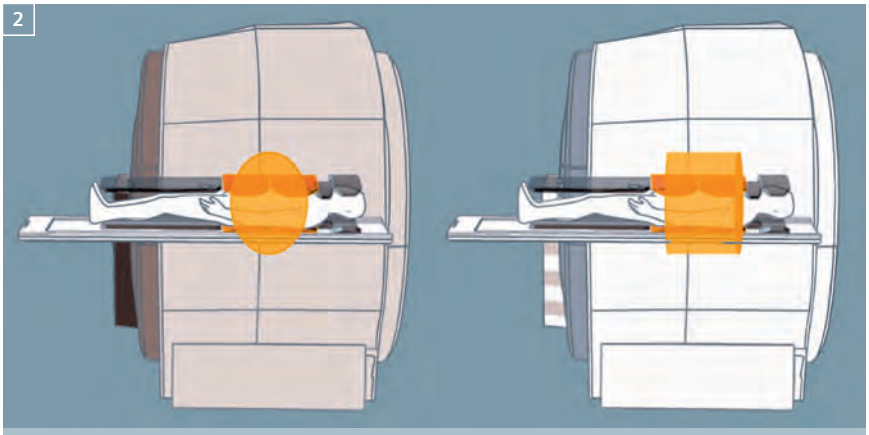

2 Visualization of the imaging volumes of a conventional magnet with spherical / ellipsoid volume (left) vs. TrueForm Magnet Design with a cylindrical volume (right).

3

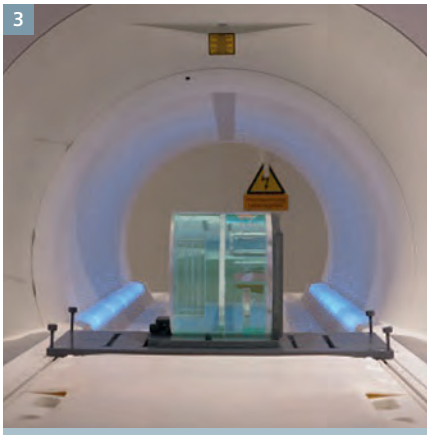

3 Vertical setup of the ACR phantom in the scanner bore for quality assurance testing of geometric distortions.

vessels [4]. These routes of spread can be depicted with DTI since water will diffuse more rapidly in the direction aligned with the internal structure of axon fibers, and more slowly as it moves perpendicular to this preferred direction. Based on the information about the principal diffusion direction in each voxel, tractography maps can be calculated and fused with morphological brain scans. The group of Berberat employs the technique with the ultimate aim "to derive a biologically targeted volume to ensure coverage of the regions at greatest risk of microscopic infiltration whilst excluding uninvolved brain."

Clinical application in brachytherapy

When considering the contribution of MRI to the treatment outcome, however, the potential advantages are still under clinical evaluation in many cases. It is all the more worth mentioning that in the treatment of cervical cancers with brachytherapy, the significance of 3D volumetric imaging in the planning process, namely with MRI, has been attested by the EMBRACE study [5]. This has shown that "with the MR image based brachytherapy approach [...] it is possible to obtain local control in over 90 percent of patients [...]".[6] In their article, Prisciandaro et al. comprehensively describe the commissioning of devices and workflows and the clinical implementation of MR-guided brachytherapy services at the University of Michigan, Ann Arbor, USA.

Prostate cancer treatment is also expected to significantly benefit from dose escalation and MR-guided brachytherapy has a great potential to contribute to this goal. In their article, Ménard et al. describe what is state-of-the-art at the Princess Margaret Hospital, Toronto, Canada, and discuss the benefits and challenges of acquiring the images in different parts of the process.

Response Monitoring

MRI information is not only able to positively impact treatment planning; it also has the potential to transform the entire care continuum. The case selection presented in the article by Padhani and Sokhi shows the ability to assess therapy efficacy in patients with metastatic disease with whole-body diffusion-weighted MRI when morphological imaging is inconclusive.

Current functional MRI techniques also show promising application in prediction as well as assessment of response, early in the course of treatment. Pham et al. have used the predecessor analysis software of what today is the *syngo*.MR OncoCare, to perform a voxel-by-voxel multiparametric analysis in order to evaluate heterogeneity within rectal cancers. This can give a quantitative assessment of the change in the tumor microenvironment resulting from chemoradiation.

Quality assurance and management of spatial accuracy

Before introducing MRI in clinical routine, physicists will look into commissioning the system and verifying its geometric performance in order to ensure a high degree of accuracy. A variety of our systems are fitted with a higher order shim, which affects the resulting image quality. More information about magnet homogeneity (Figure 2) and shimming can be found in the white paper by Blasche and Fischer [7]. Siemens also proposes a set of QA recommendations, based on the ACR phantom (Figure 3) [8].

In this section, Balter et al., Stanescu and Jaffray, as well as Paulson focus on these topics, discuss the impact of subject-induced susceptibility on distortions and share their methods for comprehensive acceptance testing and quality assurance.

Papanikolaou et al. have taken a different approach and detail how an MR scanner can be used for reading out irradiated polymer gels as a means of patient-specific dosimetric plan verification.

4 Synthetic CT generation from brain MR images using *syngo*.via Frontier*.

**syngo*.via Frontier is for research only, not a medical device.

One step closer to clinical application: synthetic CT generation and 4D MRI

In a typical 'MR enriched' workflow it is common practice to perform both (a) CT, to provide the electron density information needed for dose calculation and the geometric accuracy that is expected for planning a precise treatment, and (b) MRI, as the preferred modality for enhanced soft tissue contrast. The related additional cost and workload as well as the potential systematic error introduced by image registration have motivated researchers to focus their efforts on investigating MR-only[1] workflows for radiation therapy. Siemens Healthcare is enabling this scientific exchange by making such prototypes available on our research platform *syngo*.via Frontier (Figure 4).

In this issue, Greer et al. describe the implementation of an MR-only[1] workflow for the prostate at their institution, whereas Nyholm et al. give an overview of the technical aspects of MR-only[1] radiotherapy. Going along a similar direction, Liney et al. explore the potential of ultrashort echo time sequences, both for synthetic CT generation as well as for reducing susceptibility artifacts arising from fiducial markers.

Further to MR-only[1] workflows, current CT-based radiotherapy practice is also looking to MRI to solve another challenge, that of motion assessment. Ken et al. have looked at such a methodology for stereotactic treatment of the liver, whilst Bernatowicz et al. pose the thought-provoking question whether 4D-MRI may become the future of radiotherapy of moving targets. Siemens Healthcare has gained considerable experience in the field of 4D MRI thanks to the development of the Biograph mMR, the combined MR-PET scanner that requires time-resolved MRI for PET attenuation correction in the presence of organ motion.

I would like to thank all the authors publishing in this issue for sharing their expertise and enthusiasm with other MAGNETOM users. For those of you new to MRI in radiation therapy, I strongly encourage you to visit our online training and learn more about this exciting world at http://www.healthcare.siemens.com/radiation-oncology/imaging/magnetic-resonance/mri-training #webfeature

I wish you an enjoyable read!

Elena Nioutsikou
Global Product Marketing Manager Imaging in RT

[1] Radiotherapy Planning where MR data is the only imaging information is ongoing research. The concepts and information presented in this issue are based on research and are not commercially available. Its future availability cannot be ensured.

References

1 2014 Radiation Therapy Market Summary Report. IMV 2014.
2 Quantitative evaluation of diffusion-weighted imaging techniques for the purposes of radiotherapy planning in the prostate G P Liney et al BJR 2015.
3 Readout-segmented echo-planar diffusion-weighted imaging improves geometric performance for image-guided radiation therapy of pelvic tumors. Foltz et al Radiother Oncol (2015).
4 Giese A, Westphal M. Glioma invasion in the central nervous system. Neurosurgery 1996 39(2):235-50.
5 https://www.embracestudy.dk/
6 EMBRACE: intErnational study on MRI guided BRachytherapy in locally Advanced CErvical cancer: Small changes, big improvements. European Journal of Cancer. 2013;49:5.
7 Siemens Healthcare GmbH white paper. Magnet Homogeneity and Shimming. Mathias Blasche and Daniel Fischer. 2015 Downloadable at the MAGNETOM World RT: www.siemens.com/magnetom-world-rt
8 Siemens Healthcare GmbH white paper. MRI Geometric Distortion QA. Nina Niebuhr 2014. Downloadable at the MAGNETOM World RT: www.siemens.com/magnetom-world-rt

Content

[1] Radiotherapy planning where MR data is the only imaging information is ongoing research. The concepts and information presented in this article are based on research and are not commercially available. Its future availability cannot be ensured.

A Dedicated MRI Scanner for Radiotherapy Planning: Early Experiences

Gary Liney[1, 2]; Robba Rai[1]; Lois Holloway[1]; Shalini Vinod[1]

[1] Liverpool Cancer Therapy Centre, Sydney, Australia
[2] Ingham Institute for Applied Medical Research, Sydney, Australia

Introduction

The last decade has seen a dramatic increase in the use of MRI for radiotherapy planning. MRI has a number of advantages for the simulation of treatment plans, over the current gold standard of computed tomography (CT); Its excellent and variable soft-tissue contrast has been shown to improve the delineation accuracy of both the tumor and surrounding organs-at-risk; a range of functional techniques are able to measure and display tumor physiology in the same examination, potentially revealing sub-regions that could receive a boost in radiation dose; and finally, the absence of ionising radiation means the patient may be scanned any number of times before, during and after treatment, giving the clinician the ability to assess and adapt plans on an individual basis.

MR-simulator

In common with most radiotherapy centres, our department at Liverpool Cancer Therapy Centre (LCTC), located

1 The 3 Tesla MAGNETOM Skyra MR-Simulator at Liverpool CTC, in south western Sydney, Australia. The 30 Gauss line can be seen marked on the floor which serves to emphasise this inner controlled area for the majority of our staff who have not previously worked in MRI. The object on the bed is our 3D volumetric distortion test phantom.

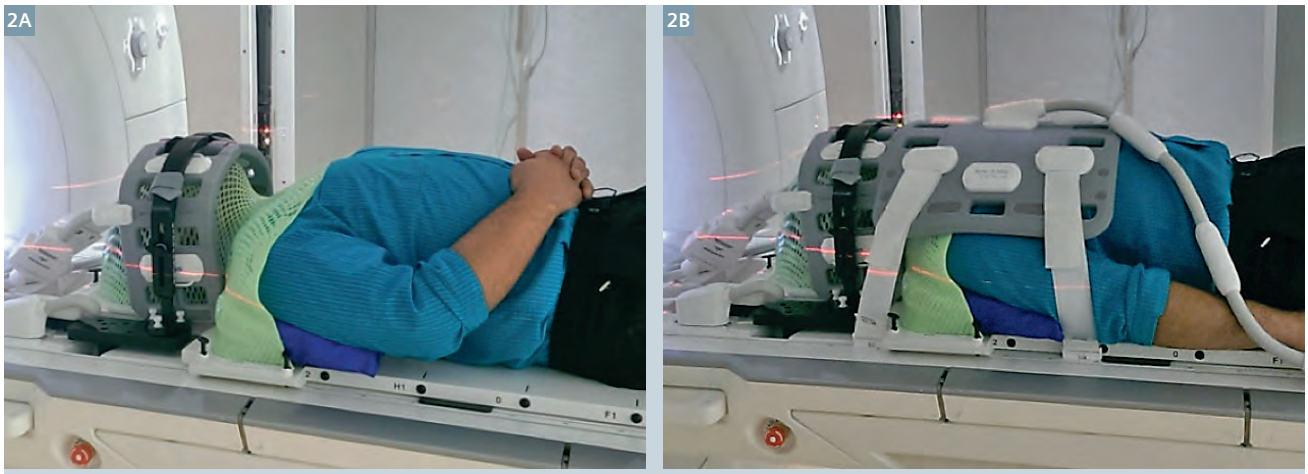

2 Photographs showing the RF coil set-up used in head and neck planning scans. **(2A)** Two small flexible coils are placed laterally around the fixation shell using two coil supports. **(2B)** The 18-channel body array is connected to one of the available ports at the bottom of the table using a long cable.

in south western Sydney, relied heavily on local radiology scanners to provide MR images. This often meant a compromise in image protocol and the limited availability of these busy scanners restricted our patient throughput and any opportunity for further development. However, in August 2013, as part of a wider investment in MRI, which will also see the Australian MR-Linac program on site, we installed our own dedicated system for the exclusive use of radiotherapy patients to provide MR-based treatment simulation scans. This scanner is a wide-bore 3 Tesla MAGNETOM Skyra with XQ gradients and 64-channel RF architecture and was purchased with the latest suite of functional imaging sequences. Our MR-Simulator (MR-sim), shown in Figure 1, is configured with a number of radiotherapy-specific features in mind including in-room lasers (as on a CT-simulator), flat indexed table top and a range of RF coils suitable for optimum imaging with the patients in the treatment position. The field strength was chosen with aspirations of incorporating functional studies into future clinical practice.

Over the last 12 months or so, our small but dedicated team has climbed a steep learning curve and implemented MR-based planning successfully into clinical practice for a variety of tumor sites. This process began even before the installation and acceptance testing of the system, with in-house safety and educational training being implemented for all radiotherapy and physics staff connected with MRI. Under normal operation, scanning is performed by our lead MR radiographer and one of a small number of specialist radiotherapists who are rotated through MR-Sim. Additional support is provided by the lead MR physicist and a radiologist. By preserving a significant portion of scan time during the week for research – one of the many advantages of having our own system – we have also been able to develop a number of studies that are beginning to explore the use of functional information and motion evaluation in treatment planning. This article serves as a brief illustration of how we are using this system in practice.

The vast majority of our workload requires MRI to be registered to CT for the electron density information needed in the dose calculation. To facilitate this, we image our patients in the treatment position and take advantage of the RF coils we have available. A good example of this is in head and neck tumors were patients lie on a flat table top and are imaged in a fixation shell placed over their head and shoulders which is attached to the table. Previous attempts to cater for this equipment on other scanners were compromised either due to a narrower 60 cm bore or unsuitable RF coils. On the MR-Sim we take advantage of the in-built 32-channel RF coil under the flat table-top and use this in conjunction with two laterally positioned 4-channel flexible coils attached to a supporting bridge. More recently we have been able to add an 18-channel body array connected at the foot of the table by a long cable (Fig. 2). This gives us vastly improved signal-to-noise ratio (SNR) and greater coverage compared to what had previously been possible as shown in Figure 3.

Imaging details

In working up our protocols, we have had to consider the specific requirements of MR-simulation, which is often quite different from standard diagnostic procedure [1]. Geometric distortion is something we have to be especially mindful of. For radial distances less than 15 cm from isocentre (i.e. up to 30 cm FOV), system distortions caused by non uniformity in B_0 and non linearity of the gradients are within our tolerance, and the dominant contribution is instead

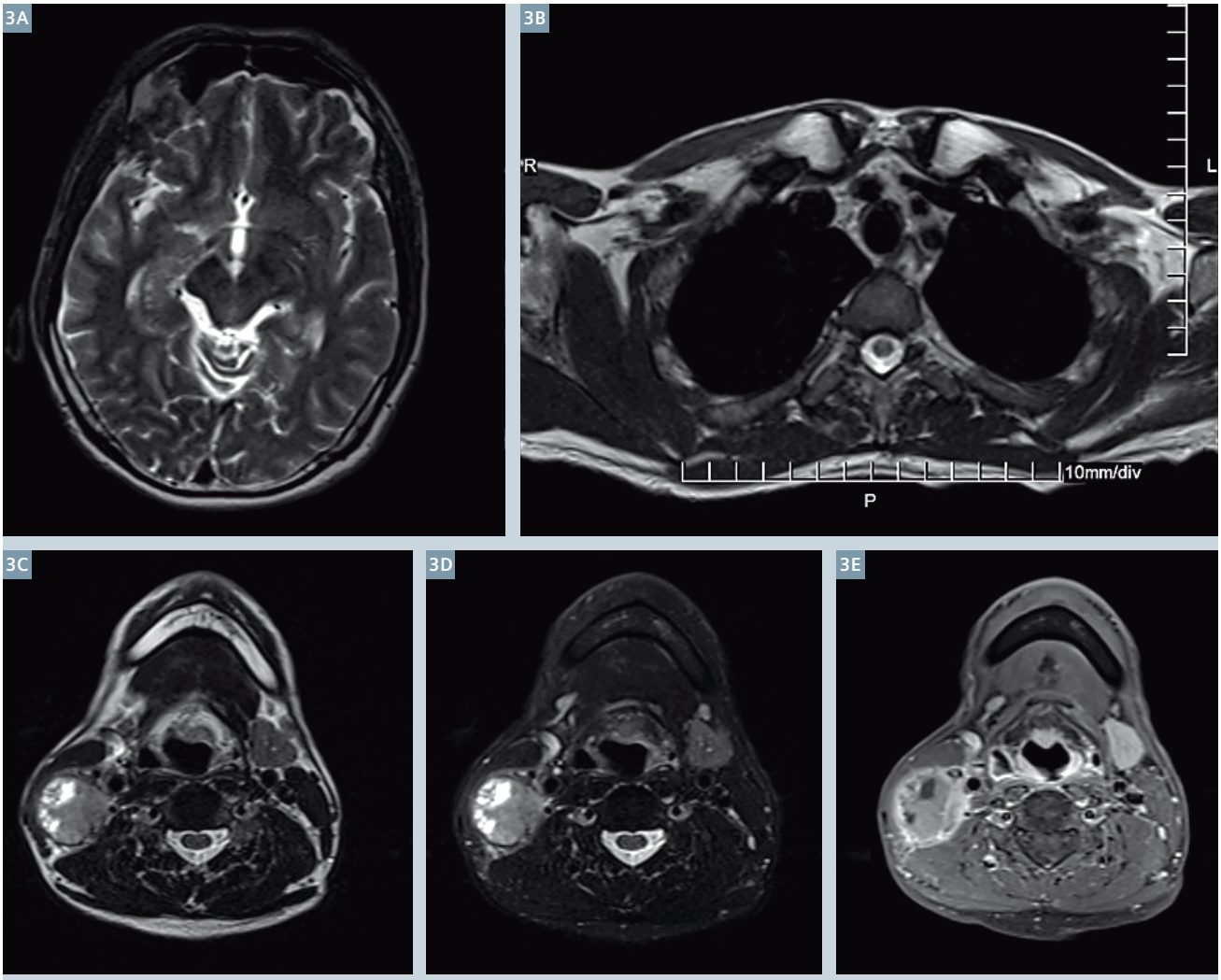

3 Example images acquired in a head and neck tumor patient. Figures **3A and B** serve to illustrate the image quality and coverage obtained using dedicated RF coils which extend from midbrain down to sternal notch. The bottom images show a slice taken through the tumor using **(3C)** Dixon T2w in-phase, **(3D)** water-only and **(3E)** Dixon T1w water-only post-contrast.

from chemical shift and magnetic susceptibility within the patient. These effects can be mitigated by use of high receiver bandwidths which we set to 440 Hz/pixel or greater. The large coverage that is required for planning creates long scan times compared to diagnostic practice and we rely heavily on iPAT technology to keep these down to an acceptable level. Nevertheless, these scan times inevitably result in some organ motion and we have found BLADE to be useful in reducing artifacts for example from bladder filling. One of our current studies is comparing the image quality of this radial *k*-space technique against the administration of anti-peristaltic agents and normal cartesian acquisition as shown in Figure 4A. Another particular interest for us is the development of a single planning scan for prostate patients with fiducial gold seeds. These exams would normally require two separate scans, a gradient-echo based sequence to identify the seed position and a second T2-weighted TSE for contouring the gland. The susceptibility artefact from the seed, while making them clearly visible, reduces positional accuracy, even with high bandwidths, and the requirement for two scans is less than ideal. However, we have begun looking at sequences such as turbo gradient spin-echo (TGSE) which offer the potential of combining both types of contrast into a single image (Fig. 4B).

To fully map out the geometric integrity of our system over large volumes, we have designed and built our own 3D phantom which covers 50 cm in each orientation (pictured in the magnet in Fig. 1). This test object has proved particularly useful in demonstrating the role of TimCT in cases when we have needed to exceed our 30 cm rule. By moving the patient through the bore while acquiring thin isocentric sections the distortion limit along the z-axis may be avoided altogether, thereby extending planning coverage. Figure 5 shows an example of this in a particularly difficult sarcoma case where more than 60 cm coverage was requested by the Oncologist and a total of 50 coil elements were used.

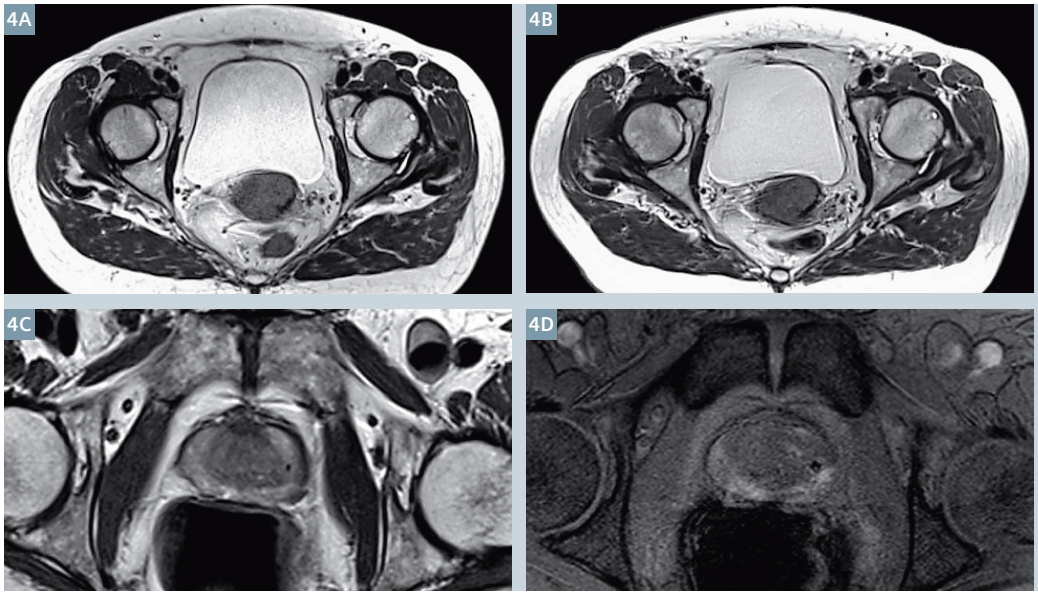

4

Developing body protocols for RT simulation; A comparison of BLADE **(4A)** versus anti-peristaltic agent **(4B)** as an effective control of organ motion artefacts. Use of the TGSE **(4C)** to provide a prostate planning scan that combines T2w contrast and gold seed visualization. **(4D)** Standard gradient-echo image used for seed localisation, which exaggerates the dimension of the marker.

Therapy response

For most examinations we are using MRI at the commencement of treatment for its soft-tissue contrast and the improvement in planning contours. Alongside this routine work, we have begun several research studies that are using MRI to assess response over the course of treatment. These studies use both diffusion-weighted imaging (DWI) and dynamic contrast enhancement (DCE) to look at changes in tumor cellularity and vascularity respectively. In the case of diffusion, the commonly-used EPI sequence produces significant distortions and artifacts that has made its application in radiotherapy planning problematic. We have recently concluded a study that compared EPI with RESOLVE, which uses multi-segmentation in the frequency encoding direction combined with navigator self-correction, and showed improvements in ADC repeatability and geometric integrity compared to a T2-weighted gold standard [2]. Figure 6 shows a DWI example in a prostate patient acquired with b = 800 s/mm^2 together with the corresponding ADC map and we have now also adopted this sequence for rectum and cervix. As part of our DCE protocol we acquire pre-contrast sequences at 2 and 15 degree flip angles to measure the native T1 prior to using dynamically acquired TWIST images. These scans are then analysed using the two compartment model which is available with the Tissue4D software.

Lung imaging

For our lung patients, we have developed an advanced imaging protocol providing a comprehensive assessment of anatomy, function and motion throughout their treatment (Fig. 7). For tumor contouring a T2-weighted HASTE sequence with a phase

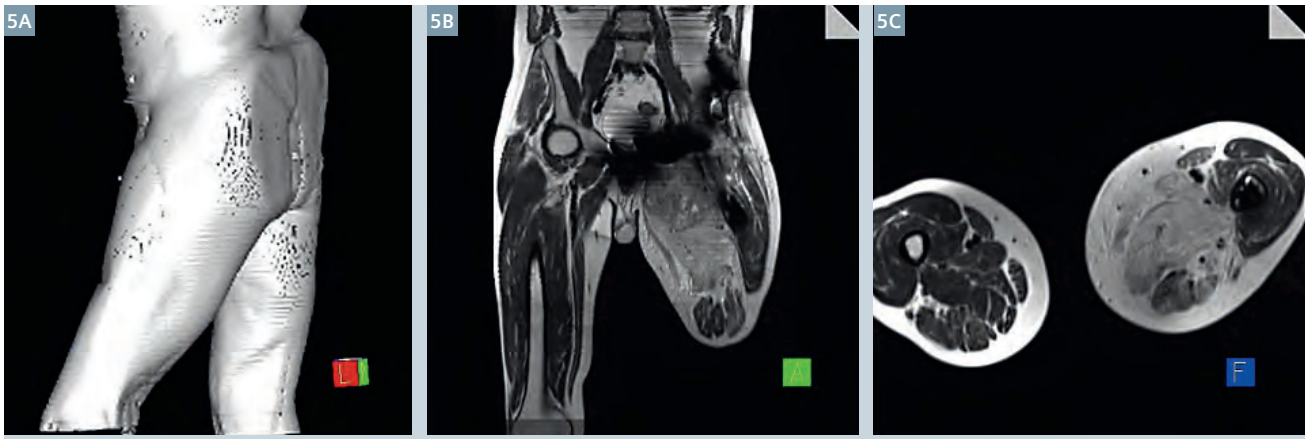

5 TimCT was used in this patient with a leg sarcoma and prosthesis *in situ* who could not straighten the effected leg. A full treatment simulation coverage of 61 cm in the head to foot direction was obtained by using the continuously moving table technique.

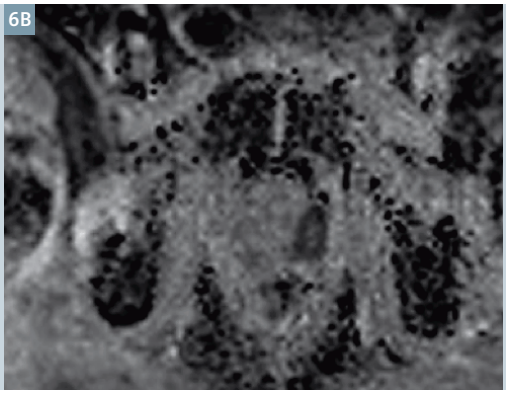

6

Diffusion-weighted imaging using the RESOLVE sequence in the prostate; **(6A)** A distortion free image with b = 800 s/mm^2 and **(6B)**, the resulting ADC map, both of which demonstrate an area of reduced diffusion in the left peripheral zone.

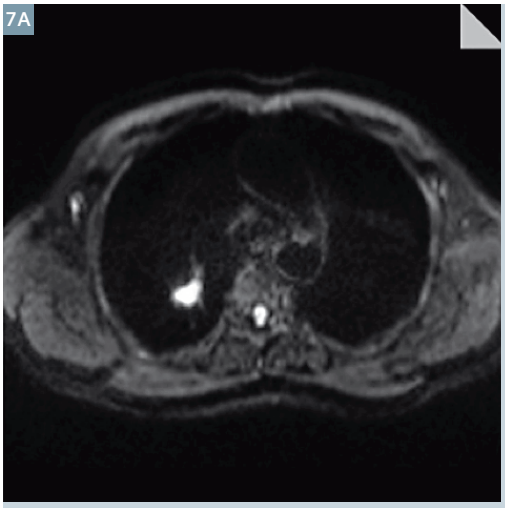

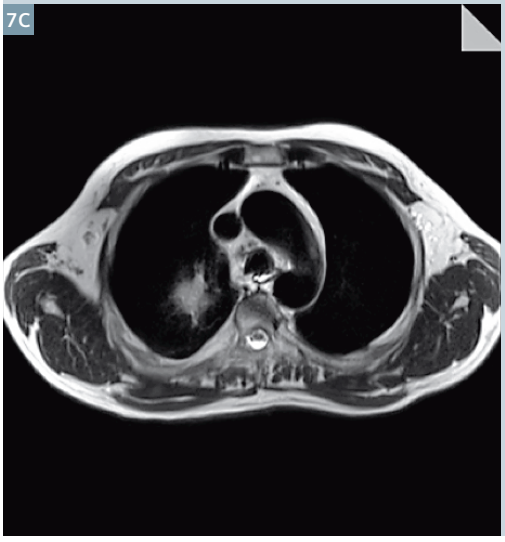

7

Example images from a lung tumor patient study; **(7A)** DWI with b = 500 s/mm^2 image, **(7B)** single frame from a coronal TrueFISP cine sequence acquired with cardiac shim, **(7C)** a late post-contrast enhanced TWIST image and **(7D)** axial HASTE acquired using a phase navigator.

navigator placed in the liver dome is used to provide artefact free images. We then acquire a diffusion-weighted sequence to measure ADC, and cine TrueFISP scans during free breathing to assess tumor motion. The protocol is completed with a DCE TWIST sequence which is modified to acquire a total of six separate short breath-hold windows from early first pass to 5 minutes post contrast. The incorporation of all this data is still in its infancy but we have already begun to use our own analysis to look at the tumor excursion and how it correlates with respiration.

Conclusion

In the future, we anticipate that it will be possible to replace CT altogether in the majority of cases. In order to do this, one of the challenges will be the need to substitute CT and provide a surrogate for electron density. As part

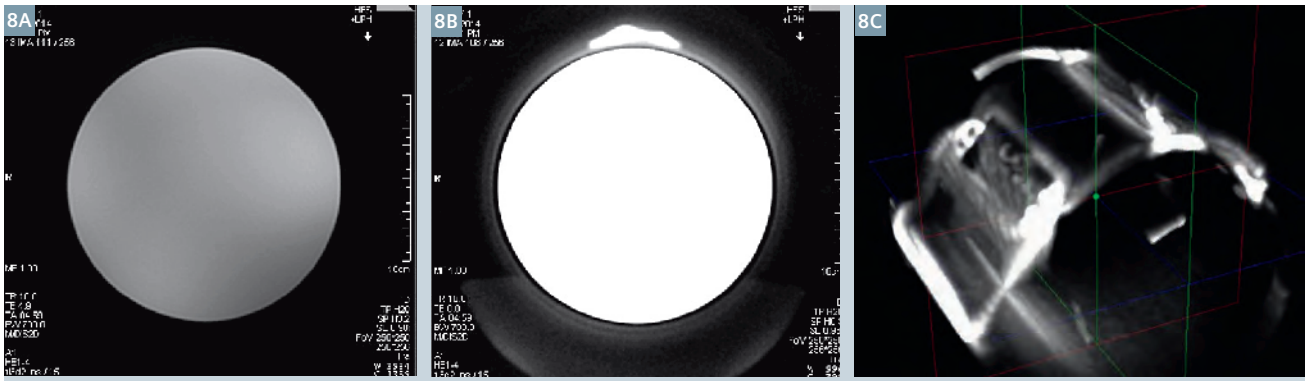

8 Examples of UTE imaging; **(8A, B)** Test object imaged at 4 ms displays signal from the fluid only but when this is repeated at 0.04 ms (40 µs) a previously invisible lump of adhesive putty placed on top and the plastic cushion underneath can also be seen. **(8C)** 3D rendering of a processed dataset which demonstrates the RF coil itself *(courtesy Jason Dowling, CSIRO)*.

of our research agreement with Siemens we are currently investigating the efficacy of ultrashort echo time (UTE) sequences to develop a strategy for MR-only planning[1]. By bringing the TE down to tens of microseconds it becomes possible to obtain signal from materials and tissues that were previously invisible (Fig. 8). These images have the potential to provide more accurate substitute CT datasets as they can map cortical bone and even the RF coil itself which will be useful on the MR-Linac.

In summary, although it is still very much early days for us, the installation of a dedicated scanner in our department has been a great success and crucial in propelling MRI into our practice. We hope that in the not-too-distant future, MR-Sim will become a fairly standard sight in many radiotherapy centres throughout Australia and indeed the rest of the world. This will certainly help to establish a standardised approach for the implementation of MRI into radiotherapy so that the full benefit of this modality can be realised.

Acknowledgements

We would like to acknowledge the following radiotherapists who make up the MR-Sim team: Lynnette Cassapi, Ewa Juresic, Jim Yakobi & Callie Choong. Also thanks to Aitang Xing, Amy Walker (radiotherapy physicists), Mark Sidom and Dion Forstner (oncologists) and Daniel Moses (MR radiologist).

References

1 GP Liney & MA Moerland. Magnetic resonance imaging acquisition techniques for radiotherapy planning, Sem Rad Onc in press, 2014.
2 GP Liney, T Al Harthi, E Juresic et al. Quantitative evaluation of diffusion-weighted imaging techniques for radiotherapy planning of prostate cancer. Proc ISMRM 2718: 2014.

[1] Radiotherapy Planning where MR data is the only imaging information is ongoing research. The concepts and information presented in this article are based on research and are not commercially available. Its future availability cannot be ensured.

Contact

Associate Professor Gary Liney (UNSW)
Hon Principal Fellow, University of Wollongong
Ingham Institute for Applied Medical Research & Radiation Oncology
Liverpool Hospital, 1 Campbell Street
Liverpool NSW 2170, Australia
Phone: +61 2 8738 9221
gary.liney@sswahs.nsw.gov.au

Evaluation of the CIVCO Indexed Patient Position System (IPPS) MRI-Overlay for Positioning and Immobilization of Radiotherapy Patients

Th. Koch[1]; K. Freundl[1]; M. Lenhart[2]; G. Klautke[1]; H.-J. Thiel[1]

[1] Klinik und Praxis für Strahlentherapie und Radioonkologie, Sozialstiftung Bamberg, Germany
[2] Klinik für Diagnostische Radiologie, Interventionelle Radiologie und Neuroradiologie, Bamberg, Germany

Abstract

The emerging development in modern radiotherapy planning (RTP) requires sophisticated imaging modalities. RTP for high precision requires exact delineation of the tumor, but this is currently the weakest link in the whole RTP process [1]. Therefore Magnetic resonance imaging (MRI) is of increasing interest in radiotherapy treatment planning because it has a superior soft tissue contrast, making it possible to define tumors and surrounding healthy organs with greater accuracy. The way to use MRI in radiotherapy can be different. The MRI datasets can be used as secondary images to support the tumor delineation. This is routinely in use in many radiotherapy departments. Two other methods of MRI guidance in the RTP process are until now only research projects, but interest in them is increasing. The first method is to use MRI data as the primary and only image dataset and the second is the application of the MRI data as reference dataset for a so-called 'MRI-guided radiotherapy in hybrid systems' (Linear Accelerator (Linac) or Cobalt RT units combined with MRI). For all cases it is essential to create the MRI datasets in the radiotherapy treatment position. For this reason the CIVCO Indexed Patient Positioning System (IPPS) MRI-Overlay was introduced and tested with our Siemens MAGNETOM Aera MRI Scanner.

Introduction

Although computed tomography (CT) images are the current gold standard in radiotherapy planning, MRI becomes more and more interesting. Whilst CT has limitations in accuracy concerning the visualization of boundaries between tumor and surrounding healthy organs, MRI can overcome these problems by yielding superior soft tissue contrast. Currently there are three different possible strategies by which MRI can help to improve radiotherapy treatment planning:

The MRI datasets can be used as secondary images for treatment planning. These MR images can be used to delineate the tumor and the surrounding organs, whilst the CT images – the primary planning data – are necessary to calculate the 3D dose distribution. The two image datasets have to be co-registered thoroughly to ensure that the anatomy correlates (see for example [2]). The registration

1 1.5T MAGNETOM Aera with the standard cushion on the MRI couch.

2 After the removal of the standard cushion the CIVCO IPPS MRI-Overlay can be mounted.

3 The lines indicate the position for the index bars.

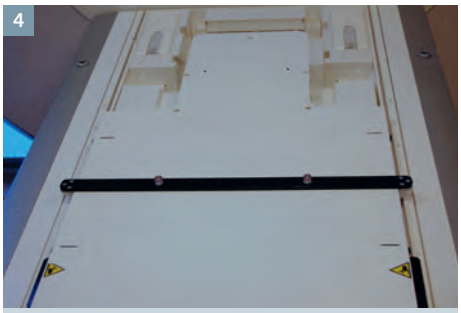

4 One index bar is latched to the MRI-Overlay.

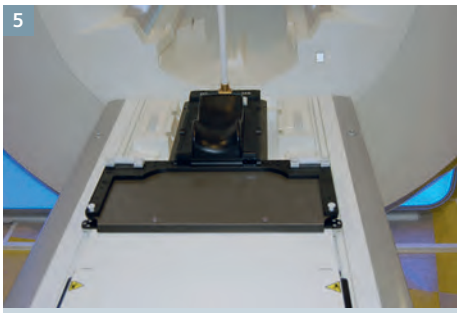

5 The mask system for head and neck fits to the index bar to avoid movement.

accuracy strongly depends on the MRI scan position. Hanvey et al. [3] and Brunt et al. [4] have shown that it is indispensable for the MRI dataset to be created in the treatment position which is primarily defined by the CT scan.

The MRI dataset can also feasibily be used as the only dataset. Because of the lack of electron density information, which is required for dosimetric calculations, bulk densities have to be applied to the MRI images. For this purpose the different anatomic regions like bone, lung, air cavities and soft tissue have to be overwritten with the physical densities. With this method it is possible to achieve dose calculation results quite similar to the calculation in the CT dataset in the head and neck region [5, 6] as well as in the pelvic region [7]. The advantage of this method is that by avoiding the CT scan you save some time and money. In this case it is necessary for the treatment position to be determined during the MRI scan, hence the MRI scanner has to be equipped with the same positioning and immobilization tools as the Linac. Further problems to overcome are the evaluation and correction of possible image distortions and the determination of accurate bulk densities.

After the RTP process there are a lot of remaining uncertainties such as set-up errors, motion of the target structures and during the treatment changes of the tumor volume and shrinking. This problem can be overcome with the so-called image-guided radiotherapy (IGRT). IGRT involves a periodical verification (weekly or more frequent) of tumor position and size with appropriate imaging systems. It is evident that IGRT is only as good as the accuracy with which the target structures can be defined. For this reason some groups try to develop hybrid systems, where a Linac or a cobalt treatment unit is combined with an MRI scanner for a so-called MR-guided radiotherapy [8-10]. Again: MR-guided radiotherapy can only be successful when the reference MRI dataset has been created in the treatment position.

In any of the above three cases, where MRI can be helpful to improve the accuracy of radiotherapy, it is strongly advised that one has a robust and reproducible patient positioning and immobilization system, mainly at the MRI scanner, which is used for MR-guided RTP. Siemens provides with the CIVCO IPPS MRI-Overlay a suitable solution. In our clinic we have introduced and tested this MRI-overlay, especially for patients with tumors in the pelvis and for brain tumors and metastasis.

Method

Our 1.5T MAGNETOM Aera system (Siemens Healthcare, Erlangen, Germany) is located in the radiology department and can temporarily be used by the staff of the radiotherapy department. For the purpose of MR-guided RTP we have equipped the MAGNETOM Aera with the CIVCO IPPS MRI-Overlay. This overlay enables the fixation of positioning and immobilization tools necessary for radiotherapy treatments. For our purpose we have used an MR compatible mask system for head and neck cases and vacuum cushions for patients with diseases in the pelvic region both from Medical Intelligence (Elekta, Schwabmünchen, Germany). These tools can all be fixed with so-called index bars (Figs. 4, 12) at the MRI-Overlay. These index bars are custom designed for our purpose by Innovative Technologies Völp (IT-V, Innsbruck, Austria) for the MRI-Overlay and for use in the high field magnetic environment. For the correct positioning of the patients, the laser system Dorado 3 (LAP, Lüneburg, Germany) was additionally installed in the MRI room. The preliminary modifications and the patient positioning is described in the following for two cases.

The first case describes the procedure for a patient with a head tumor. The first step is the removal of the standard cushion of the MRI couch and the mounting of the MRI-Overlay (Figs. 1–3). One index bar is necessary to fix the mask system on the overlay (Figs. 4, 5) to avoid movements and rotations during the scan. Because the standard head coil set cannot be used with the mask system, two flex coils (Flex4 Large) have to be prepared (Figs. 6–8). In figure 8 one can see, that the correct head angle could be adjusted. Now the patient is placed on the overlay and in the mask system. The patient's head can be immobilized with the real and proper mask made from thermoplastic material called iCAST (Medical Intelligence, Elekta, Schwabmünchen, Germany)

6
Two flex coils (Flex4 Large) are prepared.

7
The flex coils have to be positioned partly under the mask system, because the whole head of the patient should be covered.

8
It is possible to adjust the head angle in an appropriate and reproducible position that is comfortable for the patient.

9
Now the patient is immobilized using a custom-made mask made from thermoplastic material.

10
The flex coils are closed with hook-and-loop tapes.

11
The patient is ready for the scan.

12 A custom-made vacuum cushion for the lower extremities is latched to the MRI-Overlay with two index bars.

13 A second vacuum cushion is positioned on the table to fix the arms and shoulders and keep the patient in a comfortable position.

as can be seen in figure 9. Now the flex coils can be fixed with hook-and-loop tapes and placed very tight to the patient (Figs. 10, 11). Now the MRI scan can be started.

The second case describes the preparation before the MRI scan for a patient with a tumor in the pelvic region. The first two steps are identical, the remove of the standard cushion followed by the mount of the overlay (Figs.1, 2). Then a custom-made vacuum cushion for the lower extremities is attached to the overlay with two index bars (Figs. 12, 13). For a robust position of the patients with diseases in the pelvis it is very important to keep the legs in well-defined position – not only during imaging but also throughout the

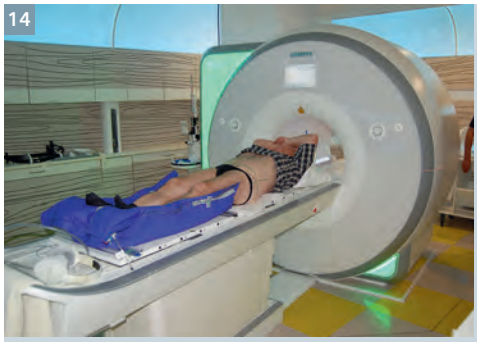

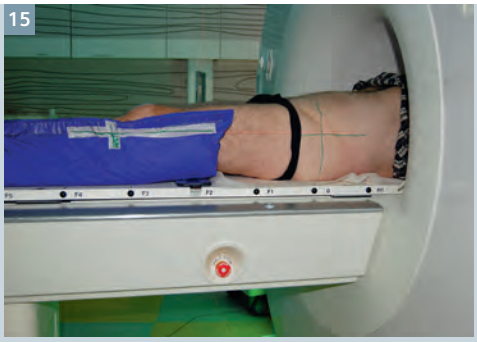

14
Now the patient can be positioned.

15
The accurate position of the patient can be adjusted with the LAP laser system.

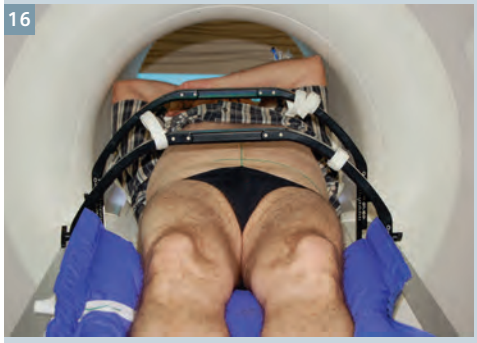

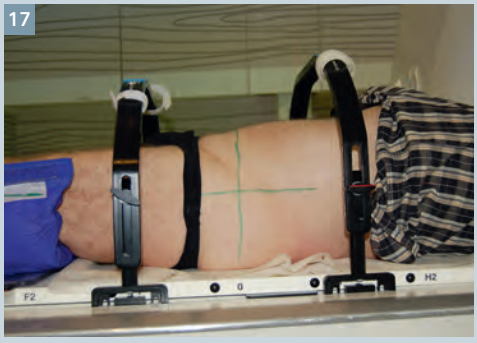

16
A mounting-frame for the flex coil has to attached to the MRI-Overlay.

17
The mounting-frame from a side view.

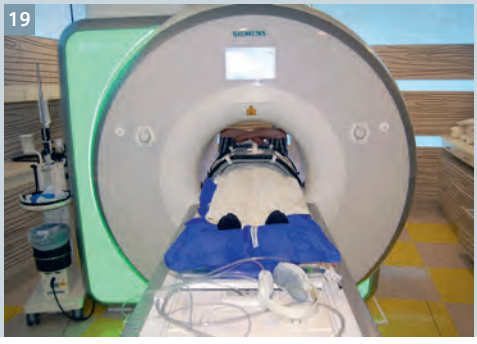

18
The flex coil is fixed to the mounting-frame with hook-and-loop tapes.

19
The patient is ready to start the scan.

whole treatment course, which spans over seven weeks. Any changes there can result in undesired rotations of the pelvis and in the end the tumor position and shape can also change. In figure 13 a second custom-made vacuum cushion can be seen. The only purpose of this vacuum cushion is to enable a comfortable position of the patient during scan and later during the treatment (Fig. 14). The more comfortably the patient lies on the table the more robust and reproducible is the positioning. Fortunately MAGNETOM Aera has a bore diameter of 70 cm, hence there are almost no limitations concerning patient positioning. Now the accurate position of the patient should be checked with the moveable laser-system (Fig. 15). This is necessary to avoid rotations of the pelvis around the patients longitudinal and lateral axis. For the fixation of the flex-coil for the pelvic region a mounting-frame has to be attached to the overlay (Figs. 16, 17). This can be done with hook-and-loop tapes (Fig. 18). Now the patient set-up is completed and the MRI scan can be started (Fig. 19).

Results

Two examples are shown in the following pictures. In Fig. 20 you can see a brain tumor in two corresponding slices. The left picture shows the CT-slice and the right picture shows the corresponding MRI slice obtained with a T1-weighted sequence with contrast agent. It is clear to see that tumor boundary is much more pronounced in the MRI image. Figure 21 shows the same slices with structures created by the radiotherapists. It is also helpful to create some control structures, such as brain and ventricles, to check the accuracy of the registration. Figures 22 and 23 give an example of a patient with prostate cancer. In this case the MRI images on the right

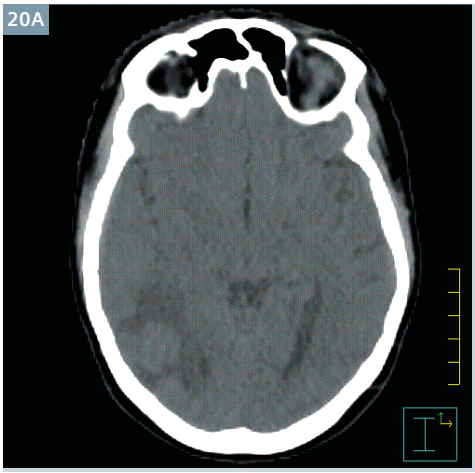

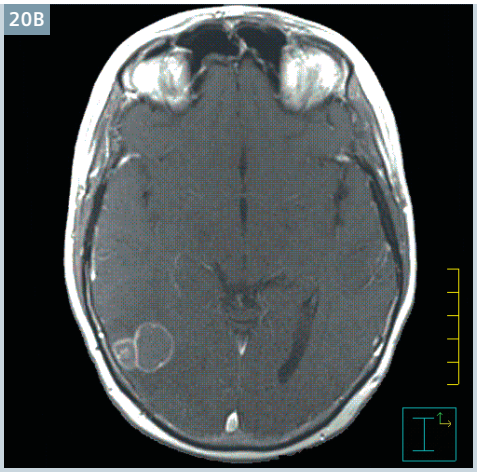

20

Two corresponding slices of a brain scan: **(20A)** CT slice and **(20B)** MRI slice obtained using a T1-weighted sequence with contrast agent.

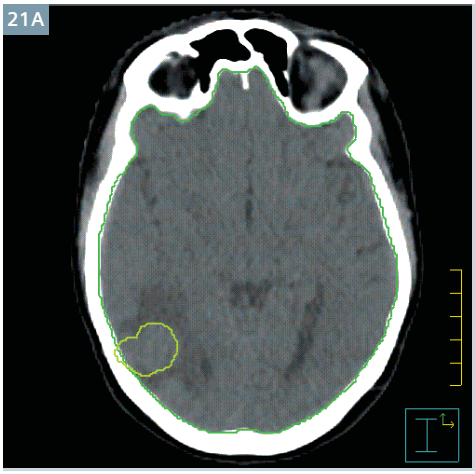

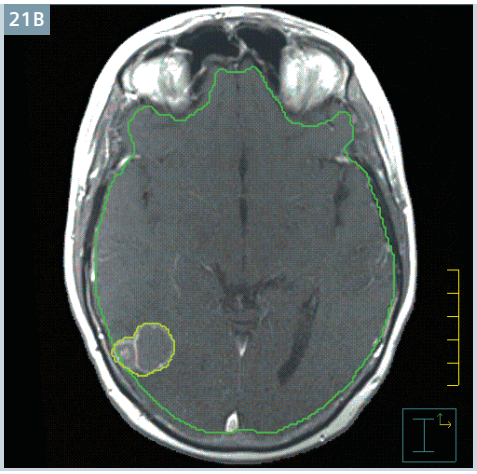

21

The same slices as in figure 20, but now with delineated tumor and help structures.

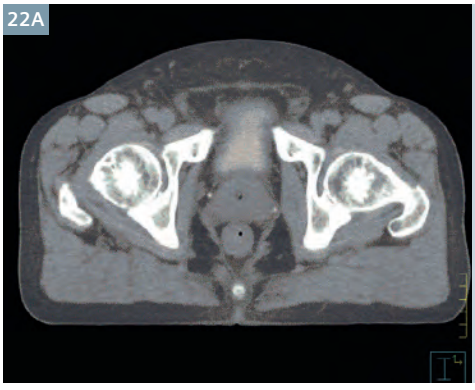

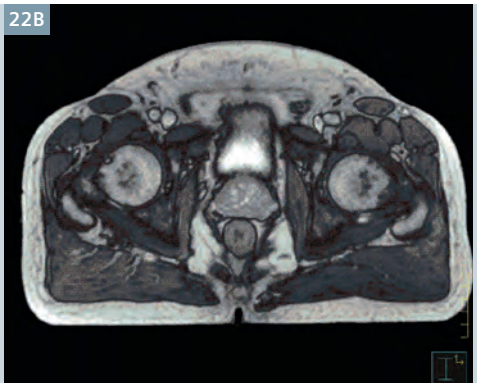

22

Two corresponding slices in the pelvic region of a patient with a prostate cancer: **(22A)** CT slice and **(22B)** MRI slice obtained with a T2-weighted TrueFISP sequence.

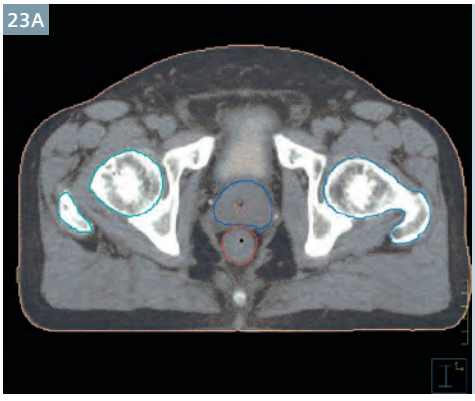

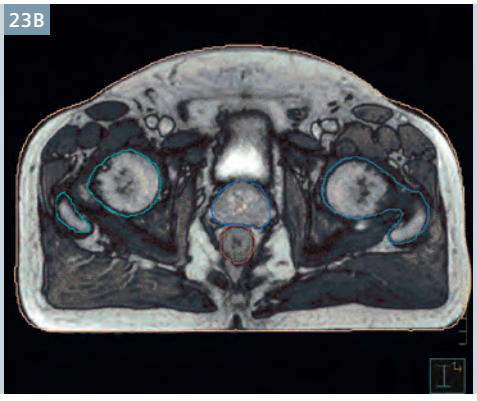

23

The important structures rectum and prostate as defined in the MRI slice are shown. The accuracy of the registration can be tested with the coincidence of help structures – like the femoral heads in this case – in both datasets.

are acquired using a T2-weighted TrueFISP sequence. The boundary of the prostate and the differentiation between prostate and rectum is much more easier to define in the MRI images. The control structures in this case are the femoral heads. For the head scans we normally use 3 sequences, a T1w SE with contrast agent, a T2w TSE and a FLAIR sequence. For the pelvis scans we normally use a T2w SPACE, a T2w TrueFISP and a T2w TSE sequence. The coordinate system should be the same for all sequences, that means same slices and same field-of-view. Hence one can use the same registration parameters for all sequences.

Conclusion and outlook

We can now look back over a period of two years working with the CIVKO IPPS MRI-Overlay. Our experience is very promising. The modifications on the table of the MRI scanner are very easy and can be executed and finished in only a couple of minutes. The procedure is well accepted by the radiologic technologists. To date, we have scanned more than 100 radiotherapy patients, mainly with diseases in the pelvis (rectum and prostate cancer) and in the head (brain tumors and metastasis). So far we have only used MRI dataset as a secondary image dataset. The co-registration with the CT datasets is now much easier because we have nearly identical transversal slices in both image datasets.

As a conclusion we can say that we are very happy with the options we have to create MRI scans in the treatment positions. It has been demonstrated that the MRI dataset is now much more helpful in the radiotherapy planning process. We should mention the need for a quality assurance program to take possible image distortions into consideration. Our next step is to install such a program, which involves the testing of suitable phantoms. A further step will be to assess whether we can use MRI datasets alone for RTP.

References

1 Njeh C. F. Tumor delineation: the weakest link in the search for accuracy in radiotherapy. J. Med. Phys. 2008 Oct-Dec; 33(4): 136-140.
2 Dean C.J. et al. An evaluation of four CT-MRI co-registration techniques for radiotherapy treatment planning of prone rectal cancer patients. Br. J. Radiol. 2012 Jan; 85: 61-68.
3 Hanvey S. et al. The influence of MRI scan position on image registration accuracy, target delineation and calculated dose in prostatic radiotherapy. Br. J. Radiol. 2012 Dec; 85: 1256-1262.
4 Brunt J.N.H. Computed Tomography – Magnetic Resonance Imaging Registration in Radiotherapy Treatment Planning. Clin. Oncol. 2010 Oct; 22: 688-697.
5 Beavis A.W. et al. Radiotherapy treatment planning of brain tumours using MRI alone. Br. J. Radiol. 1998 May; 71: 544-548.
6 Prabhakar R. et al. Feasibility of using MRI alone for Radiation Treatment Planning in Brain Tumors. Jpn. J. Clin. Oncol. 2007 Jul; 37(6): 405-411.
7 Lambert J. et al. MRI-guided prostate radiation therapy planning: Investigation of dosimetric accuracy of MRI-based dose planning. Radiother. Oncol. 2011 Mar 98: 330-334.
8 Raymakers B.W. et al. Integrating a 1.5 T MRI scanner with a 6 MV accelerator: proof of concept. Phys. Med. Biol. 2009 May; 54: 229-237.
9 Hu Y. et al. Initial Experience with the ViewRay System – Quality Assurance Testing of the Imaging Component. Med. Phys. 2012 Jun; 39:4013.
10 ViewRay. Available at: http://www.viewray.com

Contact

Thomas Koch, Ph.D.
Sozialstiftung Bamberg – Medizinisches Versorgungszentrum am Bruderwald
Praxis für Radioonkologie und Strahlentherapie
Head Medical Physics
Buger Straße 80
96049 Bamberg
Germany
Phone: +49 951 503 12931
thomas.koch@sozialstiftung-bamberg.de

RT Dot Engine

Gregor Thörmer, Ph.D.; Martin Requardt, Ph.D.

Siemens Healthcare, Magnetic Resonance Imaging, Erlangen, Germany

Background

Magnetic resonance imaging (MRI) is based on different *pulse sequences*, a combination of radio-frequency pulses and gradients that are switched on and off according to a specific scheme. The strength, duration, and spacing of these 'building blocks' are defined by imaging *parameters*. This allows the depiction of tissue in various ways, e.g. for the visualization of vessels, fat or edema, and with different spatial and temporal resolution, depending on the concrete clinical question. An imaging *protocol* allows predefined or customized parameter sets to be saved and retrieved [1].

Standard MR imaging protocols for diagnostic purposes are typically not optimized to meet the requirements of radiation therapy (RT), but can be adjusted for high spatial integrity, isotropic voxels and reduced susceptibility to motion artifacts via the underlying imaging parameters. To do so, however, the user had to be familiar with the complex system of parameters and their mutual interference up to now [2].

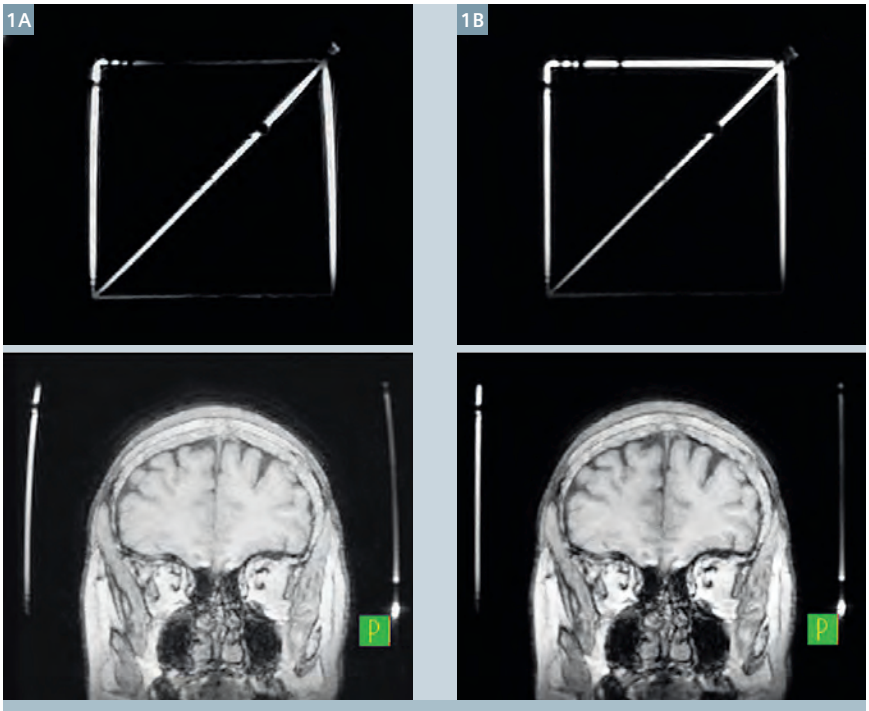

1 Left column **(1A)** shows uncorrected MR images with distortions due to gradient non-linearity. In the right column **(1B)**, these distortions are automatically corrected with 3D distortion.

RT Dot Engine

With the RT Dot[1] Engine, a comprehensive package became available addressing specifically the requirements of MR imaging for radiation therapy. The imaging protocols it provides have been developed in collaboration with RT departments experienced in using MR, in particular the group of Prof. James Balter (Michigan University, Ann Arbour, USA). Features like automatic axial image reconstruction and 'one click' integration of external laser bridges are easily accessible. All protocols in the RT Dot Engine were carefully optimized to improve spatial integrity, e.g. via high bandwidths [2] and automatic 3D distortion correction (Fig. 1). In the "Dot mode", only a limited set of routine geometry parameters is shown to the user (Fig. 2), while the "Detail mode" provides full access to imaging parameters. The product features different predefined strategies for brain and head & neck imaging and a protocol to perform external Laser QA (Fig. 3). Using this technology, Radiation Oncology staff can perform MR exams in a reliable and reproducible way. Furthermore, pictograms and hints that exemplary show how to plan an exam can be used to guide less MR-experienced users troughout the workflow. More advanced customers can use the dedicated RT Dot AddIns to build their own RT Dot Engines for other body regions. To support this, Siemens has a team of MR application specialists specifically trained for RT.

One click integration of external lasers

After patient preparation and positioning with MR compatible immobilization accessories, an external laser bridge (DORADOnova, LAP, Germany) can be used to exactly define the target position on the patient's body. In the past, the technologist had to perform this step with the built-in laser crosshair of the MRI system again; a handicap of the workflow and a source of inaccuracy. Now, a Dot AddIn takes care with 'one click' ("Laseroffset-Scan", see Fig. 3) that the position defined with the external laser beam directly goes to the center of the magnet where imaging conditions are optimal. One enabler of this technology is the ±0.5 mm positioning accuracy of the Tim Table[2].

2 User interface shows the predefined scan strategy for a brain exam with the RT Dot Engine. The queue with RT protocols is displayed in the lower half to the left. In "Dot mode" a limited set of geometry parameters is displayed on the right side to adapt scanning to patient's anatomy. By clicking the magnifying glass symbol in the lower right corner you can access and define all imaging parameters on expert level.

Fine structured scanning and spatial integrity

Imaging in the treatment position with thermoplastic masks and other equipment requires the use of flexible surface coils. Two such coils wrapped around the patient's head form an '8-channel head coil' providing 17% increase in signal-to-noise-ratio (SNR) compared to a setup with two loop coils positioned left and right of the skull. Nonetheless, the received SNR is still approximately 25% higher with a dedicated 20-channel head & neck coil.

To address this challenge, the RT Dot Engine allows acquisition of two interleaving datasets with an overlap ('negative distance factors') of the neighboring slices. To give an example: 3 mm slice thickness and a negative distance factor of 50% corresponds to an effective interslice distance of only 1.5 mm. This technique of fine structured 2D scanning not only improves the SNR of reconstructed images, it also supports 3D reformatting capabilities (Fig. 4)

3D imaging and automatic axial image reconstruction

A majority of imaging protocols in the RT Dot Engine is based on 3D sequences. 3D images inherently provide superior SNR compared to 2D imaging, allow for isotropic voxel size and can be reformatted in any desired orientation. From the point of MR physics it is sometimes beneficial to acquire these datasets with non-axial slice orientation. For some therapy planning systems, however, axial image orientation is mandatory.

3 Scan strategies within the RT Dot Engine for MAGNETOM Skyra [204x48].

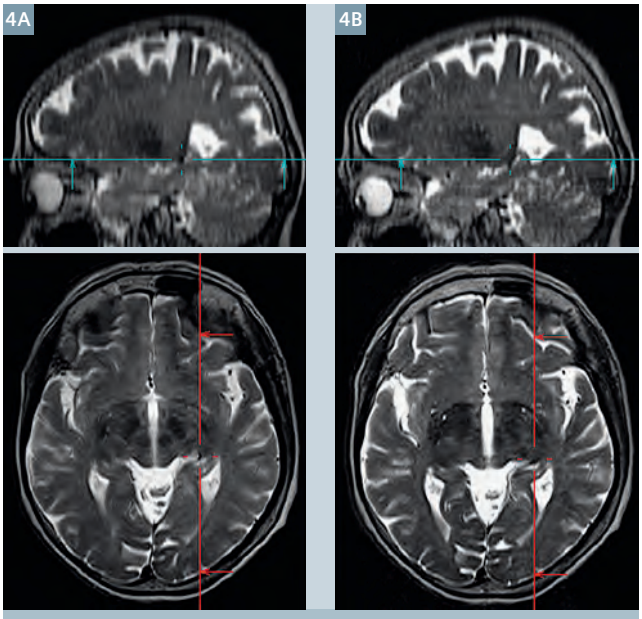

4 Comparison of a standard axial 2D TSE scan with no gap between the slices **(4A)** and a fine structured 2D TSE volume scan **(4B)**. These images provide both better SNR and good delineation of anatomical structures along the slice axis. The technique is applicable to every 2D sequence protocol.

5 Screenshot of multiplanar reconstruction (MPR) planning AddIn. Assigned image data sets (here: 4 t1_spc_sag_reformat_tra and 5 t2_spc_flair_reformat_tra) are automatically reconstructed according to the defined parameters.

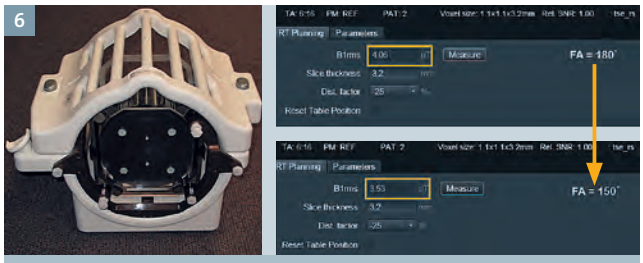

6 Left: Coordinate Frame G inside a Tx/Rx (transmit/receive) head coil. By clicking "measure" the B1 rms value for a protocol is calculated. In the example shown here, the flip angle, which correlates with the power of the applied refocusing RF pulses was reduced from 180° to 150° resulting in a respective decrease of the applied average RF power.

In the RT Dot Engine an AddIn ensures that axial images are automatically reconstructed in a predefined way which then can be sent to the planning system (Fig. 5). If a user always wants to have 1.5, 3 and 6 mm axial slices, for example, this can be defined via a respective preset.

B1 rms calculation

Some radiation therapy scenarios involve the use of special equipment, like dedicated stereotactic head-frames to fixate the patient's skull. For some devices special regulations exist, i.e. to operate these devices with protocols under restricted RF-deposition in order to reduce the risk of heating during imaging[3]. The functionality "B1 rms" (Root mean square of the B1 field) enables easy access to SAR (specific absorption rate) deposition with a specific imaging protocol (Fig. 6). Before starting the actual measurement, the user can verify if certain safety conditions are fulfilled and change imaging parameters if necessary.

References

1 Rumpel H, et al. How Modules of Imaging Sequences Fit Together: An Overview of Recent Advances in MR Imaging. MAGNETOM Flash #60 (5/2014) p86-92.

2 Graessner J. Bandwidth in MRI? MAGNETOM Flash #52 (2/2013) p122-127. http://www.healthcare.siemens.com/magnetic-resonance-imaging/magnetom-world/clinical-corner/application-tips/bandwidth-mri

Contact

Gregor Thörmer, Ph.D.
Global Segment Manager Men's and Women's Health
Siemens Healthcare
Karl-Schall-Str. 6
91052 Erlangen
Germany
gregor.thoermer@siemens.com

[1] Dot (Day optimizing throughput) includes different features like Dot AddIns to assist the user, standardize procedures and automate recurrent workflow steps.

[2] Specifications MAGNETOM Aera and MAGNETOM Skyra. Datasheet.

[3] Specifications and terms of use are defined and provided by the manufacturer of the equipment.

SIEMENS

siemens.com/imaging-for-RT

Imaging Solutions that empower Radiation Therapy

Look closer. See further.

As therapeutic and technological capabilities in RT evolve, so does the need for a partner who combines therapy experience with leading imaging expertise. Siemens Healthcare is that partner: For access to high-quality anatomical and functional imaging information that helps RT professionals to make confident treatment decisions.

Siemens' advanced imaging tools can help you reach your most important clinical goals: achieve a complete response, reduce the risk of normal tissue toxicity, and improve the chances of disease-free survival for an increasing number of patients.

Siemens solutions can be easily implemented in RT environments and are customized to fit the way RT professionals work – ensuring a smooth and efficient workflow supported by some of the finest imaging tools available.

With tailor-made imaging solutions for RT, Siemens enables you to look closer and see further than ever before, to place you at the forefront of truly individualized therapy.

Significant Benefit of Optimized 3D SPACE Sequences in Radiation Therapy Treatment

Maja Sohlin, Ph.D.[1]; Karin Petruson, M.D., Ph.D.[2]

[1] Sahlgrenska University Hospital, Medical Physics and Biomedical Engineering, Gothenburg, Sweden
[2] Sahlgrenska University Hospital, Department of Oncology, Gothenburg, Sweden

MR images used in radiation therapy have other requirements than conventional diagnostic MR images. In radiation therapy, the exact extent and position of lesions in relation to critical structures have to be determined in order to ensure an effective and safe treatment of the patient. This requires high in-plane spatial resolution, thin slices without slice gaps, and a minimal geometric distortion. In addition, due to image registration and patient fixation, a sub-optimal patient set-up is often required, including flexible coil solutions and a flat table top.

MR imaging struggles with system-related and patient-induced geometric distortions. For radiation therapy, the imaging protocols must be optimized to give minimal geometric distortions in the imaging volume. In general, the geometric integrity is best preserved by using spin-echo based sequences with high acquisition bandwidth. In the current workflow, MR images used for therapy planning have to be registered to a CT dataset. The imaging protocol must thus also be optimized to give sufficient image contrast and adequate spatial resolution to ensure an accurate image registration, with a trade-off between registration accuracy and image quality. Acquiring thin slices (<2-3 mm) without slice gaps using standard 2D multi-slice acquisitions results in either low signal-to-noise ratio or unreasonably long acquisition times, the latter not only inconvenient for the patient but also an increased risk of introduction of motion artefacts in the images.

Although still not optimal for all applications, we found several examinations to benefit from the use of optimized fast isotropic 3D acquisitions. Utilization of the SPACE sequence for therapy planning has increased the possibilities we have to delineate small tumors intended for treatment with high-dose radiotherapy. The sequence has shown to be very helpful in defining small benign as well as malignant brain tumors. At our clinic, these tumors are treated with stereotactic radiotherapy that involves a very narrow margin between the gross tumor volume and the planning target volume intended for treatment, which makes an exact tumor volume definition essential for successful treatment.

Further, we are in the initial stages of incorporating MRI in the workflow for brachytherapy for head-and-neck cancer patients. At our clinic, patients with cancer in the tongue and the base of tongue without nodal spread receive external radiotherapy combined with chemotherapy to the primary tumor site and to non-engaged lymph node sites. Some of the patients also receive an additional brachytherapy boost to the primary tumor site. The volume intended to receive the boost has been decided by the head-and-neck radio oncologist after a digital examination prior to brachy loop implantation. We have seen a great benefit of using a T1 3D SPACE MRI after the brachy loop implantation to reconstruct the loops and to verify that the tumor remnant is within reach of the radiotherapy. The possibility to reconstruct images in any arbitrary plane combined with the excellent image quality will increase the possibilities for us to offer patients a more exact treatment, sparing the salivary glands and mandibular bone. In conclusion, we are so far very satisfied with the SPACE sequence for several applications in radiation therapy and we see a great advantage of investing further optimization work to introduce the sequence in the treatment of other anatomical areas.

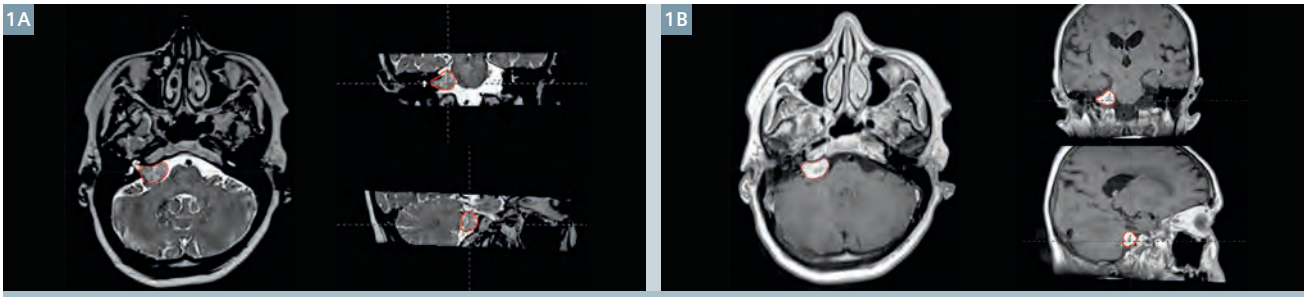

1 The gross tumor volume of a vestibular schwannoma on the T2-weighted SPACE **(1A)**, and T1-weighted contrast enhanced SPACE **(1B)**. The high (1 mm) and isotropic resolution of the SPACE sequence is highly beneficial for therapy planning of vestibular schwannoma as many schwanomma are as small as a few millimeters. The excellent image contrast on the T2-weighted SPACE may eliminate the need for contrast enhanced acquisitions.

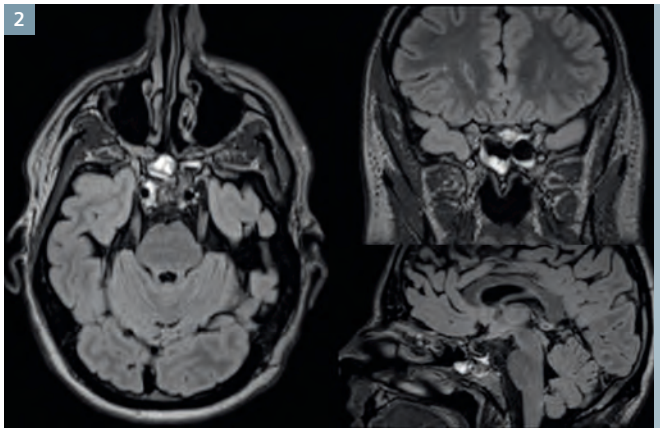

2 A patient diagnosed with a chordoma. Initial surgery was due to technical difficulties not completely radical and the patient will receive adjuvant radiotherapy to the remaining chordoma. Due to the close vicinity to the optical nerves it is extremely important to be able to define the exact volume of the tumor in order to minimize negative treatment effects of the radiotherapy. A T2-weighted SPACE dark fluid.

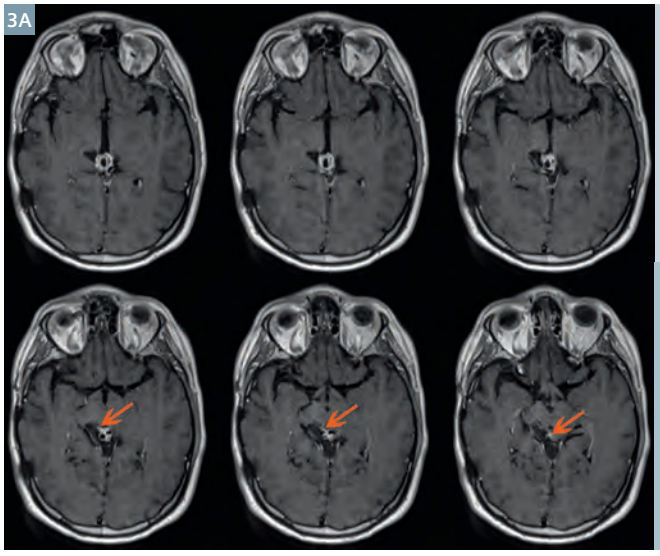

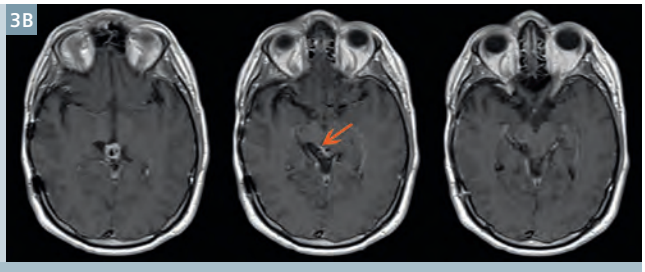

3 A patient who was diagnosed with a germinoma of the corpus pineale five years ago. He was initially treated with radio-chemotherapy and now shows a local recurrence. T1-weighted contrast-enhanced SPACE **(3A)** and standard T1-weighted contrast enhanced 2D TSE with a slice thickness of 3 mm **(3B)**. The standard 2D TSE was not sufficient to determine the extent of the recurrent tumor.

4 Dose distribution for a brachytherapy patient on a T1-weighted SPACE **(4A-C)**, and with an applicator reconstructed **(4D-E)**.

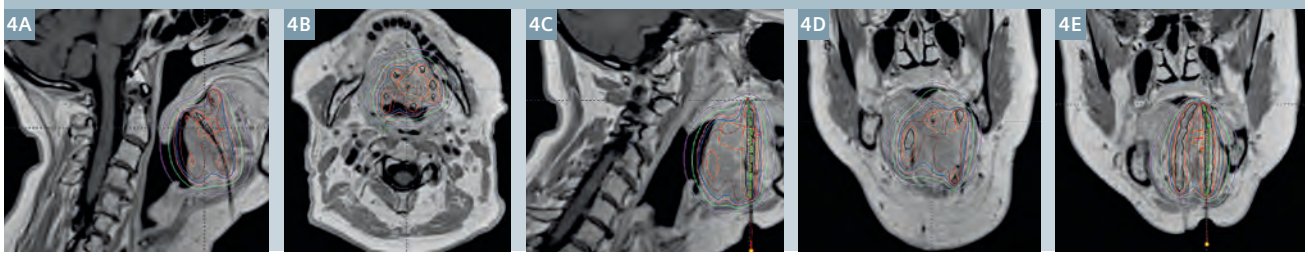

Contact

Karin Petruson, M.D., Ph.D.
Radiation Oncologist
Sahlgrenska University Hospital
Department of Oncology
Blå stråket 2
413 45 Gothenburg
Sweden
karin.petruson@vgregion.se

Contact

Maja Sohlin, Ph.D.
Medical Physicist
Sahlgrenska University Hospital
Medical Physics and Biomedical Engineering
Bruna stråket 13
413 45 Gothenburg
Sweden
maja.sohlin@vgregion.se

Anatomical and Functional MRI for Radiotherapy Planning of Head and Neck Cancers

Maria A. Schmidt, Ph.D.; Rafal Panek, Ph.D.; Erica Scurr, DCR(R), MSc; Angela Riddell, MD FRCS FRCR; Kate Newbold, MD MRCP FRCR; Dow-Mu Koh, MD MRCP FRCR; Martin O. Leach, Ph.D. FMedSci

Cancer Imaging Centre, Royal Marsden NHS Foundation Trust and Institute of Cancer Research, Sutton, UK

Introduction

Head and Neck cancers are relatively common: squamous cell carcinoma of the head and neck (SCCHN) has a worldwide incidence of approximately 500,000 cases per annum [1]. Treatment is a combination of surgery, chemotherapy and radiotherapy (RT), devised to maximize the probability of eradicating the disease while retaining organ function [2-5]. Recent technical advances in RT include high-precision conformal techniques such as intensity-modulated RT (IMRT) and volumetric intensity modulated arc therapy (VMAT), which enable dose escalation to lesions without exceeding recommended exposure levels for organs at risk (OAR). However, these techniques require accurate anatomical information to contribute towards improving disease control.

High-resolution Magnetic Resonance Imaging (MRI) has increasingly been used to plan Head and Neck RT [6-10]. MRI and CT images are registered, combining the advantageous soft tissue contrast of MRI examinations and the required CT-based electron density. However, MR images are often distorted due to magnetic field inhomogeneity and non-uniform gradients [11-13], and the use of CT-MR fusion requires geometrically accurate MRI datasets. This article describes the equipment, protocols and techniques used in Head and Neck MRI at the Royal Marsden NHS Foundation Trust to ensure that the MRI examinations undertaken for RT planning purposes achieve the required geometric accuracy.

1 Receiver coil arrangement used at the Royal Marsden NHS Foundation Trust to perform Head and Neck MRI for RT planning. A standard MR-compatible baseboard is employed, enabling the use of a thermoplastic mask. The large flex-coil is positioned above the neck and used in conjunction with elements of the spine array.

High resolution anatomical imaging in the radiotherapy planning position

At the Royal Marsden NHS Foundation Trust clinical Head and Neck MRI examinations for RT planning are undertaken at 1.5T in the 70 cm bore MAGNETOM Aera (Siemens Healthcare, Erlangen, Germany). Patients are scanned in the RT position using an appropriate head rest and thermoplastic shell immobilisation attached to an MR-compatible headboard, modified to remain accurately positioned on the Aera patient couch. In addition to the elements of the posterior spine coil selected at the level of the lesion, a large flex-coil is also placed anteriorly, in line with the tumor, employing a custom-built plastic device to keep the coil curved, following the neck anatomy. This arrangement achieves a high signal-to-noise ratio, allows effective use of parallel imaging and keeps patient comfort in the RT planning position (Fig. 1).

The MRI protocol covers the primary tumor and neck lymph nodes with approximately isotropic T1-weighted sagittal 3D acquisition (TE 1.8 ms, TR 880 ms, 160 x 1 mm slices, 250 mm x 250 mm FOV, 256 x 256 image matrix). Images are acquired post contrast-agent injection (single dose). This dataset is subsequently registered with the RT planning CT examination, and for this reason its geometric integrity is checked periodically with a large linear test object, previously described [14], consisting of sets of straight tubes in three

orthogonal directions. Figure 2 shows images of the test object without and with post processing to correct image distortion. The 3D distortion correction built into the scanner software is essential for RT planning, and always used. The maximum displacement found within the volume encompassed by head and neck examinations is less than 1 mm. In addition, the imaging protocol employs a 500 Hz/pixel bandwidth, ensuring chemical shift related displacements in the readout direction remain under 0.5 mm.

Having characterized the geometric integrity of the protocol employed, it is also essential to characterize any further distortion associated with the distribution of magnetic susceptibility values within the subjects. In Head and Neck a large number of air-tissue interfaces in the vicinity of the tumors gives rise to localized magnetic field inhomogeneity, detrimental to the geometric integrity of the images. For this purpose, the field inhomogeneity in this region was estimated in five Head and Neck subjects. Transaxial gradient-echo images were acquired with fat and water in phase (TE values 4.76 and 9.53 ms), and the phase images were subtracted. The local field inhomogeneity was measured after phase unwrapping. Displacements associated with the airways were mostly under 0.5 mm with this sequence. Displacements only reach 1 mm in the vicinity of dental implants, and only very few pixels are affected.

Functional imaging

In addition to the clinical service providing anatomical images for RT planning, functional MRI is also employed to characterize lesions pre and post treatment and to investigate prediction of treatment response both at 1.5T (MAGNETOM Aera) and 3T (MAGNETOM Skyra). In RT planning, the ultimate aim of functional imaging techniques is to identify radio-resistant disease and thus provide a biological target volume for dose boosting. Geometric accuracy is therefore essential to allow correct registration of functional MR images with anatomical MRI and CT datasets. In Head and Neck cancers, both diffusion-weighted imaging (DWI) and Dynamic Contrast-Enhanced (DCE) MRI have been explored [15-21].

Diffusion-weighted imaging with readout segmentation of long variable echo-trains (RESOLVE): EPI-based DWI is sensitive to the mobility of water molecules and to their environment. In cancer, cell proliferation is often associated with an increase in cell density and in extracellular space tortuosity. This leads to lower values of the Apparent Diffusion Coefficient (ADC), compared to healthy tissues [22-23]. ADC values have thus been used for tumor detection, prediction and assessment of treatment response.

EPI in regions adjacent to air-tissue interfaces is known to suffer from poor geometric integrity [24]. Because this affects Head and Neck studies, strategies to reduce the echo-train length were sought. In addition to parallel imaging, the RESOLVE technique was also employed to acquire multi-shot DWI using a navigator signal to enable accurate multi-echo combinations. In Head and Neck studies, DWI with RESOLVE was employed, covering the volume of interest to identify restricted diffusion within primary lesions and affected lymph nodes.

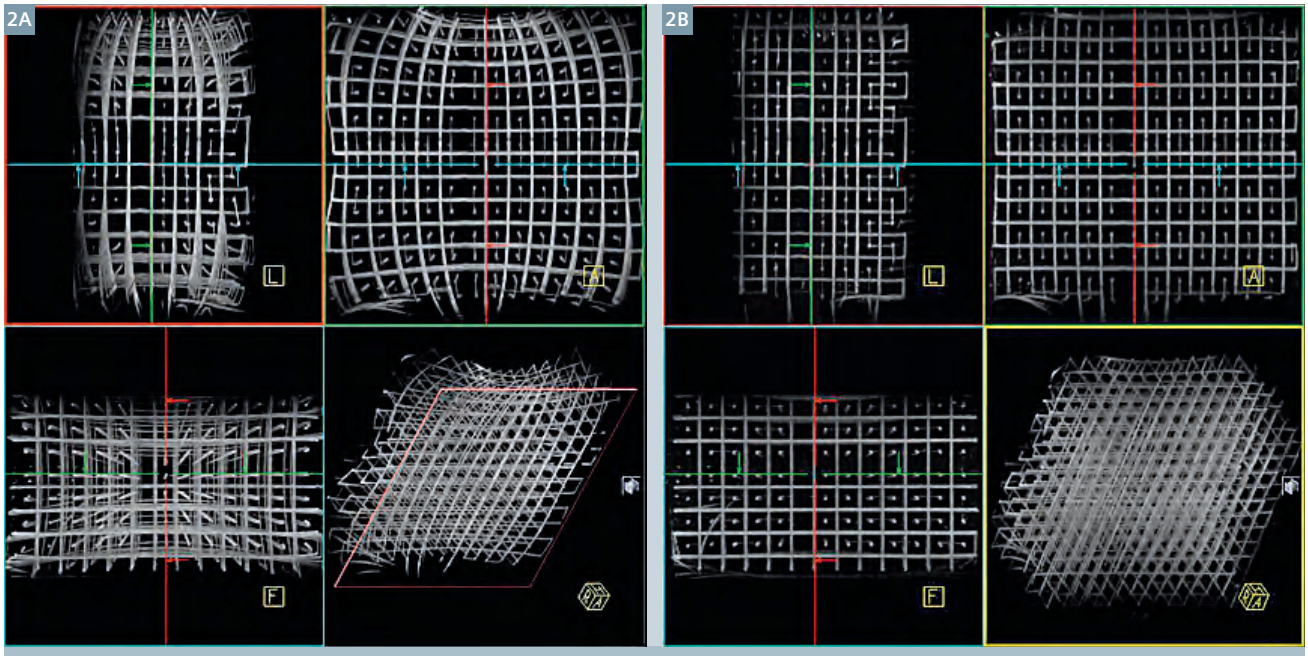

2 Images of the Linear Test Object (described by Doran et al. [14]) acquired using a 3D T1-weighted sequence with bandwidth 500 Hz/pixel, without distortion correction **(2A)** and with 3D distortion correction **(2B)**. Each picture shows three maximum intensity projections (sagittal, coronal and transaxial) and a 3D view of the test object.

3 A comparison of conventional single shot DWI **(3A)** and RESOLVE DWI **(3B)** in a head examination. The ADC calculated with the RESOLVE DWI **(3C)** retains the geometric integrity. Standard DWI parameters: TE 98 ms, TR 7000 ms, receiver bandwidth 1040 Hz/pixel, matrix 192 x 192, FOV 230 mm x 230 mm, 3 averages, slice thickness 4 mm. RESOLVE DWI parameters: TE 58 ms, TR 5700 ms, receiver bandwidth 950 Hz/pixel, matrix 128 x 128, FOV 240 mm x 240 mm, slice thickness 4 mm.

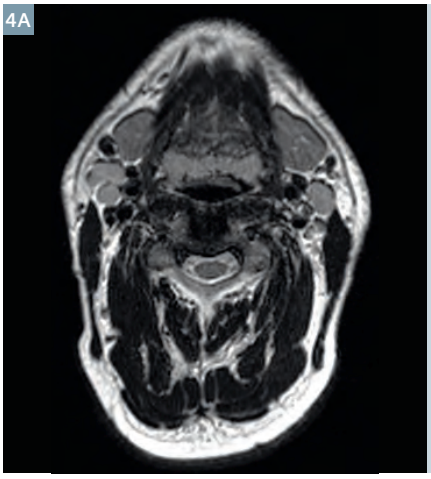

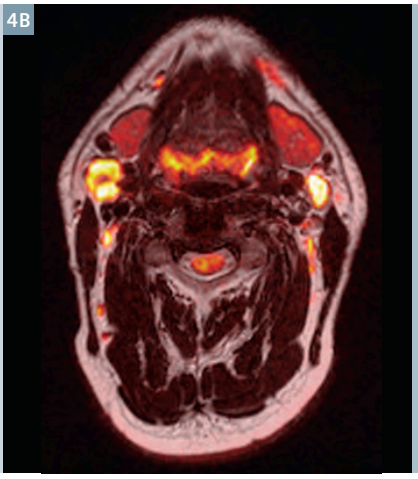

4 Head and Neck T2-weighted image **(4A)** with co-registered RESOLVE diffusion-weighted image **(4B)**. Restricted diffusion (high intensity) can be observed in nodes, spinal cord, tonsils and submandibular glands with no apparent geometrical distortion.

Figure 3 compares DWI acquired without and with the RESOLVE technique for a Head subject, in a slice comprising air spaces. The clear improvement in geometric integrity achieved with RESOLVE DWI allows the registration of anatomical and functional images, thus allowing the use of DWI in RT planning for Head and Neck cancers (Fig. 4).

Dynamic contrast-enhanced MRI with CAIPIRINHA-VIBE and TWIST view-sharing*:
In dynamic contrast-enhanced (DCE)-MRI a series of 3D T1-weighted images is acquired to monitor contrast-agent uptake following an intravenous injection of contrast-agent. Using reference images, this technique can be quantitative and provide a dynamic calculation of T1 for each voxel. This enables pharmacokinetic modelling, providing information on tumor microcirculation, vascularity, blood volume and vessel permeability [25, 26]. This quantitative approach to DCE requires high temporal resolution to maintain accuracy. However, this conflicts with the need for high spatial resolution in RT planning applications.

The combination of flex-coil and spine coil elements has been used for DCE employing TWIST view-sharing and CAIPIRINHA reconstruction to produce high resolution images (voxel size 2 mm isotropic x 44 slices, CAIPIRINHA parameters: 2x2) with 2.5 s temporal resolution (TWIST parameters: A = 33% B = 33%). An example of TWIST/CAIPIRINHA DCE with a generous superior/inferior coverage to include both primary site and local involved lymph nodes is shown in figure 5. Isotropic voxels allow for a good 3D delineation of a biological target volume. In addition, Dixon reconstruction of fat and water images also provides information on fat content within the imaged volume, which might be important in the context of tumor response to treatment. Figure 6 shows T1-weighted water-Dixon signal change after Gd injection for a given representative slice containing a primary tumour. Last frame shows K**trans** map within the region of interest.

* The product is still under development and not commercially available yet. Its future availability cannot be ensured.

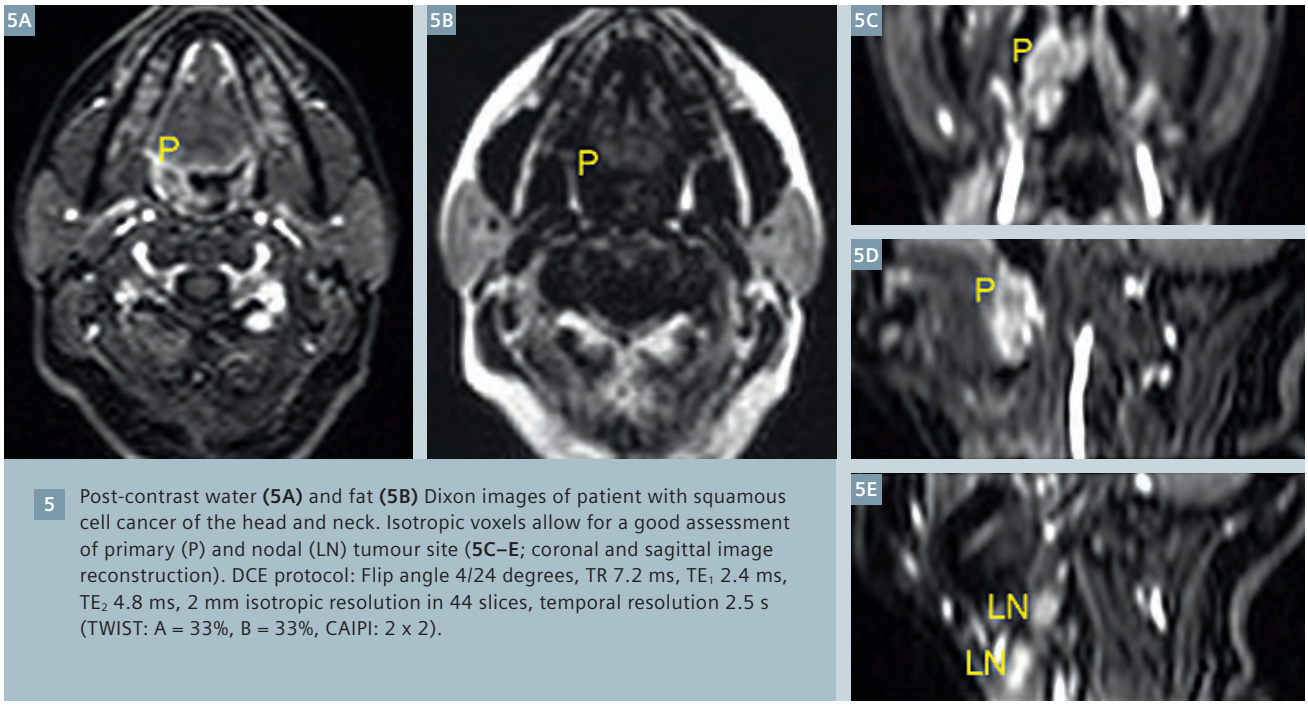

5 Post-contrast water **(5A)** and fat **(5B)** Dixon images of patient with squamous cell cancer of the head and neck. Isotropic voxels allow for a good assessment of primary (P) and nodal (LN) tumour site (**5C–E**; coronal and sagittal image reconstruction). DCE protocol: Flip angle 4/24 degrees, TR 7.2 ms, TE_1 2.4 ms, TE_2 4.8 ms, 2 mm isotropic resolution in 44 slices, temporal resolution 2.5 s (TWIST: A = 33%, B = 33%, CAIPI: 2 x 2).

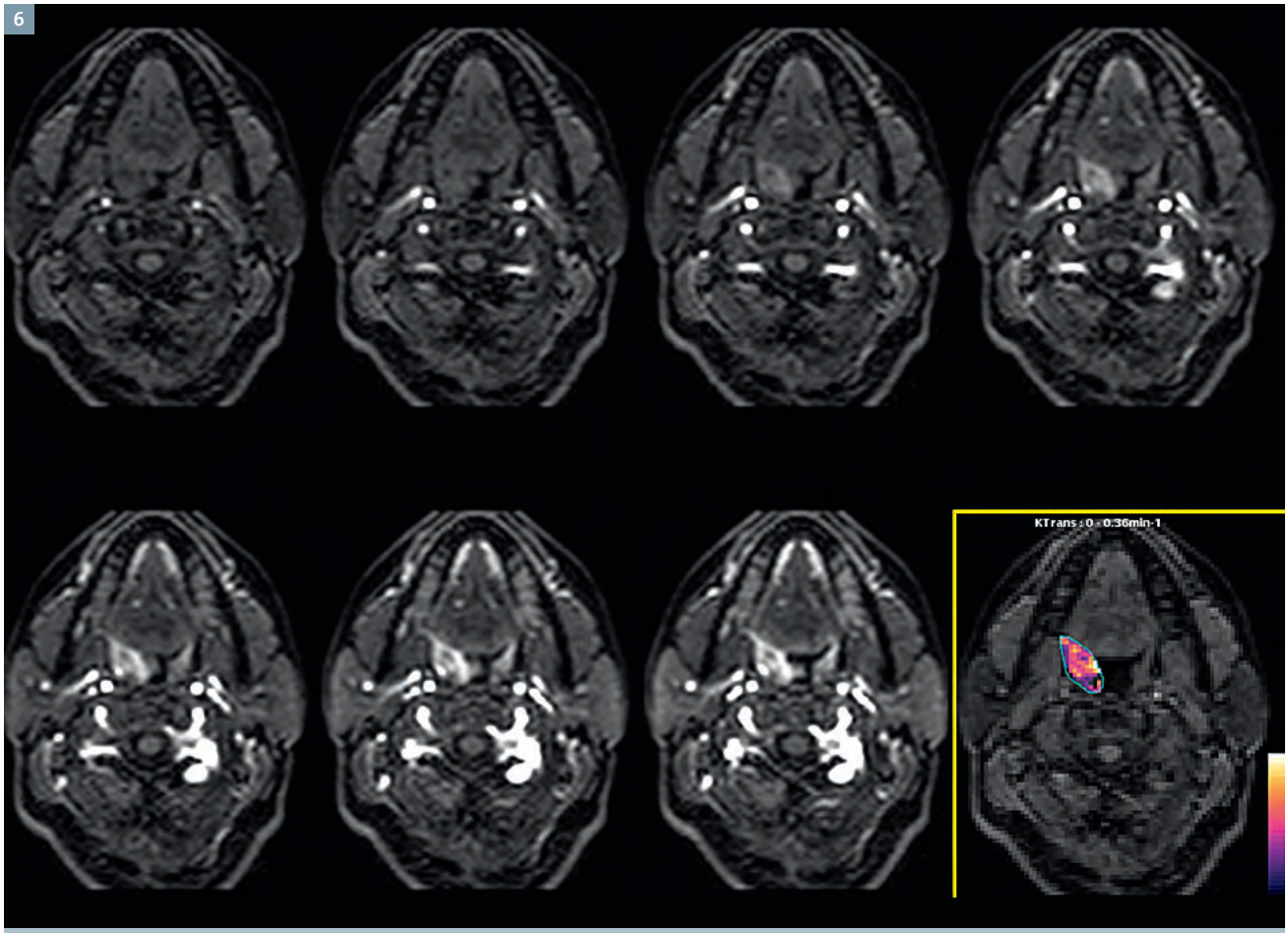

6 T1-weighted Dixon/water signal change after contrast agent injection, showing progressive enhancement and washout of Head and Neck cancer lesion. Last frame shows K**trans** for a region of interest over a primary tumor site.

Conclusion

Geometrically accurate anatomical and functional imaging for RT planning of Head and Neck cancers were acquired in the RT planning position in standard clinical scanners; this service was developed to meet the clinical and research needs of the users, using custom built coil positioning devices and test objects.

Acknowledgments

The authors wish to thank D. Nickel, R. Kroeker and P. Ravell (Siemens Healthcare) for the provision of the works-in-progress package WIP771 (VIBE with View Sharing TWIST). The authors acknowledge the support of CRUK and EPSRC to the Cancer Imaging Centre at ICR and RMH in association with MRC & Department of Health C1060/A10334, C1060/A16464 and NHS funding to the NIHR Biomedicine Research Centre and the Clinical Research Facility in Imaging. This work was also supported in part by Cancer Research UK Programme Grants C46/A10588 and C7224/A13407. MOL is an NIHR Senior Investigator.

Radiotherapy Planning where MR data is the only imaging information is ongoing research. The concepts and information presented in this article are based on research and are not commercially available. Its future availability cannot be ensured.

Contact

Dr. Maria A. Schmidt
MRI Unit
Royal Marsden NHS
Foundation Trust
Downs Rd
Sutton SM2 5PT
UK
Phone: +44 (0)20 8661 3353
maria.schmidt@icr.ac.uk

References

1 Parkin DM, Bray F, Ferlay J, Pisani P. Estimating the world cancer burden: Globocan 2000. International Journal of Cancer. 2001;94(2):153–6.
2 Bentzen SM, Trotti A. Evaluation of early and late toxicities in chemoradiation trials. J Clin Oncol 2007; 25:4096-4103.
3 Harrington KJ, et al. Interactions between ionising radiation and drugs in head and neck cancer: how can we maximise the therapeutic index? Curr Opin. Investig Drugs 2002; 3: 807-11.
4 Lefebvre JL, et al. Larynx preservation clinical trial design: key issues and recommendations - a consensus panel summary. Int J Radiat Oncol Bioi Phys. 2009; 73: 1293-303.
5 Kazi R, et al. Electroglottographic comparison of voice outcomes in patients with advanced laryngopharyngeal cancer treated by chemoradiotherapy or total laryngectomy. Int J Radiat Oncol Bioi Phys. 2008; 70: 344-52.
6 Ahmed M, Schmidt M, Sohaib A, Kong C, Burke K, Richardson C, Usher M, Brennan S, Riddell A, Davies M, Newbold K, Harrington KJ & Nutting CM. The value of magnetic resonance imaging in target volume delineation of base of tongue tumours – a study using flexible surface coils. Radiother Oncol 2010; 94, 161-7.
7 Bhide SA, Ahmed M, Barbachano Y, Newbold K, Harrington KJ & Nutting CM. Sequential induction chemotherapy followed by radical chemo-radiation in the treatment of locoregionally advanced head-and-neck cancer. Br J Cancer 2008; 99, 57-62.
8 Gregoire V et al. Radiotherapy for head and neck tumours in 2012 and beyond: conformal, tailored, and adaptive? Lancet Oncol. 2012; 13(7), pp.e292-300.
9 Nuyts S. Defining the target for radiotherapy of head and neck cancer. Cancer Imaging.2007;7(Special Issue A):S50–S55.
10 Newbold K, Partridge M, Cook G, Sohaib SA, Charles-Edwards E, Rhys-Evans P, et al. Advanced imaging applied to radiotherapy planning in head and neck cancer: a clinical review. Br J Radiol. 2006 Jul 1;79(943):554–61.
11 Wang D & Doddrell DM. Geometric distortion in structural magnetic resonance imaging. Current Medical Imaging Reviews 2005; 1: 49-60.
12 Wang H, Balter J & Cao Y. Patient-induced susceptibility effect on geometric distortion of clinical brain MRI for radiation treatment planning on a 3T scanner. Phys Med Biol. 2013; 58: 465-77.
13 Reinsberg SA, Doran SJ, Charles-Edwards EM & Leach MO. A complete distortion correction for MR images: II. Rectification of static-field inhomogeneities by similarity-based profile mapping. Phys Med Biol 2005; 50: 2651-61.
14 Doran SJ, Charles-Edwards L, Reinsberg SA & Leach MO. A complete distortion correction for MR images: I. Gradient warp correction. Phys Med Biol. 2005; 50: 1343-61.
15 Thoeny HC, de Keyzer F & King AD. Diffusion-weighted MR imaging in the head and neck. Radiology, 2012; 263(1): pp.19-32.
16 Vandecaveye, V. et al. Evaluation of the larynx for tumour recurrence by diffusion weighted MRI after radiotherapy: initial experience in four cases. The British Journal of Radiology 2006; 79: 681-687.
17 Sumi M, Sakihama N, Sumi T, Morikawa M, Uetani M, Kabasawa H, et al. Discrimination of metastatic cervical lymph nodes with diffusion-weighted MR imaging in patients with head and neck cancer. AJNR Am J Neuroradiol 2003; 24(8):1627-34.
18 Powell C, Schmidt M, Borri M, Koh DM, Partridge M, Riddell A, Cook G, Bhide S A, Nutting CM, Harrington KJ & Newbold KL. Changes in functional imaging parameters following induction chemotherapy have important implications for individualised patient-based treatment regimens for advanced head and neck cancer. Radiother Oncol. 2013; 106, 112-
19 Quon H, Brizel DM. Predictive and prognostic role of functional imaging of head and neck squamous cell carcinomas. Semin Radiat Oncol. 2012 Jul; 22(3):220–32.
20 Wang P, Popovtzer A, Eisbruch A, Cao Y. An approach to identify, from DCE MRI, significant subvolumes of tumours related to outcomes in advanced head-and-neck cancer. Medical Physics. 2012; 39(8):5277–85.
21 Srinivasan A, Mohan S & Mukherji SK. Biological imaging of head and neck cancer: the present and the future. AJNR Am J Neuroradiol. 2012; 33(4), pp. 1-9.
22 Padhani et al. Diffusion-Weighted Magnetic Resonance Imaging as a Cancer Biomarker: Consensus and Recommendations, Neoplasia 2009; 11(2):102-125.
23 Galbán CJ et al. The parametric response map is an imaging biomarker for early cancer treatment outcome. Nature medicine, 2009;15(5): pp.572-6.
24 Jezzard P. Correction of geometric distortion in fMRI data. Neuroimage 2012; 62: 648-51.
25 Walker-Samuel S, Leach MO, Collins DJ. Evaluation of response to treatment using DCE-MRI: the relationship between initial area under the gadolinium curve (IAUGC) and quantitative pharmacokinetic analysis. Phys Med Biol. 2006 Jul 21; 51(14):3593–602.
26 O'Connor J P B, Jackson A , Parker G J M and Jayson G C. DCE-MRI biomarkers in the clinical evaluation of antiangiogenic and vascular disrupting agents. British Journal of Cancer 2007; 96: 189–195. doi:10.1038/sj.bjc.6603515.

Clinical Application of Diffusion Tensor Imaging in Radiation Planning for Brain Tumors

S. Rogers[1]; S. Bodis[1]; G. Lutters[1]; L. Remonda[2]; J Berberat[1, 2]

[1]Radiation Oncology, Canton Hospital, Aarau, Switzerland
[2]Neuro-radiology, Canton Hospital, Aarau, Switzerland

Malignant brain tumors (glioma WHO grade III-IV) are notoriously difficult to treat despite an intensive combination of surgery, radiation and chemotherapy. Although there is an increasing number of 5-year survivors with this combined modality therapy, the median survival remains in the order of 14 months [1]. Pathological studies have demonstrated preferential tumor cell dissemination spread along white matter tracts and brain vessels [2], which limits the efficacy of both microsurgical resection and radiation therapy. The target for postoperative therapeutic radiation after maximal safe resection includes the resection cavity and any residual tumor visible on the postoperative T1-weighted Gadolinium-enhanced MRI. When surgery is not possible due to a high risk of neurological damage, a diagnostic biopsy is undertaken, followed by radiotherapy. To maximise the probability of including relevant microscopic spread from a glioblastoma (glioma WHO grade IV), uniform wide planning margins of up to 30 mm are typically added (Fig. 2B, green line). Some centres further extend this to include all visible edema on the T2-weighted imaging. Recent studies on the pattern of relapse in patients with high-grade glioma (HGG), predominantly glioblastoma, have suggested that tumor recurrence after maximal combined modality therapy occur within 2 cm of the original tumor location [3, 4]. This has led to a suggestion that a

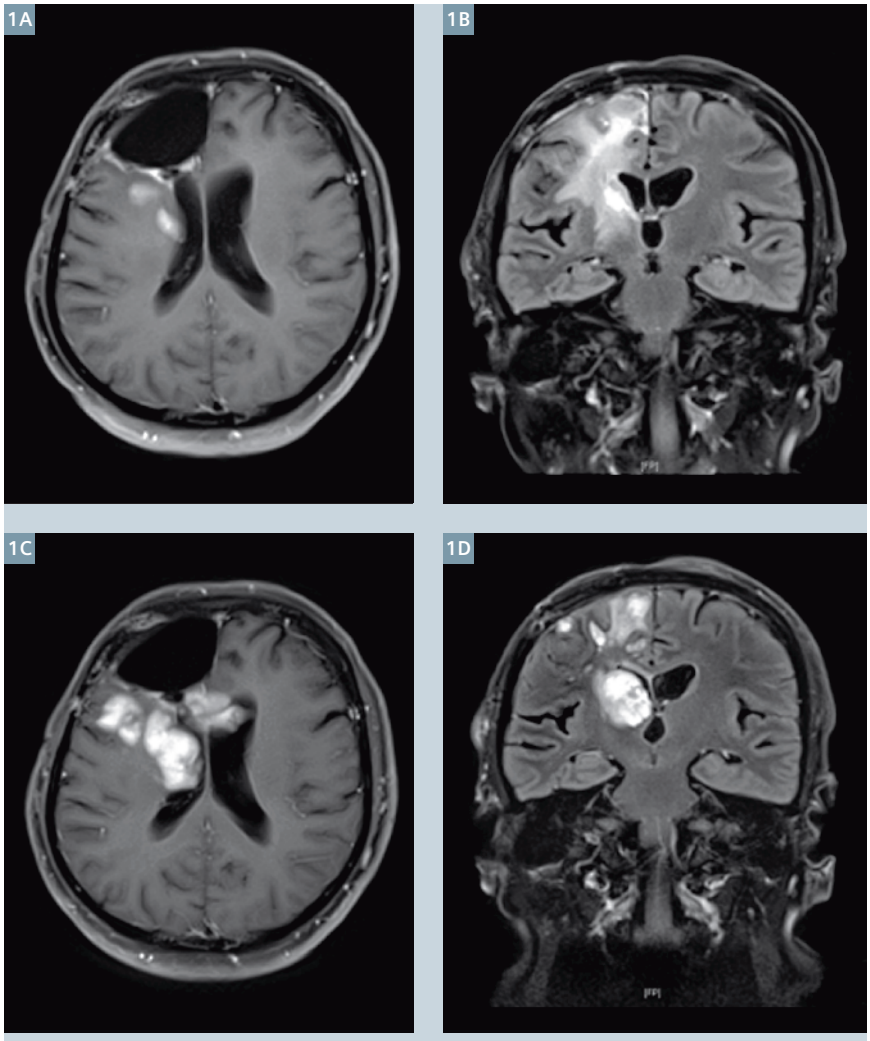

1 Transverse (T1w BLADE fs) and coronal (T2w TIRM dark fluid fs) MR images **(1A, B)** 12 months and **(1C, D)** 16 months after the operation. The patient developed a progressive tumor recurrence contiguous with residual tumor with subsequent extension along neighboring white matter tracts.

reduced margin, for example 1 cm, may be sufficient for the high-dose volume [3].

The addition of temozolomide chemotherapy as a radiation sensitizer and as adjuvant therapy is reported to be associated with an increased risk of normal brain toxicity (radionecrosis) of up to 20% [5]. Radiation-related side effects are dependent on both the prescription dose and the irradiated volume. A dose of at least 60 Gy has been shown to be necessary to control HGG, therefore it is compelling to instead reduce the planning target volume (PTV) where possible without compromising efficacy. Our aim is to derive a biologically targeted volume to ensure coverage of the regions at greatest risk of microscopic infiltration whilst excluding uninvolved brain. To this end, we have explored diffusion tensor imaging (DTI) and fractional anisotropy (FA) to identify areas of tumor infiltration, beyond that visible on T1w contrast-enhanced MRI. The method is derived from the isotropic (p) and anisotropic (q) maps of water diffusivity [6] and based on clinically validated data from patients with HGG [7].

Our technique is best illustrated using a clinical case as an example. This patient with histologically confirmed glioblastoma (GBM), showed tumor progression after surgery and radiation and developed a new lesion in the right thalamus (Fig. 1). The initial preoperative work-up included DTI to assist the neurosurgeons in the identification and avoidance of apparently uninvolved white matter tracts to minimize the neurological sequelae of the surgery. All the MR imaging was done using a MAGNETOM Avanto 1.5T whole body scanner (Siemens Healthcare, Erlangen, Germany). These same scans were further analysed to extract data

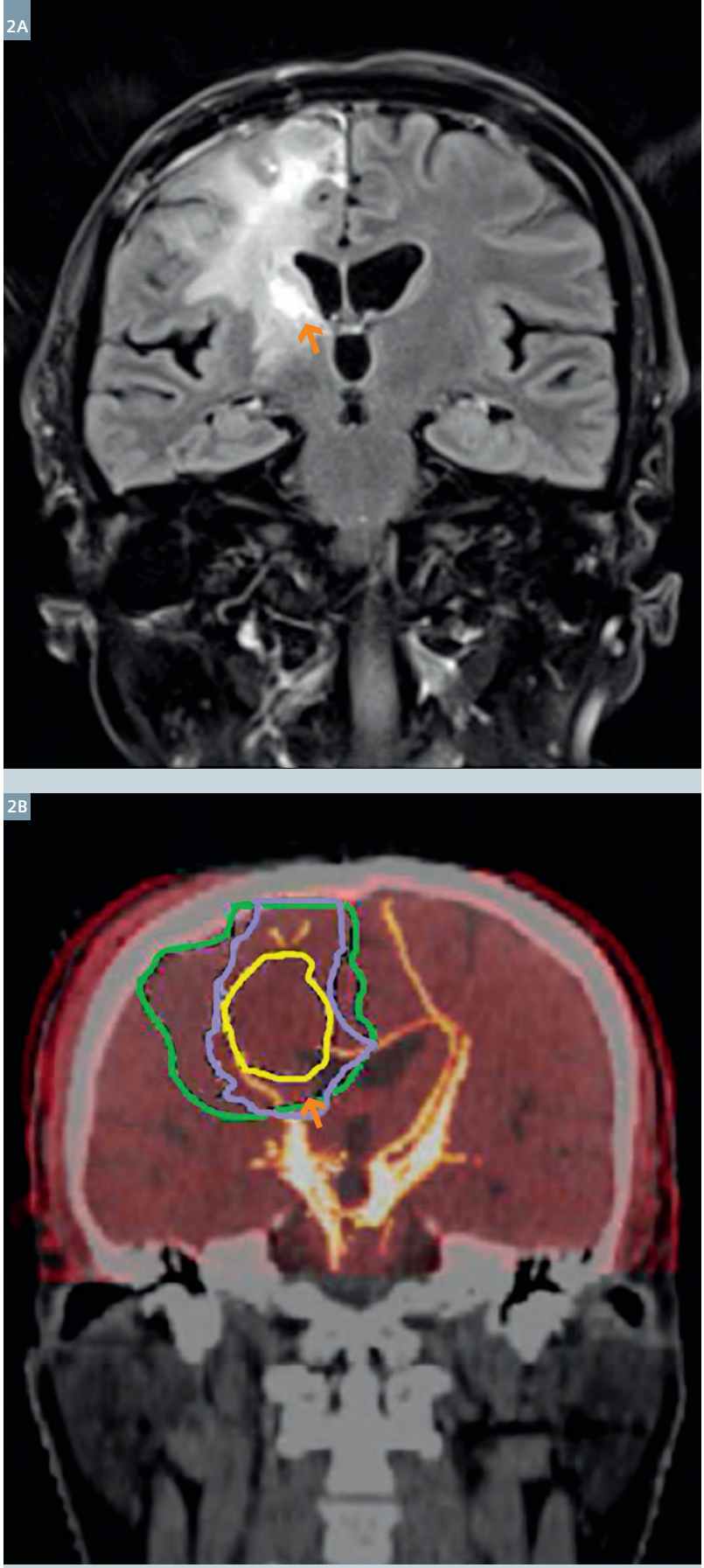

2 Fusion of the MRI at recurrence 12 months post op with the DTI at recurrence 12 months post op suggests a route of spread via the radiologically abnormal right corticospinal tract.

regarding water diffusivity. The initial steps of the radiation planning technique were to co-register the T1w contrast-enhanced MRI with the planning CT scan. The residual enhancing tumor was contoured accordingly and the volume expanded by 1 cm (Fig. 2B, yellow line) to include brain at highest risk of infiltration. In addition, the DTI scan was co-registered and the volume was extended further along the tracts (Fig. 2B, purple line) in contact with the tumor to encompass likely microscopic spread. Any additional regions of tumor and infiltration, as detected by the p and q maps, were delineated and then combined into the target volume by the planning software. This final volume was used to generate intensity modulated radiotherapy (IMRT) plans that were not used for clinical treatment (Fig. 2).

Using an in-house software program, we have developed a technique to incorporate regions of altered water diffusivity, reported to correspond with macroscopic tumor or microscopic infiltration, into the radiotherapy planning process. Conventional large volume irradiation for high-grade glioma carries an inevitable risk of neuro-toxicity, which may be enhanced by combination with radiosensitizers. DTI and FA have previously been reported as diagnostic tools to assist with differential diagnosis, tumor grading, identifying tumor margins and predicting tumor relapse [7-9]. As white matter tracts and alterations in water diffusivity can also be targeted, we believe that future developments in radiation planning for HGG should endeavour to reduce the irradiated volume whilst maintaining adequate coverage of such regions likely to mediate relapse and spread.

References

1 Stupp R, Hegi ME, Mason WP, van den Bent MJ, Taphoorn MJ, Janzer RC, Ludwin SK, Allgeier A, Fisher B, Belanger K, Hau P, Brandes AA, Gijtenbeek J, Marosi C, Vecht CJ, Mokhtari K, Wesseling P, Villa S, Eisenhauer E, Gorlia T, Weller M, Lacombe D, Cairncross JG, Mirimanoff RO; European Organisation for Research and Treatment of Cancer Brain Tumour and Radiation Oncology Groups; National Cancer Institute of Canada Clinical Trials Group. Effects of radiotherapy with concomitant and adjuvant temozolomide versus radiotherapy alone on survival in gliobastoma in a randomized phase III study: 5-year analysis if the EORTC-NCIC trial. Lancet Oncol. 2009 10(5):459-66.

2 Giese A, Westphal M. Glioma invasion in the central nervous system. Neurosurgery 1996 39(2):235-50.

3 McDonald MW, Shu HK, Curran WJ Jr, Crocker IR. Pattern of failure after limited margin radiotherapy and temozolomide for glioblastoma. Int J RadiatOncol-BiolPhys 2011 1;79(1):130-6.

4 Milano MT, Okunieff P, Donatello RS, Mohile NA, Sul J, Walter KA, Korones DN. Patterns and timing of recurrence after temozolomide-based chemoradiation for glioblastoma. Int J RadiatOncolBiol Phys. 2010 15;78(4):1147-55.

5 Rusthoven KE, Olsen C, Franklin W, KLeinschmidt-DeMasters BK, Kavanagh BD, Gaspar LE, Lillehei K, Waziri A, Damek DM, Chen C. Favorable prognosis in patients with high gradeglioma with radiation necrosis: the University of Colorado experience. Int J Radiat Oncol Biol Phys. 2011 1;81(1):211-7.

6 Basser PJ, Mattiello J, LeBihan D. Estimation of the effective self-diffusion tensor form the NMR spin echo. J MagnReson B 1994 103(3):247-54.

7 Price SJ, Jena R, Burnet NG, Hutchinson PJ, Dean AF,Peña A, Pickard JD, Carpenter TA, Gillard JH. Improved delineation of glioma margins and regions of infiltration with the use of diffusion tensor imaging: an image-guided biopsy study. AJNR Am J Neuroradiol 2006 27(9):1969-74.

8 Byrnes TJ, Barrick TR, Bell BA, Clark CA. Diffusion tensor imaging discriminates between glioblastoma and cerebral metastases in vivo. NMR Biomed 2011 24(1):54-60.

9 Mohsen LA, Shi V, Jena R, Gillard JH, Price SJ. Diffusion tensor invasive phenotypes can predict progression-free survival in glioblastomas. Br J Neurosurg 2013 27 [Epub ahead of print].

Contact

Jatta Berberat, Ph.D.
Canton Hospital
Tellstrasse
5001 Aarau
Switzerland
jatta.berberat@ksa.ch

MR-guided Gynecological High Dose Rate (HDR) Brachytherapy

Joann I. Prisciandaro[1]; James M. Balter[1]; Yue Cao[1]; Katherine Maturen[2]; Amir Owrangi[1]; Shruti Jolly[1]

[1] Department of Radiation Oncology, University of Michigan, Ann Arbor, MI, USA
[2] Department of Radiology, University of Michigan, Ann Arbor, MI, USA

Introduction

Brachytherapy is a form of radiation therapy that is delivered using sealed radioactive sources positioned in close proximity to tissues with cancer. The term derives from the Greek meaning short distance therapy. It is one of the original forms of radiation therapy, and emerged shortly after the discovery of radium in the early 1900's. Up until the 1990's, little had changed in the way brachytherapy treatments were planned and delivered. The nominal workflow consisted of the selection and *in vitro* placement of the appropriate applicator (a device that contains the radioactive source(s)), acquisition of 2D radiographic images to determine the position of the applicator and sources relative to the patient's anatomy, determination of the desired dose to the cancerous tissues and dose limits to neighboring normal tissues, and development of a treatment strategy to deliver the dose. The last two steps are iterative, as one tries to optimize the position and length of time the radioactive source(s) may reside in the applicator to deliver the highest possible dose to the defined region of interest, while minimizing dose to neighboring normal tissues. However, 2D imaging presents limitations to the development of an optimal treatment plan. Although radiographs provide sharp subject contrast and detail between objects with highly varying attenuation, such as bone and air, the limited differences in attenuation between different types of soft tissue make them difficult to discern (Fig. 1A). As a result, brachytherapy treatment plans have traditionally been designed to deliver the desired dose to a geometrically defined reference point relative to the applicator to which anatomic significance is attached. This approach limits the ability to individualize the patient's radiation to their specific tumor and normal tissues.

In the 1990's, as computed tomography (CT) and magnetic resonance imaging (MRI) became more widely available at clinics and hospitals, brachytherapy imaging began to transition from the use of planar to volumetric imaging. Unlike radiographs, volumetric images support some visualization of tumors and adjacent normal soft tissues (Figs. 1B, C). Compared to CT, MR images have the advantage of superior soft tissue resolution, and clear distinction of pelvic structures such as the uterus and cervix. Since local tumor control is strongly dependent on appropriately defined tumor volumes and the accurate delivery of radiation, the ability to visualize and delineate soft tissue is expected to improve target coverage and normal tissue sparing [1].

Beginning in 2000, GEC-ESTRO (the Groupe Européen de Curiethérapie – European SocieTy for Radiotherapy & Oncology) recognized the significance of volumetric imaging in the movement toward 3D treatment planning for gynecological diseases, namely cervical cancer, with the formation of the gynecological (GYN) GEC-ESTRO work group [1]. In the fourteen years

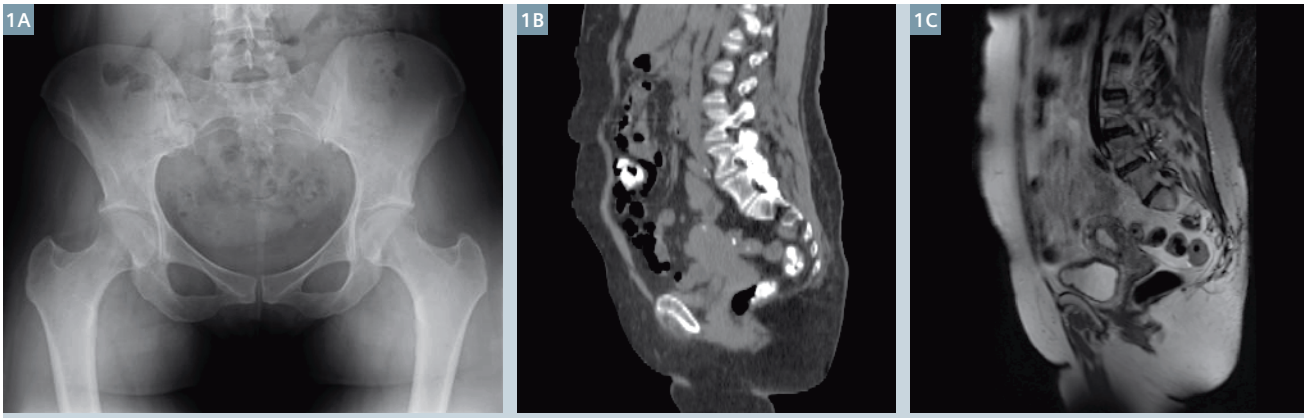

1 Example **(1A)** anterior pelvic radiograph [10], **(1B)** sagittal view of a pelvic CT simulation, and **(1C)** a sagittal reconstruction of a T2w 3D (SPACE) coronal image.

since its creation, the work group has released a series of recommendations to help standardize the approach to image-based brachytherapy treatment planning [1-4]. This has included the definition of a common language and means of delineating the target volumes (i.e., Low Risk-Clinical Target Volume (CTV), Intermediate Risk-CTV and High Risk-CTV for definitive treatment of cervix cancer), discussion on issues related to applicator reconstruction, and suggestions on the appropriate MR imaging sequences to utilize for treatment planning. Although these recommendations are helpful, there is a significant learning curve for each clinic during the clinical commissioning of MR-guided brachytherapy that is dependent on their specific MRI unit and brachytherapy applicators.

MR-simulator

In 2012, a 3T wide-bore MRI-simulator was installed in the department of Radiation Oncology at the University of Michigan (MAGNETOM Skyra, Siemens Healthcare, Erlangen, Germany). This unit was purchased for the express purpose of complementing, and at times, replacing CT treatment simulations, and has been outfitted with a laser marking system (LAP, Lueneburg, Germany) and detachable couch [5]. The couch supports imaging and treatment of brachytherapy patients, eliminating the need to transfer patients to other tables and the risk of inadvertently modifying the local geometry of the applicator and surrounding tissues. The brachytherapy suite is directly across the hall from the MRI-simulator, and an access door and path was built into the room design to permit wheeling the couch directly to the treatment suite following scanning.

Clinical commissioning

Prior to the clinical implementation of MR-guided brachytherapy, it is imperative to commission the process and workflow. Commissioning varies based on the desired treatment site, and involves the determination of the optimal imaging sequences for anatomical and applicator visualization. Care must be taken to ensure an MR conditional or compatible applicator is selected prior to the simulation. For treatment planning purposes, the images are imported into a software package (treatment planning system) that allows the user to identify the position of the applicator/potential source positions (a process known as applicator reconstruction) and the relevant patient anatomy. This software can then be used to optimize the length of time the radioactive source(s) should reside in various positions along the length of the applicator in order to deliver the desired dose and dose distribution to the patient. While the applicator, in particular the source channel (i.e., the hollow channel within the applicator where the source(s) may reside), is well-visualized in planar and CT imaging with the use of x-ray markers, this task is challenging with MRI. At present there are few MR markers that are commercially available to assist with applicator reconstruction. Additionally, the presence of the applicator, especially titanium applicators, produces image artifacts and distortions. Since dose calculations are dependent on the accurate definition of the applicator, namely the source position(s), relative to the patient's anatomy, geometrical uncertainties may result in dosimetric uncertainties to the target volume(s) and neighboring normal structures [3]. Thus, it is critical to evaluate these uncertainties prior to the clinical implementation of MR-guided brachytherapy.

2

Common brachytherapy applicators used for vaginal brachytherapy delivery, **(2A)** vaginal cylinder (Varian Medical Systems, Palo Alto, CA, USA) and **(2B)** ovoids (modified from the Fletcher Williamson Applicator Set, Nucletron/Elekta, Veenendaal, The Netherlands).

a. Vaginal high dose rate (HDR) brachytherapy

Clinically, vaginal brachytherapy is most often used in the adjuvant treatment of uterine cancer post hysterectomy to reduce the risk of cancer recurrence in the vagina. Vaginal brachytherapy can also be used for treatment of other gynecologic cancers, including cervix, primary vaginal and vulvar cancer as clinically indicated. The typical applicators used for the delivery of vaginal brachytherapy are the vaginal cylinder and ovoids [6] (see Fig. 2). A vaginal cylinder is typically a smooth, plastic cylinder with a dome shaped apex that is available in diameters ranging from approximately 2.0 – 4.0 cm, depending on the patient's anatomy. The applicator typically has a single, hollow channel that runs along the center of the device; however, multichannel variants are also available. Ovoids are hollow egg or cylinder-shaped capsules that are inserted into a patient's vagina and pressed up against the cervix if present or apex of the vaginal vault. Whereas the ovoids may be used to treat the upper

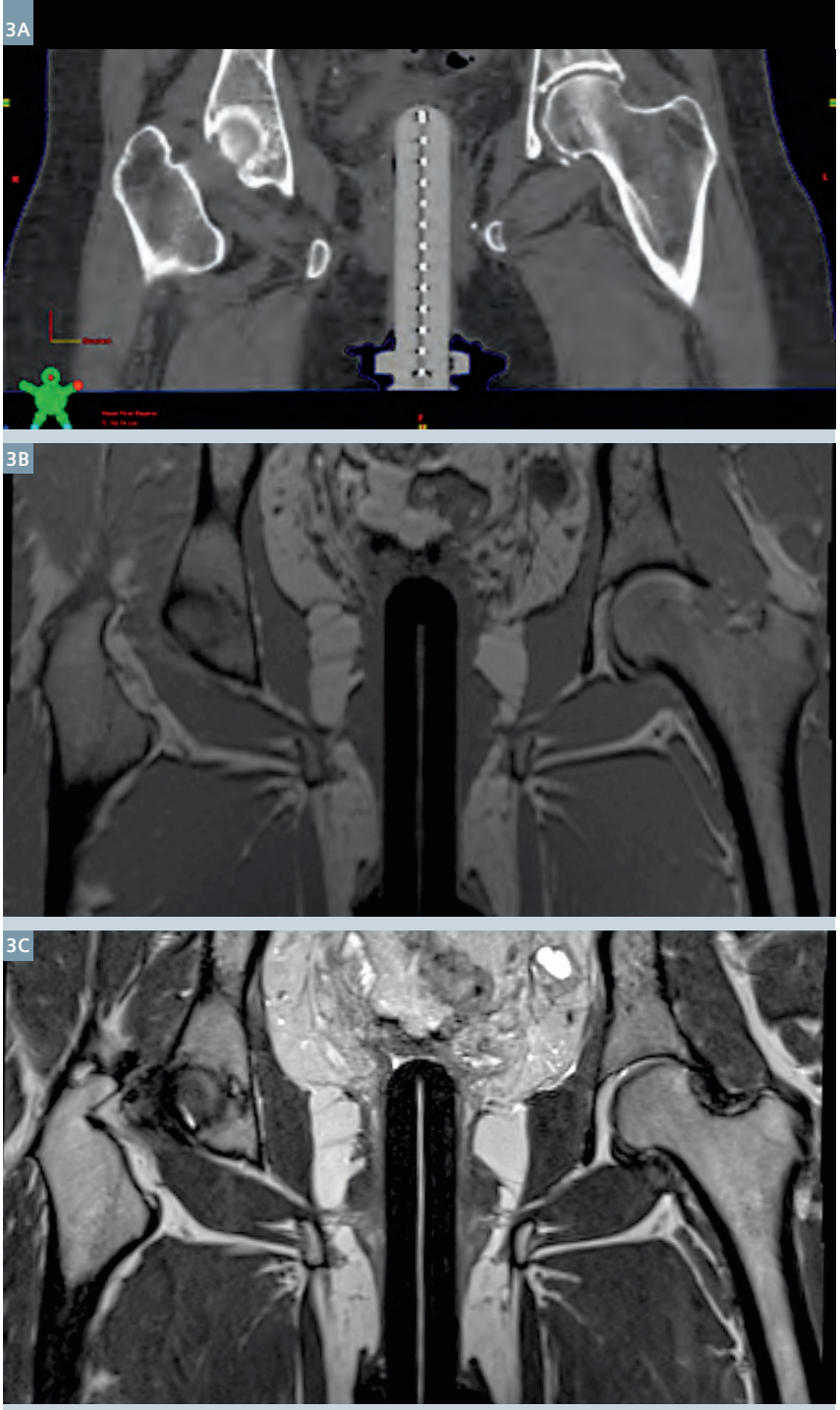

3 Coronal view of a patient with a vaginal cylinder on **(3A)** CT, **(3B)** 3D T1w (MPRAGE) MR, and **(3C)** 3D T2w (SPACE) MR. To assist with the visualization of the central source channel, the appropriate marker (x-ray for CT and contrast filled for MR) was inserted in the applicator prior to simulations.

portion of the vagina (known as the vaginal cuff), the vaginal cylinder offers the flexibility of treating the entire length of the vaginal vault [6].

During the clinical commissioning of MR-guided vaginal brachytherapy at the University of Michigan between August and September of 2013, three patients received a CT simulation preceding each HDR treatment with a Philips Brilliance CT scanner (Philips Medical, Chesterfield, MO, USA), followed by an MRI simulation using a Siemens MAGNETOM Skyra 3T scanner. The patients were positioned supine with their legs straight. The CT scan was acquired with a 1 mm slice thickness with an x-ray marker in place (see Figure 3A). The MRI was acquired with T1 and T2-weighted 3D imaging sequences. The following MRI sequences were used: 3D T2 (SPACE) coronal (FOV 320 × 320 × 176 mm, voxel size 0.94 × 0.94 × 1 mm, TR 1700 ms, TE 88 ms) and 3D T1 (MPRAGE) coronal (FOV 300 × 300 × 166.4 mm, voxel size 1.17 × 1.17 × 1.3 mm, TR 1900 ms, TE 2.35 ms, TI 900 ms, flip angle 9°). In order to identify the applicator channel, an MR marker was made in-house using a thin (0.046" outer diameter), hollow nylon tube (Best Medical International, Springfield, VA, USA) filled with gadolinium-doped water (T1 contrast) or either water or 0.2% Agarose Gel (T2 contrast), then sealed. Several different techniques were tested to seal the catheter ends including a heat seal with and without hot glue, bone wax with cyanoacrylate, and Water Weld™ with and without cyanoacrylate.

Although the applicator channel was easily visualized with the presence of the appropriate MR marker in both the T1w and T2w images as illustrated in Figures 3B and 3C, the applicator tip proved difficult to identify due to challenges in achieving a watertight seal. This resulted in observed displacements of the catheter tip, at times exceeding 1 cm. As such, an alternative method was investigated for applicator reconstruction using a solid model of the applicator available in the treatment planning software (BrachyVision 8.11, Varian Medical Systems, Palo Alto, CA, USA). Using T1w and/or T2w images, the solid model was aligned to the perimeter of the applicator (see Fig. 4). Deviations between the central source positions identified via aligning the applicator surface model to MR versus using the x-ray marker on CT to reconstruct the applicator (the conventional method) ranged from 0.07 – 0.19 cm and 0.07 – 0.20 cm for T1w and T2w images, respectively. Based on this study, vaginal brachytherapy patients at the University of Michigan now routinely undergo a single, T2w SPACE scan with approximately 1 mm isotropic voxel size. The applicator and related source positions for treatment planning are determined by alignment of the applicator model to the vaginal cylinder outline as observed on MRI.

b. Cervical HDR brachytherapy

While cervical cancer remains the most common gynecologic cancer worldwide, in the United States, the incidence of cervical cancer has decreased significantly since the widespread use of Papanicolaou (pap) smears in preventative care. Currently, approximately 12,000 new cases of cervical cancer are diagnosed per year. Treatment options are dependent on the stage of the disease upon clinical exam. Early stage cervical cancers are treated primarily by surgery. Occasionally, postoperative radiation or chemotherapy may be needed. When cervical tumors are not considered to be small enough to be removed by definitive hysterectomy, then curative or neoadjuvant radiation therapy with chemotherapy is the standard of care. In such situations, the patient undergoes combined external beam radiation with brachytherapy to provide high doses of radiation close to the tumor. Such treatments employ a variety of brachytherapy applicators. For most cases, the cervix can be treated using a combination of a tandem and ovoids, ring, or cylinder applicators [7]. However, when significant vaginal and/or parametrial involvement are present, then an interstitial brachytherapy implant may be needed to safely bring the required high doses of radiation to those areas.

At the University of Michigan, a plastic MR compatible ring and tandem applicator (GM11001220 and GM1100760, Varian Medical Systems, Palo Alto, CA, USA) has typically been used for HDR brachytherapy treatment of cervical cancer. This applicator system consists of an intrauterine catheter (tandem) and a circular, ring shaped device that allows the sealed source to be placed adjacent to the cervix (see Fig. 5A). During applicator commissioning which commenced in November 2013, 3D T2 (SPACE) sagittal images (FOV 300 × 300 × 79.2 mm, voxel size 0.94 × 0.94 × 0.9 mm, TR 1700 ms, TE 88 ms), 3D T1 (MPRAGE) sagittal images (FOV 300 × 300 × 79.2 mm, voxel size 1.17 × 1.17 × 0.9 mm, TR 1900 ms, TE 2.49 ms, TI 932 ms, flip angle 9°), and multi-planar 2D T2w images at 2–3 mm slice thickness, were acquired with in-house MR markers in each applicator. Although the

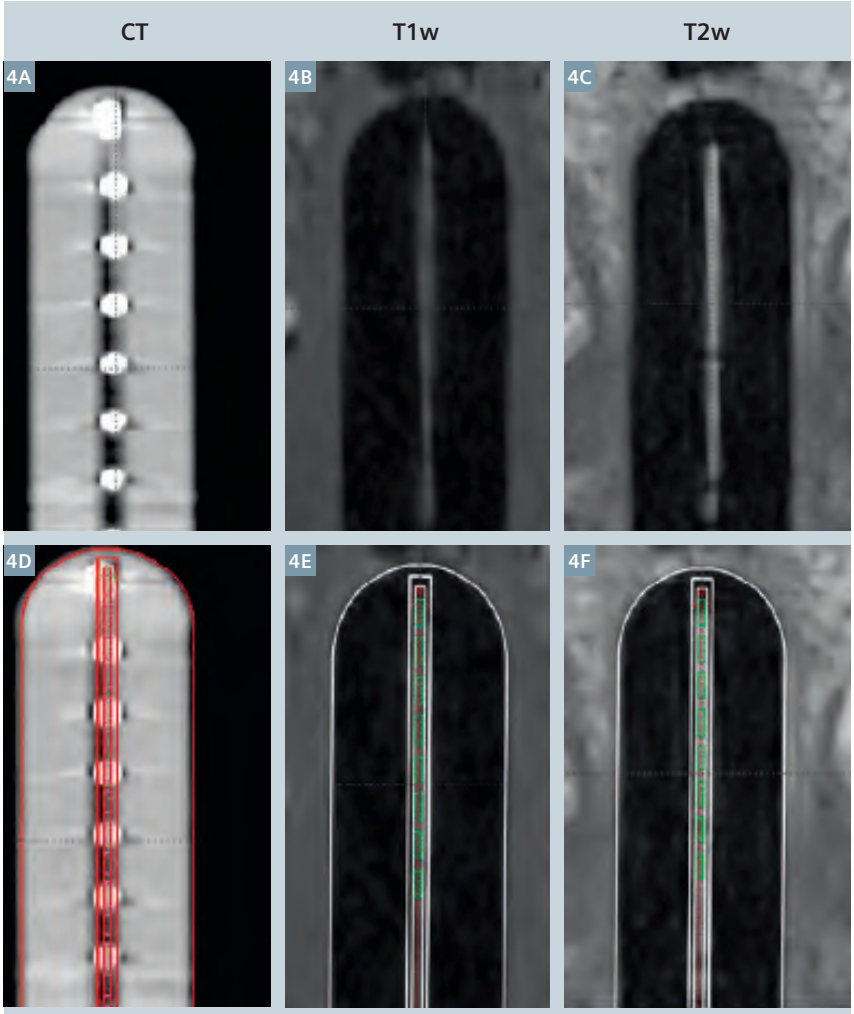

4 Para-coronal view of the vaginal cylinder on **(4A)** CT, **(4B)** 3D T1w (MPRAGE) MR, and **(4C)** 3D T2w (SPACE) MR. Following alignment, the overlay of the solid applicator model is depicted for each imaging set in **(4D–F)**.

5 The **(5A)** plastic and **(5B)** titanium ring and tandem applicator system used at the University of Michigan (Varian Medical Systems, Palo Alto, CA, USA).

The MRI restrictions (if any) of the metal implant must be considered prior to patient undergoing MRI exam. MR imaging of patients with metallic implants brings specific risks. However, certain implants are approved by the governing regulatory bodies to be MR conditionally safe. For such implants, the previously mentioned warning may not be applicable. Please contact the implant manufacturer for the specific conditional information. The conditions for MR safety are the responsibility of the implant manufacturer, not of Siemens.

tip of the tandem and ring was not visualized reproducibly due to the compromised seal of the MR markers, the source path and MR marker was discernable on the T1w images (see Fig. 6). As a result of the significantly higher acquisition time for the T2w versus T1w images (nearly twice the scan time), the source channel and MR markers were blurred due to patient and organ motion on the T2w images (see Fig. 6). To minimize scan time, multi-planar 2D T2w images as well as a 3D T1 (VIBE) sagittal scan with approximately 1 mm voxel size are acquired. Although the 2D T2w planar scans improve the quality of the resulting images, due to the large slice thickness of the 2D versus 3D MRI images, the MR marker was not visible on the 2D images. Therefore, 2D multi-planar T2w images as well as a small FOV 3D T2 (SPACE) sequence are acquired for soft tissue details, and 3D T1 (VIBE) sagittal images are acquired for applicator reconstruction. Prior to treatment planning, the registration of the T1w and T2w images is verified. If significant patient motion is observed, the images are manually registered in the treatment planning software.

Unlike the vaginal cylinder, a solid applicator model was not available in the treatment planning system for the utilized plastic ring and tandem system. As such, a user defined library plan and applicator model was developed based on the CT reconstruction of the applicator. When a new treatment planning simulation is acquired, the library plan is imported, and the

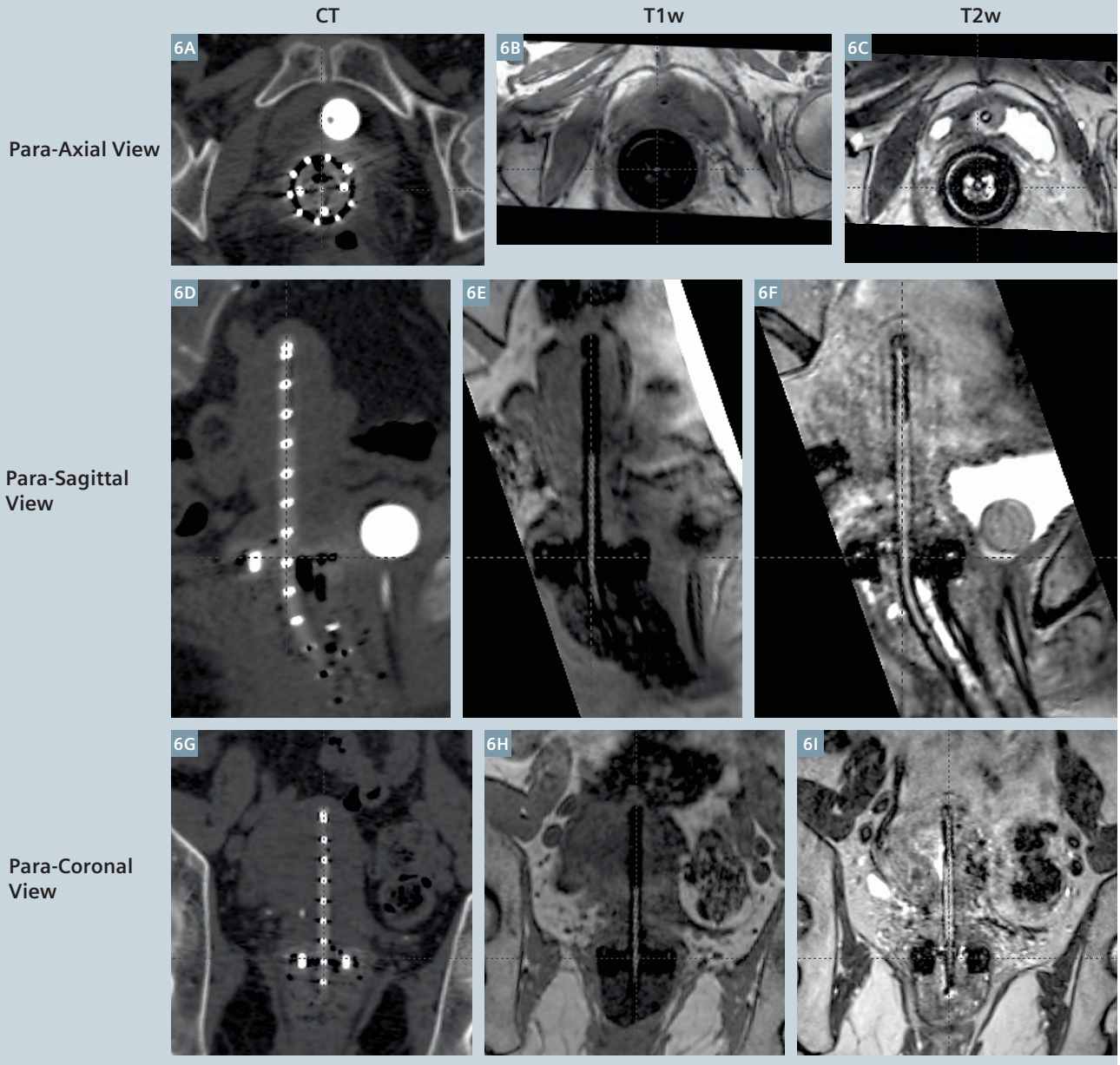

6 Comparison of CT, 3D T1w (MPRAGE), and 3D T2w (SPACE) images through the plastic ring and tandem system.

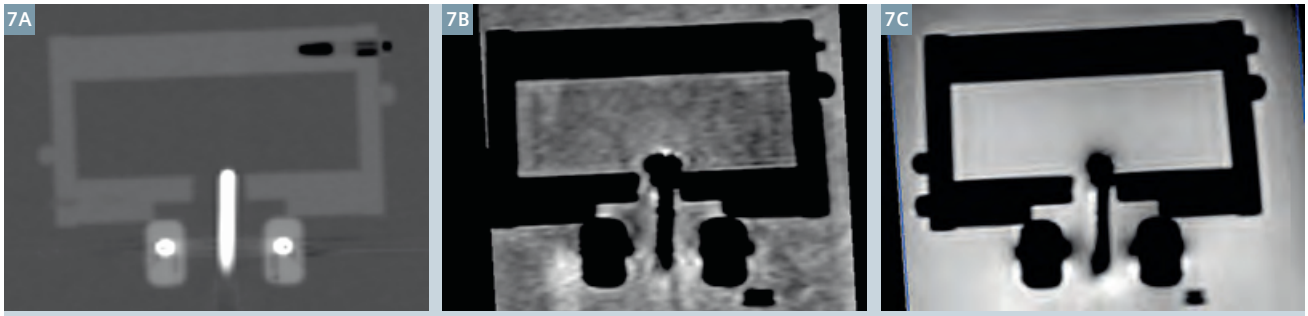

7 Comparison of **(7A)** CT, **(7B)** 3D T1w (MPRAGE), and **(7C)** 3D T2w (SPACE) sagittal images of the titanium ring and tandem system. The applicator set was scanned in a custom phantom designed to hold the applicator in a fixed position (based on [8, 9]). Prior to imaging, the phantom was filled with gadolinium-doped water. As compared to the CT image, magnetic susceptibility effects produce a mushroom effect off the tip of the tandem in the T1w and T2w images, resulting in uncertainties in the identification of the applicator tip on MRI.

applicator model is aligned based on the visible portions of the source channel, specifically focusing on the curvature of the tandem and/or ring.

Following a recent recall of the plastic ring and tandem system (PN BT-01366 Rev A, Varian Medical Systems, Palo Alto, CA, USA), a new titanium ring and tandem system (AL13017000, Varian Medical Systems, Palo Alto, CA, USA) has been purchased by the University of Michigan (see Fig. 5B). Due to susceptibility artifacts, the MR marker is not visible in the titanium applicator [8]. Additionally, these artifacts result in a mushroom effect off the tip of the applicator, making it challenging to accurately identify the applicator tip on MR (see Fig. 7). Kim *et al.* [9] have reported this effect to be considerably smaller when using a small slice thickness (i.e., 1 mm) T1w versus T2w MRI. With the recent arrival of the titanium ring and tandem system at our institution, the clinical commissioning of this applicator set is currently in progress.

Conclusions

MRI based image guided brachytherapy has the potential to significantly change the treatment planning process. Soft tissue contrast allows the user to customize treatment plans to accurately deliver therapeutic doses to the region-of-interest, while minimizing dose to the normal structures in the vicinity of the tumor, potentially resulting in fewer treatment-related complications. However, the transition from point to volume-based planning requires the user to perform a thorough set of commissioning tests to determine the geometric uncertainties related to their imaging and the associated dosimetric uncertainties.

References

1 Haie-Meder C, R. Potter, E. Van Limbergen et al., Recommendations from Gynaecological (GYN) GEC-ESTRO Working Group (I): concepts and terms in 3D image based 3D treatment planning in cervix cancer brachytherapy with emphasis on MRI assessment of GTV and CTV, Radiotherapy & Oncology, 2005;74:235-245.

2 R. Potter CH-M, E. Van Limbergen et al., Recommendations from gynaecological (GYN) GEC ESTRO working group (II): Concepts and terms in 3D image-based treatment planning in cervix cancer brachytherapy – 3D dose volume parameters and aspects of 3D image-based anatomy, radiation physics, radiobiology, Radiotherapy & Oncology, 2006;78:67-77.

3 Hellebust TP, C. Kirisits, D. Berger et al., Recommendations from Gynaecological (GYN) GEC-ESTRO Working Group: Considerations and pitfalls in commissioning and applicator reconstruction in 3D image-based treatment planning of cervix cancer brachytherapy, Radiotherapy & Oncology, 2010;96:153-160.

4 Dimopoulos JCA, P. Petrow, K. Tanderup et al., Recommendations from Gynaecological (GYN) GEC-ESTRO Working Group (IV): Basic principles and parameters for MR imaging within the frame of image based adaptive cervix cancer brachytherapy, Radiotherapy & Oncology, 2012;103: 113-122.

5 Balter J, Y. Cao, H. Wang et al., Optimizing MRI for Radiation Oncology: Initial Investigations, MAGNETOM Flash, 2013(April): 45-49.

6 Small W, S. Beriwal, D.J. Demanes et al., American Brachytherapy Society consensus guidelines for adjuvant vaginal cuff brachytherapy after hysterectomy, Brachytherapy, 2012;11:58-67.

7 Viswanathan AN, and B. Thomadsen, American Brachytherapy Society consensus guidelines for locally advanced carcinoma of the cervix. Part I: General principles, Brachytherapy, 2012;11:33 - 46.

8 Haack S, S.K. Nielsen, J.C. Lindegaard et al., Applicator reconstruction in MRI 3D image-based dose planning of brachytherapy for cervical cancer, Radiotherapy & Oncology, 2009;91:187-193.

9 Kim Y, M. Murugandandham, J. M Modrick et al., Evaluatin of artifacts and distortions of titanium applicators on 3.0-Tesla MRI: Feasibility of titanium applicators in MRI-guided brachytherapy for gynecological cancer, Int. J. Radiation Oncology Biol. Phys., 2011;80(3):947-955.

10 Jones, Jeremy. http://images.radiopaedia.org/images/16912/7bb87421cbd7be3955346f5c27ef93.jpg. Accessed June 29, 2014.

Contact

Joann I. Prisciandaro, Ph.D., FAAPM, Associate Professor
Dept. of Radiation Oncology
University of Michigan
Ann Arbor, MI
USA
Phone: +1 (734) 936-4309
joann@med.umich.edu

Joann Prisciandaro

Shruti Jolly

MRI-Guided HDR Brachytherapy for Prostate Cancer

Cynthia Ménard[1,2,3,4]; Peter Chung[1,4]; Anna Simenov[1]; Alejandro Berlin[1,4]; Alexandra Rink[1,3,4]; Warren Foltz[1,3,4]; David Jaffray[1,3,4]

[1] Radiation Medicine Program, Princess Margaret Cancer Centre, Toronto, ON, Canada
[2] Centre Hospitalier de l'Université de Montréal (CHUM), Montréal, QC, Canada
[3] Techna Institute, University Health Network,Toronto, ON, Canada
[4] Department of Radiation Oncology, University of Toronto, Toronto, ON, Canada

Introduction

Prostate brachytherapy, either as monotherapy or as a boost to external beam radiotherapy, can achieve unparalleled dose escalation, with doses (EQD2) upwards of 150 Gy when the dose gradient is taken into account [1]. As evidence mounts supporting the value of dose-escalation [2, 3], so has the adoption of high-dose-rate brachytherapy in clinical practice across the world.

Although trans-rectal ultrasound (TRUS) remains the standard-care interventional imaging modality for guidance of prostate brachytherapy, it falters in its depiction of implanted devices, such as brachytherapy needles, and/or catheters due to substantial echogenic artifact that degrades image quality as the implant progresses. It also fails in depicting regions of tumor burden that should be considered in the implant and treatment.

MRI is considered state-of-the-art for local tumor staging and visualization. A diagnostic acquisition protocol that includes high-resolution T2-weighted FSE and diffusion-weighted imaging (DWI) with or without dynamic imaging during IV contrast injection, can accurately identify regions of gross tumor burden (GTV) and the presence of gross extracapsular extension or seminal vesicle invasion (stage T3) [4].

The prostate gland is a flawed surrogate target for cancer as a target for brachytherapy, as cancer is neither defined nor confined to the boundaries of the prostate gland. The gross target volume (GTV) should be considered in planning and executing brachytherapy for prostate cancer, and in this regard, MRI prior to implantation is paramount. The introduction of MRI to augment or replace the TRUS workflow has logically progressed over the past decades. Here we present our current state-of-the-art approach to interventional MRI applied to HDR brachytherapy for prostate cancer.

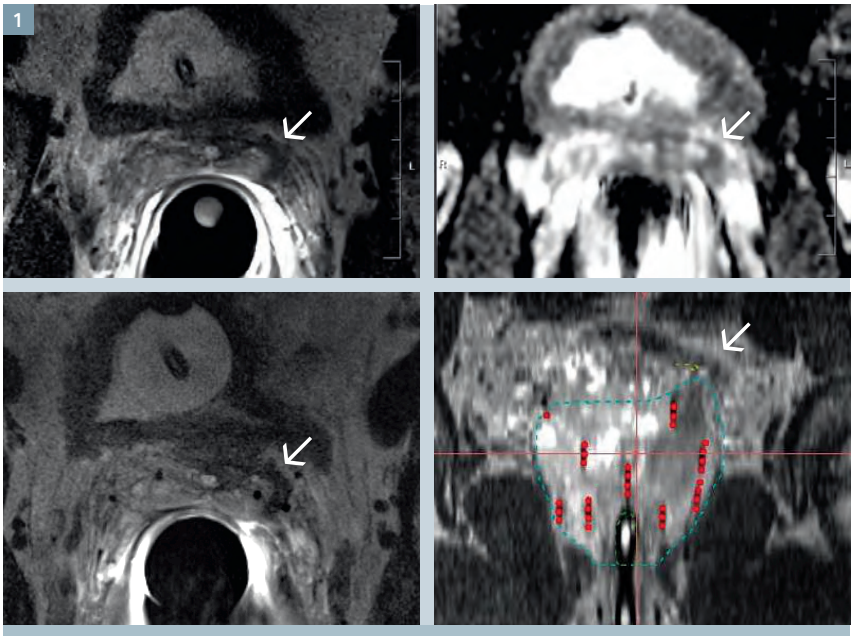

1 Patient with left seminal vesicle invasion (arrow). Catheters (signal void) are implanted deep and adjacent to extraprostatic disease (bottom), which can then be included in the target volume (turquoise) for HDR. brachytherapy.

Why MRI after catheter placement?

Dose plans in HDR brachytherapy are generated after catheter insertion in order to prescribe the time that the radioactive source spends at each pre-defined 'dwell' position. Dwell-time optimization is a powerful variable after catheter placement by which dose is focused on targets at risk while reducing exposures to nearby organs and structures at risk of injury, such as the rectum. By replacing standard TRUS or CT with MRI for treatment planning, depiction of anatomic boundaries relative to implanted catheters is vastly improved [5].

In the absence of commercial MRI markers, catheter signatures can be accentuated as signal voids in a high-resolution FSE image using an intermediate echo-time (TE) (Fig. 1),

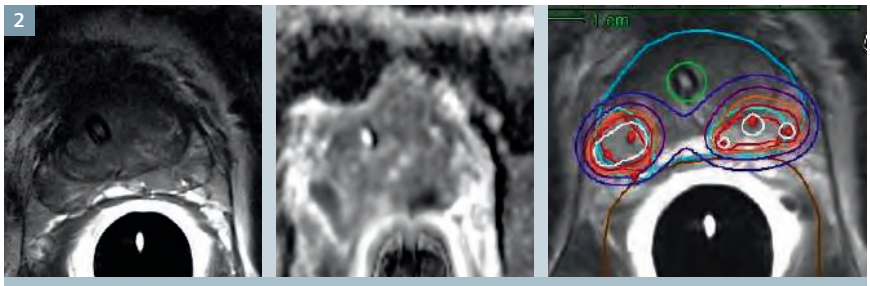

2 Patient with intermediate-risk prostate cancer and two gross target volumes in the right lateral peripheral zone, and left medial peripheral zone. Both targets are implanted for a boost to external bean radiotherapy in order to improve tumor control (isodose plan, right).

or by using a dual-echo FSE acquisition in order to acquire a proton-density-weighted (PD) image for device reconstruction, and a matched T2-weighted FSE image for anatomic delineation. Although this approach presents an improvement in accuracy of delineating the prostate gland, blurring of the apical boundary can occur due to acute needle trauma and bleeding. Depiction of gross tumor is also degraded by edema and bleeding compared with MRI prior to catheter insertion.

Why MRI before catheter placement?

MRI acquired prior to brachytherapy is most critical, whereby the appropriateness of the treatment is confirmed, and images cognitively 'fused' or considered during the implant to avoid marginal miss of gross tumor. This approach results in a change in treatment plan in a substantial proportion of patients, either through the addition of hormonal therapy, the addition of external beam radiotherapy, and/or modification of the implant itself by including sites of extraprostatic extension and/or seminal vesicle invasion [6] (Fig. 1). Sites of tumor burden can also be considered when trading off target coverage and dose to adjacent organs at risk, such that undercoverage is permitted only in regions that do not harbor gross tumor.

The next step is to differentially dose escalate visible tumor, and potentially de-escalate dose to microscopically involved prostate gland tissues distant to the GTV. A number of publications, predominantly in HDR applications, have demonstrated ease of escalating dose to tumors without incurring elevated dose to organs-at-risk (OARs) [7]. We await results of prospective trials to better ascertain the relative gain in effectiveness with this approach. It remains that the success or failure of tumor boost and/or focal-only therapies hinge on highly accurate techniques (Fig. 2). Sources of error and uncertainty introduced with MRI-TRUS registration remain to be addressed.

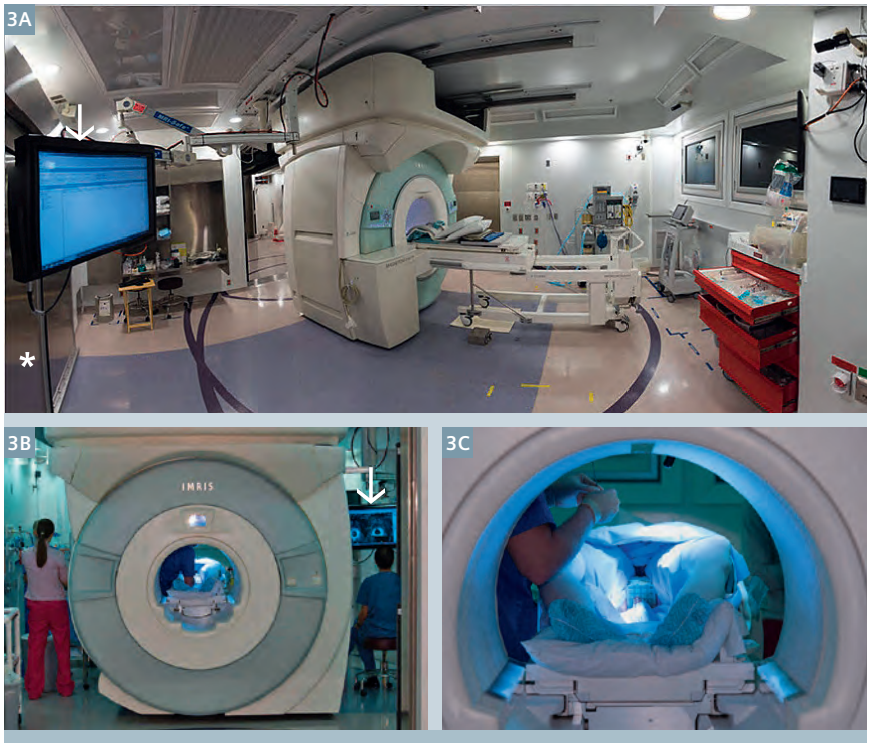

3 MRgBT suite at the Princess Margaret in Toronto. A 1.5T MRI scanner on rails is brought into the brachytherapy suite. Equipment that is not MRI safe (including HDR afterloader) is stored behind RF doors **(3A, see ✱)**. Brachytherapy catheters are inserted stereotactically with patient in frog-leg fashion using a positioning system and endorectal coil (Sentinel Endocoil Array), and a custom perineal template. In-room navigation display **(3A and 3B, arrow)** improves workflow.

Why an MRI-only prostate brachytherapy workflow?

An MRI-only workflow permits MRI to be acquired prior to and during catheter insertion to aid in implant guidance, and after catheter insertion for MRI-based treatment planning. In this manner, registration errors are largely circumvented. The requirement for a separate visit for a diagnostic MRI prior to brachytherapy is also removed. We demonstrate our installation that integrates an MRI scanner (1.5T MAGNETOM Espree, Siemens Healthcare) with the HDR delivery (Elekta MicroSelectron HDR) suite, removing the need for patient transfer between treatment-planning MRI and delivery of HDR brachytherapy dose [8] (Fig. 3). Errors due to motion or swelling are

thereby further mitigated, and imaging immediately after (or during) delivery can confirm delivered (in contrast to planned) dose.

The Interventional MRI procedure

Patients are placed in frog-leg on a patient positioning system atop the diagnostic table. An endorectal coil (Sentinelle Endocoil Array, Siemens Healthcare) is secured and fixed perpendicular to a custom perineal template. The perineum is prepped and draped with patients under general anesthesia (continuous infusion propofol). Diagnostic imaging ensues with the devices registered in MRI space for stereotactic targeting. For catheter insertion, the table is withdrawn, and needles inserted based on navigation software (Aegies, Hologic Inc.). The table is translated to isocenter for imaging verification every 1-3 catheters until the implant is complete. High-resolution images are then acquired for treatment planning of HDR brachytherapy. During treatment planning, the table is undocked, and the magnet driven out of the shielded brachytherapy suite. Once MRI safe, doors to the equipment room can be opened and the HDR afterloader can be connected to the catheters. Delivery proceeds with the patient under anesthesia, and all staff outside the treatment room. After radiation is delivered, catheters are removed and the patient is recovered. The overall procedure time is approximately 2 hours.

The imaging protocol includes diagnostic T2w TSE (TE: 103 ms; TR 5280 ms; 20 x 20 cm FOV with 320 x 320 matrix for 0.6 mm in-plane resolution; 2 mm slice thickness; 40 slices for 80 mm coverage; R/L phase encoding with 100% phase oversampling; iPAT factor 2; 200 Hz/pixel readout bandwidth; turbo factor 25; 2 averages; scan time 4 min 47 sec), and diagnostic DWI (TE 100 ms; TR 4000 ms; 20 x 20 cm FOV with 128 x 128 matrix for 1.6 mm in-plane resolution; A/P phase-encoding with 30% phase oversampling and 6/8 phase partial fourier; 3 mm slice thickness; 10 slices for 30 mm coverage; iPAT factor 2; 1148 Hz/pixel readout bandwidth; fat saturation; isotropic diffusion sampling; 4 b-values of 0, 100, 600, 1000 s/mm²; 8 averages; scan time 5 min 34 sec). The transperinal template is also imaged for registration and navigation (TE 95 ms; TR 2000 ms; 18 x 18 cm FOV with 256 x 256 matrix for 0.7 mm in-plane resolution; A/P phase-encoding with 50% phase oversampling; 4 mm slice thickness; 5 slices for 20 mm coverage; iPAT factor 2; 199 Hz/pixel readout bandwidth; turbo factor 25; 3 averages; scan time 1 min 42 sec). Needle position is verified using short TSE imaging (TE 11 ms; TR 1300 ms; 20 x 20 cm FOV with 256 x 256 matrix for 1.0 x 0.8 mm in-plane resolution; R/L phase encode with 100% phase oversampling; 3 mm slice thickness; 14 slices for 42 mm coverage; iPAT factor 2; 190 Hz/pixel readout bandwidth; turbo factor 10; 1 average scan time 31 sec). Finally, images are acquired for treatment planning once catheters are locked in placed. (Axial TSE: TE 108 ms; TR 5760 ms; 18 x 18 cm FOV with 320 x 320 matrix for 0.6 mm in-plane resolution; R/L phase encoding; with 80% phase oversampling; 2 mm slice thickness; 46 slices for 92 mm coverage; 200 Hz/pixel readout bandwidth; turbo factor 20; 3 averages; scan time 8 min 51 sec).

References

1 Hannoun-Levi, J.M., et al., Dose gradient impact on equivalent dose at 2 Gy for high dose rate interstitial brachytherapy. J Contemp Brachytherapy, 2012. 4(1): p. 14-20.

2 Kuban, D.A., et al., Long-term failure patterns and survival in a randomized dose-escalation trial for prostate cancer. Who dies of disease? Int J Radiat Oncol Biol Phys, 2011. 79(5): p. 1310-7.

3 Hoskin, P.J., et al., Randomised trial of external beam radiotherapy alone or combined with high-dose-rate brachytherapy boost for localised prostate cancer. Radiother Oncol, 2012. 103(2): p. 217-22.

4 Weinreb, J.C., et al., PI-RADS Prostate Imaging - Reporting and Data System: 2015, Version 2. Eur Urol, 2016. 69(1): p. 16-40.

5 Menard, C., et al., MRI-guided HDR prostate brachytherapy in standard 1.5T scanner. Int J Radiat Oncol Biol Phys, 2004. 59(5): p. 1414-23.

6 Murgic, J., et al., Lessons learned using an MRI-only workflow during high-dose-rate brachytherapy for prostate cancer. Brachytherapy, 2016.

7 Bauman, G.H., M., van de Heide, U., Menard, C., Boosting of Dominant Prostate Tumors: A Systematic Review. Radiother Oncol, 2013. 107(3): p. 274-81.

8 Menard, C., et al., MR-guided prostate biopsy for planning of focal salvage after radiation therapy. Radiology, 2015. 274(1): p. 181-91.

Contact

Cynthia Ménard, M.D., FRCPC
Centre hospitalier de l'Université de Montréal
Cancer Clinical Research Unit (CCRU)
Princess Margaret Cancer Centre
1560 Sherbrooke St E
Montréal, QC
Canada, H2L 4M1
cynthia.menard@umontreal.ca

Whole Body Diffusion-Weighted MRI for Bone Marrow Tumor Detection

Heminder Sokhi, MBCHB, MRCS, FRCR; Anwar R. Padhani, MB BS, FRCP, FRCR

Paul Strickland Scanner Centre, Mount Vernon Cancer Centre, Northwood, Middlesex, UK

Background

Recent years have seen the evolution of body diffusion-weighted MRI (DWI) into an exciting, whole body (WB-DWI) imaging technique with a distinct clinical utility, particularly in the context of cancer imaging [1-3]. It is clear that, with its excellent sensitivity for detecting marrow infiltration and good spatial resolution, WB-DWI has the capability of providing functional information which complements conventional anatomic MRI methods. At our institution, we use WB-DWI principally for evaluation of bone marrow metastases, both for detection and for evaluating disease response to therapy, where we have found particular utility for multiple myeloma, breast and prostate cancer. The technique is particularly useful when there is a need to minimize radiation exposure for serial evaluation of younger patients, pregnant women with cancer and in those in whom intravenous contrast medium is contraindicated (allergy or impaired renal function). This article focuses on the technique for Siemens systems, common artifacts encountered in clinical practice, and alludes to its clinical utility regarding skeletal metastases detection. We do not discuss response assessment of malignant bone marrow disease in any detail but there are clear strengths in this regard also [2].

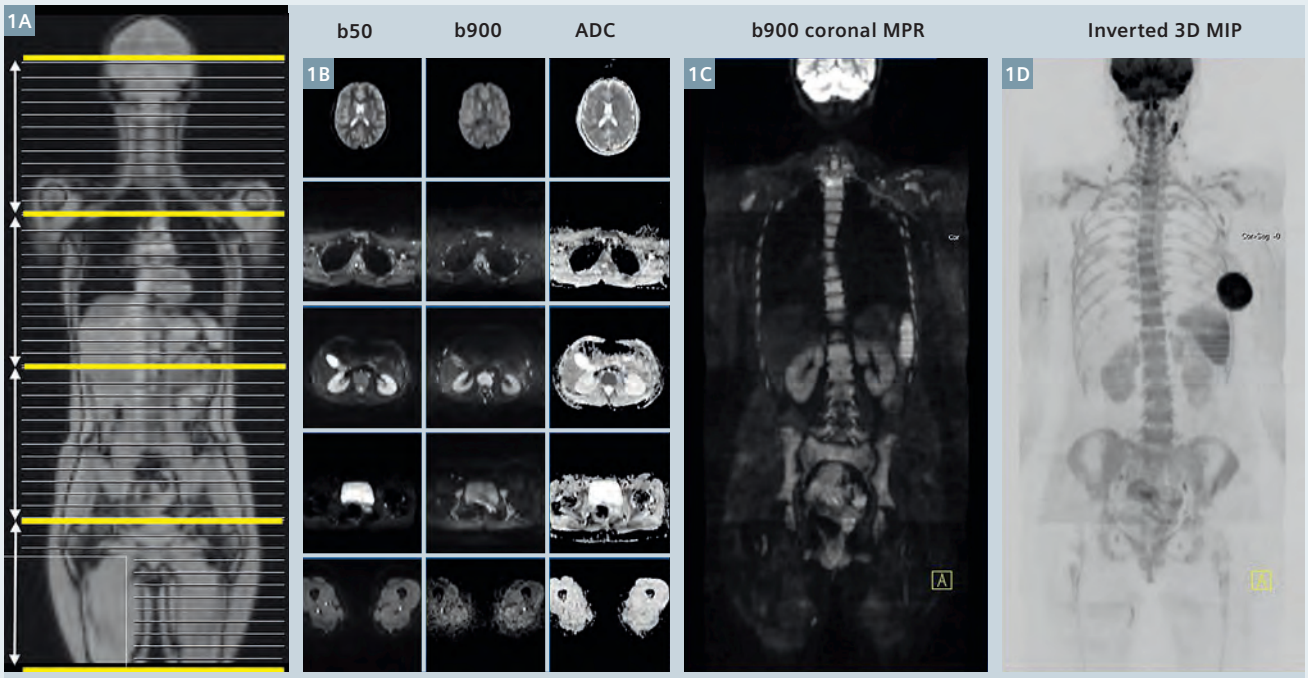

1 **WB-DWI workflow.** 27-year-old woman with sarcomatoid left breast cancer. The bone marrow pattern is normal for age. Axial DWI from the skull base to the mid-thigh is performed using 2 b-values (50 and 900 s/mm^2) with a slice thickness of 5 mm in 4 stations. The b900 images are reconstructed into the coronal plane (5 mm) and displayed as thick 3D MIPs (inverted grey scale). ADC images are computed inline with mono-exponential fitting of b50 and b900 signal intensities.

Technique of whole body DWI

Although imaging at 3T increases the signal-to-noise ratio, WB-DWI at this field strength remains challenging because of increased susceptibility artifacts and poorer fat suppression; currently, we find that WB-DWI is best performed on a longer bore 1.5T scanner. All our WB-MRI scans are done on a Siemens MAGNETOM Avanto scanner equipped with a continuous moving table option (TimCT) and total imaging matrix (Tim) body surface coils. We always acquire morphologic images to accompany the WB-DWI images.

Our morphologic images consist of

1 whole spine: T1-weighted, turbo spin-echo sagittal images (acquisition time 2:21 minutes),

2 whole spine: T2-weighted, turbo spin-echo sagittal images with spectral fat suppression (acquisition time 2:36 minutes),

3 whole body: T1-weighted, gradient-echo axial 2-point Dixon sequence (acquisition time 3:00 minutes) that automatically generates four image-sets (in-phase, opposed phase, water-only (WO), and fat-only (FO)) from which T1w fat% and non-fat% images can be calculated if needed.

4 Finally whole body (vertex to upper mid thighs): T2-weighted, short-tau inversion recovery (STIR) axial images with half-Fourier single shot turbo spin-echo (HASTE) readouts (acquisition time 4:00 minutes) is also undertaken.

The axial images from the skull vault to the mid-thighs are acquired using the continuous table movement technology, employing multiple breath-holds for image acquisitions of the chest, abdomen, pelvis and upper thighs.

Axial DWI from the skull vault to the mid-thighs is then performed using b-values of 50 s/mm^2 and a b-value of 900 s/mm^2 with a slice thickness of 5 mm. The axial DWI acquisition is usually achieved in 4 contiguous stations using a free-breathing technique, with each station taking approximately 6 minutes to acquire. Our preferred

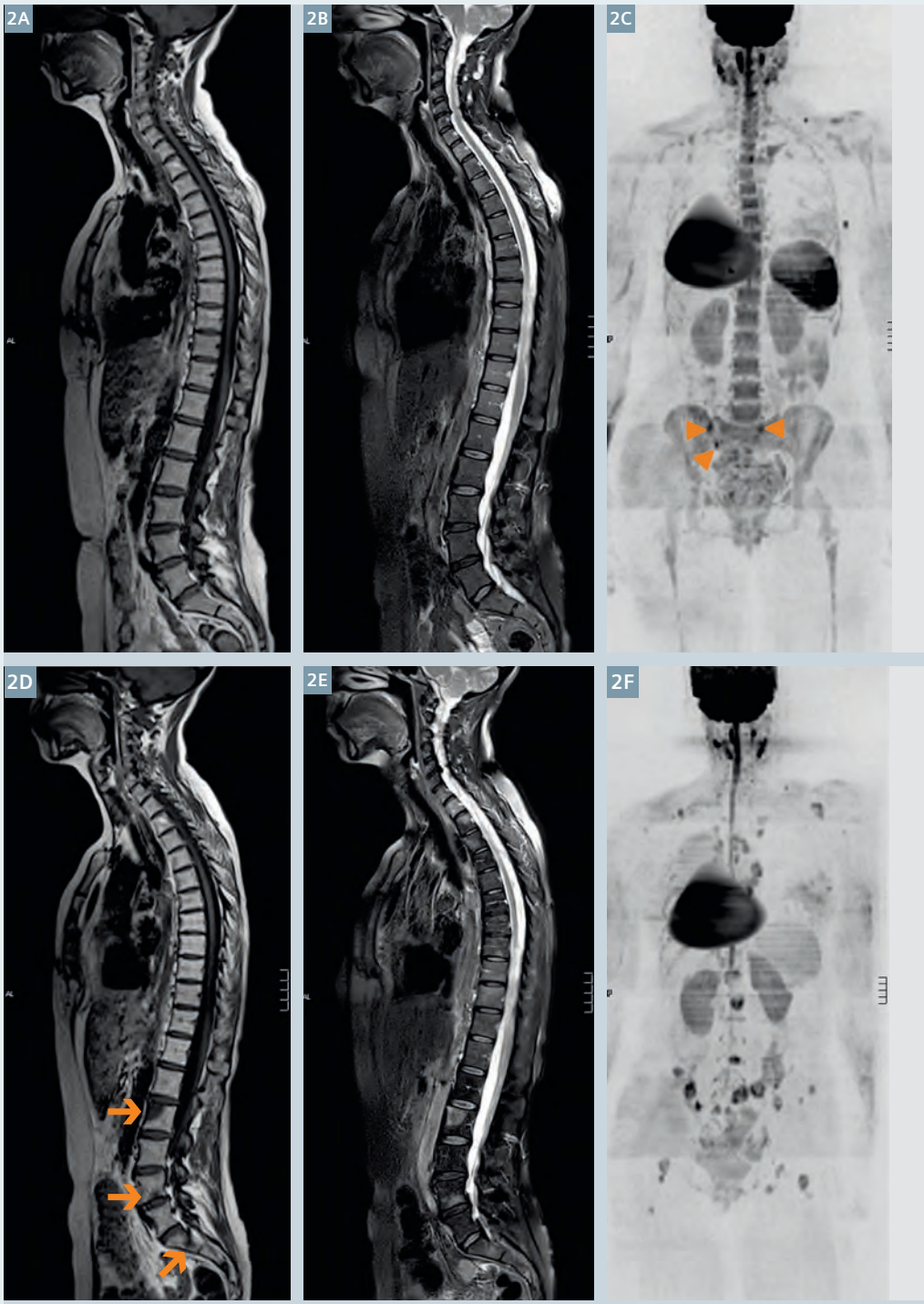

2 **Bone marrow hypoplasia due to chemotherapy with disease progression.** 49-year-old woman with metastatic breast cancer before and after 3 cycles of carboplatin chemotherapy. Both rows left-to-right: spine T1w spin-echo, spine T2w spin-echo with spectral fat saturation and b900 3D MIP (inverted scale) images.
Top row before chemotherapy shows normal background bone marrow pattern with superimposed small volume bone metastases (arrow heads).
Bottom row after chemotherapy shows disease progression with enlarging and new bony metastases (arrows). Note that bone marrow hypoplasia has developed in the ribs, spine and pelvis. Note reductions of signal intensity of the spleen secondary to iron deposition due to blood transfusions. There is a right sided silicone containing breast enhancement bra pad in place on both examinations.

3 **Poor visibility of treated metastases and osteoblastic metastases.** 69-year-old with metastatic prostate cancer on long term, third line hormonal therapy with abiraterone being evaluated for rising serum prostate specific antigen (PSA) levels. He has had an excellent response to 2 years of treatment with residual abnormalities in his bone marrow visible on T1w **(3A)** and T2w (with fat suppression) spinal images. No hyperintensity is seen on the b900 3D MIP (inverted scale) image **(3C)** indicating the absence of highly cellular infiltrative disease. Bone scan **(3D)** shows a focal area of osteoblastic uptake in the intertrochanteric region of the left femur (arrow) which is not visible as a discrete region on the b900 3D inverted MIP image.

method for fat suppression uses inversion recovery because it allows uniform fat suppression over large fields-of-view [4]. An artificially 'fractured spine' observed on the post processed stitched images as a consequence of alignment mismatch can be minimized by manually adjusting and maintaining the transmitter frequency for each station. The b900 value images are reconstructed in the coronal plane (5 mm) and as thick 3D maximum intensity projections (MIPs) which are displayed using an inverted grey scale. ADC maps are computed inline with system software using mono-exponential fitting in which each voxel reflects the tissue diffusivity (units: $\mu m^2/s$) (Fig. 1).

Detailed scanning parameters for each sequence have been published [4, 5]; the entire examination takes 52 minutes to complete. The illustrations of this article were obtained from more than 2,000 WB-DWI scans done at our institution in the last 4 years using this protocol.

Normal bone marrow signal on WB-DWI

A thorough understanding of normal bone marrow signal distribution on b900 value images is vital for the accurate detection, characterization and treatment assessment of skeletal metastases [5]. This is because the bone marrow distribution can be visualized by WB-DWI. The normal adult bone marrow pattern which is established by the age of 25 years can be seen as uniformly distributed, intermediate high signal intensity distributed in the axial skeleton (mixed red bone marrow); yellow marrow in the appendicular skeleton shows no/lower signal intensity (Fig. 1). The changing distribution of the normal marrow is also exquisitely demonstrated on WB-DWI. Red marrow conversion to yellow marrow is dependent on patient age, gender and underlying medical conditions [6]. Both bone marrow hypo- and hypercellularity are well depicted on WB-DWI.

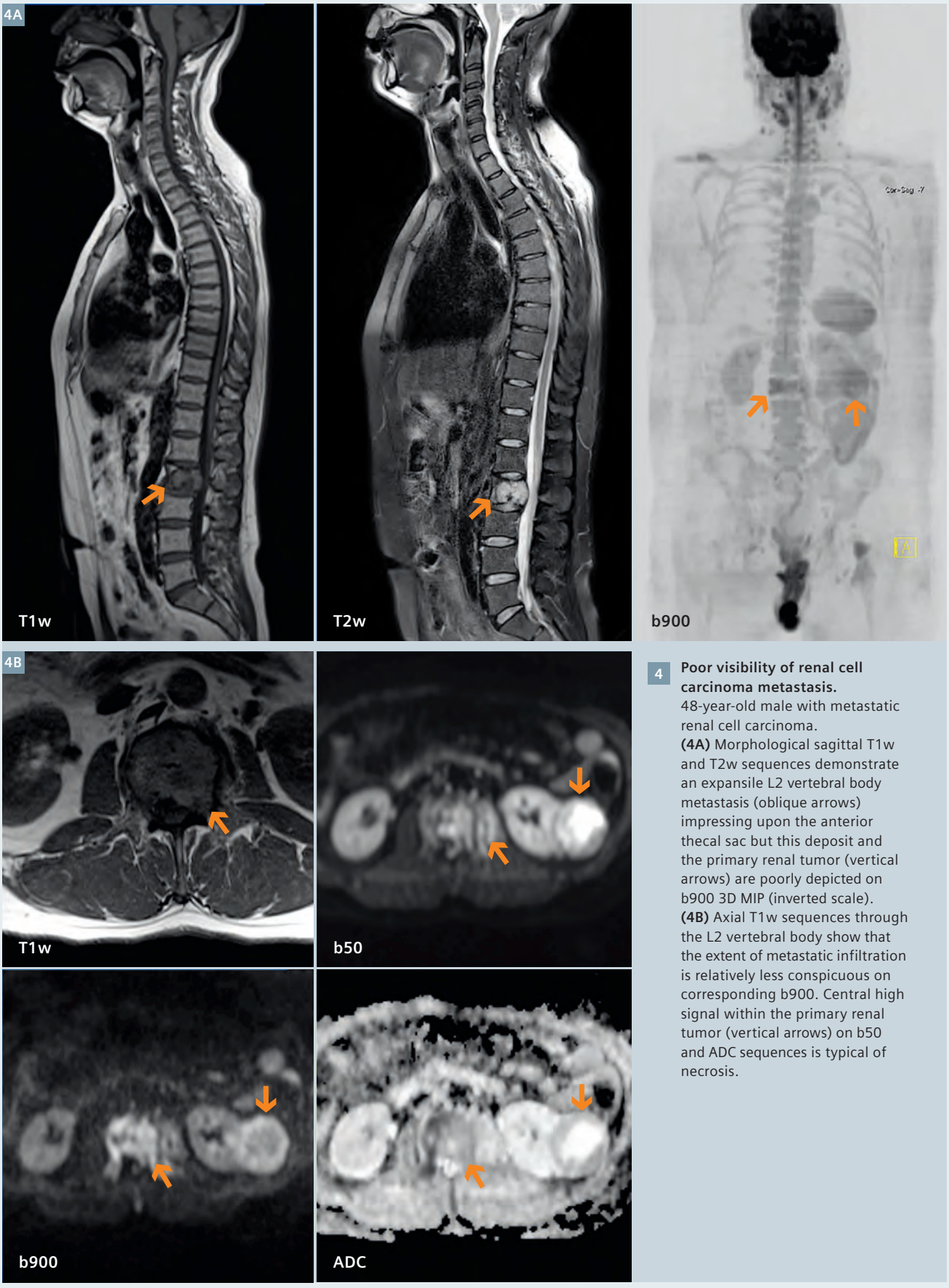

4 **Poor visibility of renal cell carcinoma metastasis.**
48-year-old male with metastatic renal cell carcinoma.
(4A) Morphological sagittal T1w and T2w sequences demonstrate an expansile L2 vertebral body metastasis (oblique arrows) impressing upon the anterior thecal sac but this deposit and the primary renal tumor (vertical arrows) are poorly depicted on b900 3D MIP (inverted scale).
(4B) Axial T1w sequences through the L2 vertebral body show that the extent of metastatic infiltration is relatively less conspicuous on corresponding b900. Central high signal within the primary renal tumor (vertical arrows) on b50 and ADC sequences is typical of necrosis.

The relationship between bone marrow cellularity and ADC values is non linear and highly dependent on the water, cellular and fat content of the marrow. The reduced water content [6], the larger-sized fat cells, the hydrophobic nature of fat and poorer perfusion all contribute to lower diffusion-weighted signal intensities and ADC values of the yellow bone marrow. On the other hand, with increasing cellularity and water content and greater perfusion, mixed yellow-red bone marrow returns higher signal intensities and paradoxically higher ADC values [5, 7-9].

Skeletal metastases detection

Skeletal metastases appear as focal or diffuse areas of high-signal intensity on high b-value WB-DWI (Fig. 2). The ability to detect bone marrow lesions is dependent on the intrinsic signal intensity of the deposits and the background bone marrow. Other factors determining the visibility of bone lesions include their anatomic location and treatment status. It is imperative that WB-DWI is performed and interpreted in conjunction with conventional morphological WB-MRI sequences rather than in isolation.

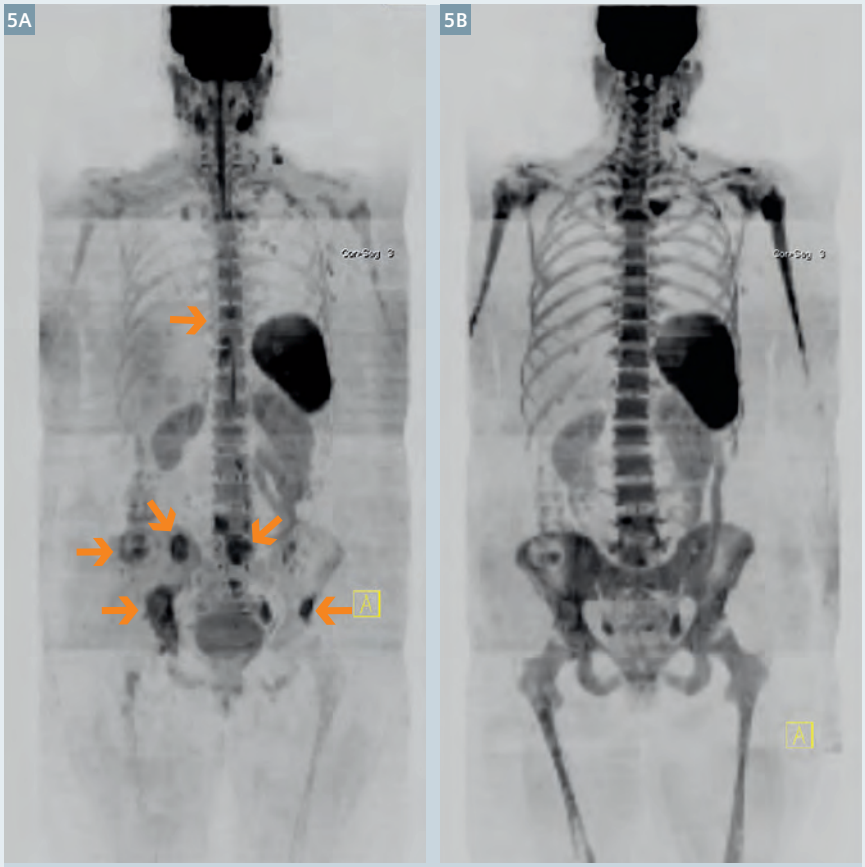

5 **Bone marrow hyperplasia induced by G-CSF therapy obscuring metastases.** 50-year-old woman with metastatic breast cancer before and after 3 cycles of erubulin chemotherapy with growth-colony stimulating factor (G-CSF) given to prevent neutropenia. b900 3D MIP (inverted scale) images. Image 5A shows multiple bone metastases (arrows). Image 5B after 3 cycles of chemotherapy shows increases in signal intensity of the bone marrow leading to the decreased visibility of the bone metastases. The splenic size has also increased. The increased signal intensity of the background bone marrow should not be misinterpreted as malignant progression.

This is because false positive and negative lesions do occur. This assertion was highlighted by a recent meta-analysis, which demonstrated that the high sensitivity of WB-DWI to detect metastases was at the expense of specificity [1].

Generally, infiltrative cellular lesions are better detected than *de-novo* sclerotic or treated lytic/sclerotic lesions (Fig. 3). This is due to the lower water and cellular content of sclerotic and treated metastases [7, 10]. This is the likely reason for the improved visibility of bone metastases of untreated breast cancer compared to prostate cancer; *de-novo* sclerotic metastases are commoner in prostate cancer. WB-DWI is better at detecting skeletal lesions from smaller cancer cell infiltrations such as those due to breast cancer, myeloma, lymphoma and small cell cancers as well as neuroendocrine tumors. On the other hand, bony metastases from clear cell renal cancers are sometimes poorly depicted (the presence of necrosis, large sized tumor cells and inherent lipogenesis contribute to the poorer visualization) (Fig. 4). On occasion, the high magnetic field susceptibility of melanin can also impair depiction of melanoma metastases.

The detection of skeletal metastases on WB-DWI may be impaired in areas of movement such as the anterior ribs and sternum. Visibility of skull vault infiltrations can be impaired because of the adjacent high signal of the normal brain. The visibility of skull base disease is impaired because of susceptibility effects.

Other causes for false-negative findings are low levels of bone marrow infiltration such as in smoldering multiple myeloma (when plasma cell infiltration fraction is less than background cell bone marrow cellularity) or when bone marrow hyperplasia results in diffuse increase in signal on high b-value images obscures the presence of metastases [2, 5] (Fig. 5). Relative bone marrow hypercellularity is observed in children and adolescents, chronic anemia, in smokers, chronic cardiac failure, in pregnancy

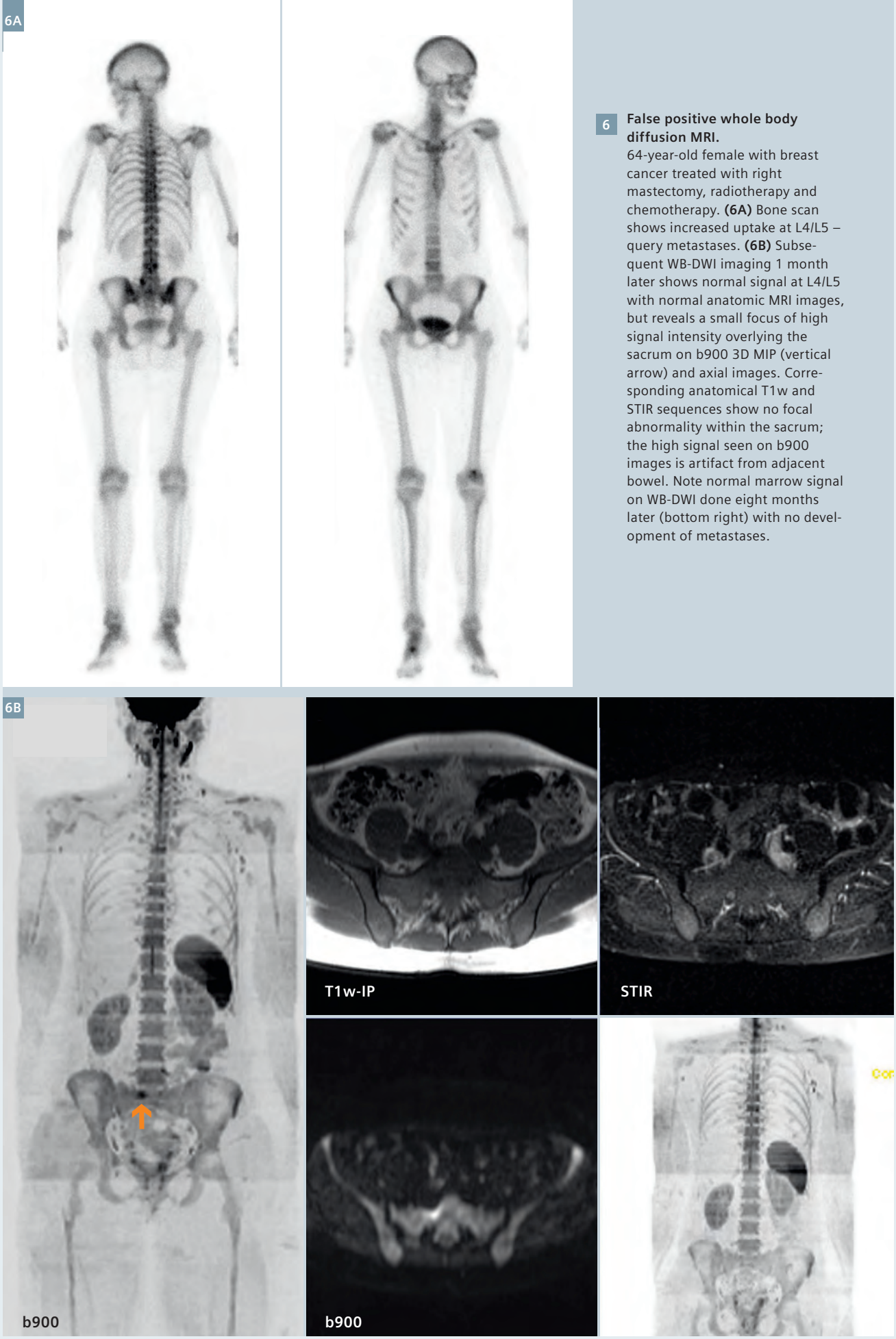

6 False positive whole body diffusion MRI.
64-year-old female with breast cancer treated with right mastectomy, radiotherapy and chemotherapy. **(6A)** Bone scan shows increased uptake at L4/L5 – query metastases. **(6B)** Subsequent WB-DWI imaging 1 month later shows normal signal at L4/L5 with normal anatomic MRI images, but reveals a small focus of high signal intensity overlying the sacrum on b900 3D MIP (vertical arrow) and axial images. Corresponding anatomical T1w and STIR sequences show no focal abnormality within the sacrum; the high signal seen on b900 images is artifact from adjacent bowel. Note normal marrow signal on WB-DWI done eight months later (bottom right) with no development of metastases.

and in patients treated with hematopoietic growth factors such as granulocyte-colony stimulating factors (G-CSF).

Causes for false-positive findings include bone marrow edema caused by fractures, osteoarthritis, infection, bone infarcts, vertebral hemangiomas, isolated bone marrow islands and 'T2 shine through' – the latter observed in treated metastases. A variety of internal metallic* (orthopedic) and silicone (breast) prostheses are routinely encountered in clinical practice. Magnetic field inhomogeneities secondary to metal and air interfaces will cause artifacts that cause false positive lesions (Fig. 6) and at the same time may obscure metastatic lesions in the adjacent bones. Many of these false-positive findings can be identified as not representing metastases by correlating the appearances of DW images with corresponding ADC maps and anatomical sequences [5].

Conclusions

WB-DWI is a contemporary imaging technique serving as an adjunct to conventional morphological whole body MRI, with high intrinsic sensitivity for detecting skeletal bone marrow metastases. However, there are several pitfalls that are encountered in routine clinical practice, the majority of which can be overcome by judicious interpretation of images in conjunction with standard anatomical sequences in light of relevant clinical knowledge.

*The MRI restrictions (if any) of the metal implant must be considered prior to patient undergoing MRI exam. MR imaging of patients with metallic implants brings specific risks. However, certain implants are approved by the governing regulatory bodies to be MR conditionally safe. For such implants, the previously mentioned warning may not be applicable. Please contact the implant manufacturer for the specific conditional information. The conditions for MR safety are the responsibility of the implant manufacturer, not of Siemens.

References

1 Wu LM, Gu HY, Zheng J, et al. Diagnostic value of whole-body magnetic resonance imaging for bone metastases: a systematic review and meta-analysis. J Magn Reson Imaging 2011;34:128-135.
2 Padhani AR, Gogbashian A. Bony metastases: assessing response to therapy with whole-body diffusion MRI. Cancer Imaging 2011;11 Spec No A:S129-145.
3 Padhani AR. Diffusion magnetic resonance imaging in cancer patient management. Semin Radiat Oncol 2011;21:119-140.
4 Koh DM, Blackledge M, Padhani AR, et al. Whole-Body Diffusion-Weighted MRI: Tips, Tricks, and Pitfalls. AJR Am J Roentgenol 2012;199:252-262.
5 Padhani AR, Koh DM, Collins DJ. Whole-body diffusion-weighted MR imaging in cancer: current status and research directions. Radiology 2011;261:700-718.
6 Hwang S, Panicek DM. Magnetic resonance imaging of bone marrow in oncology, Part 1. Skeletal Radiol 2007;36:913-920.
7 Messiou C, Collins DJ, Morgan VA, Desouza NM. Optimising diffusion weighted MRI for imaging metastatic and myeloma bone disease and assessing reproducibility. Eur Radiol 2011;21:1713-1718.
8 Hillengass J, Bauerle T, Bartl R, et al. Diffusion-weighted imaging for non-invasive and quantitative monitoring of bone marrow infiltration in patients with monoclonal plasma cell disease: a comparative study with histology. Br J Haematol 2011;153:721-728.
9 Nonomura Y, Yasumoto M, Yoshimura R, et al. Relationship between bone marrow cellularity and apparent diffusion coefficient. J Magn Reson Imaging 2001;13:757-760.
10 Eiber M, Holzapfel K, Ganter C, et al. Whole-body MRI including diffusion-weighted imaging (DWI) for patients with recurring prostate cancer: Technical feasibility and assessment of lesion conspicuity in DWI. J Magn Reson Imaging 2011;33:1160-1170.

Contact

Professor Anwar R. Padhani, MB BS, FRCP, FRCR
Paul Strickland Scanner Centre
Mount Vernon Cancer Centre
Rickmansworth Road
Northwood
Middlesex HA6 2RN
United Kingdom
Phone: +44 (0) 1923-844751
Fax: +44 (0) 1923-844600
anwar.padhani
@stricklandscanner.org.uk

Multi-parametric MRI at 3 Tesla for Prediction of Treatment Response in Rectal Cancer

Trang Pham[1,3]; Michael Barton[1,3]; Robba Rai[1]; Dale Roach[4]; Karen Wong[1,3]; Daniel Moses[5]; Christopher Henderson[2,6]; Mark Lee[1,2]; Benjamin Schmitt[7]; Gary Liney[1,3]

[1] Liverpool Cancer Therapy Centre, Liverpool Hospital, Sydney, Australia
[2] Faculty of Medicine, University of New South Wales, Sydney, Australia
[3] Ingham Institute for Applied Medical Research, Sydney, Australia
[4] Faculty of Physics, University of Sydney, Sydney, Australia
[5] Department of Radiology, Prince of Wales Hospital, Sydney, Australia
[6] Department of Anatomical Pathology, Liverpool Hospital, Sydney, Australia
[7] Siemens Healthcare, Macquarie Park, Australia

Introduction

Current functional MRI techniques have shown promising results for prediction and assessment of response to chemoradiotherapy (CRT) in rectal cancer [1,2], but lack sufficient accuracy for clinical use. There is a wide variation in performance of functional MRI in response prediction reported. Most studies describe single parameter values from either diffusion or perfusion MRI. Single parameter measurements, such as mean ADC or K^{trans}, do not adequately reflect tumor heterogeneity. Multi-parametric MRI using quantitative diffusion-weighted and dynamic contrast-enhanced imaging in combination can assess tumor heterogeneity and its response to treatment. This strategy has the potential to better reflect tumor heterogeneity and improve the accuracy of therapeutic response prediction and assessment in rectal cancer.

Since 2014 we have been conducting treatment response studies on our dedicated MRI system ('MR-Simulator' shown in Figure 1) which was installed in our Radiation Oncology Centre to provide MRI planning and guidance in various tumor sites. This report describes our results in rectal cancer.

Imaging details

Patients with locally advanced rectal cancer undergoing preoperative CRT prospectively underwent multi-parametric MRI on our 3T wide bore MAGNETOM Skyra (Siemens Healthcare, Erlangen, Germany) at 3 time-points: Pre-CRT, week 3 CRT, and post-CRT. The imaging protocol consisted of:

(i) T2-weighted image.

(ii) DWI using RESOLVE, which has been previously shown to be robust with respect to geometrical distortions [3]. Images were acquired with b-values 50 and 800 s/mm^2 and 1 & 3 averages. ADC maps and calculated b = 1400 s/mm^2 images were produced as part of protocol.

(iii) DCE consisted of pre-contrast VIBE scans with flip angles 2° and 15° in order to calculate native T1, followed by gadoversetamide (0.1 mM/kg) injection and 60 phases using TWIST with a 5 s temporal resolution. Buscopan was administered intravenously prior to the functional sequences to reduce rectal peristaltic motion.

1 The 3 Tesla MAGNETOM Skyra MR-Simulator at Liverpool Cancer Therapy Centre in Sydney, Australia.

Multi-parametric analysis and therapy monitoring

We developed a voxel-by-voxel multi-parametric histogram analysis strategy to assess tumor heterogeneity and its changes in response to combined chemotherapy and radiotherapy. A complete protocol and analysis strategy was developed which has utilized commercial, in-house developed and works-in-progress (Siemens' OncoTreat[1]) software. For DCE analysis, registration of the pre-contrast flip angle sequences to dynamic images was a crucial step in producing a pixel-by-pixel T1 map to ensure accurate voxel-by-voxel calculation of K^{trans}. Images were manually pre-registered in Siemens 3D fusion software and the headers of registered images were re-written with an in-house code to enable these images to be analyzed in

[1] The product is still under development and not commercially available yet. Its future availability cannot be ensured.

2

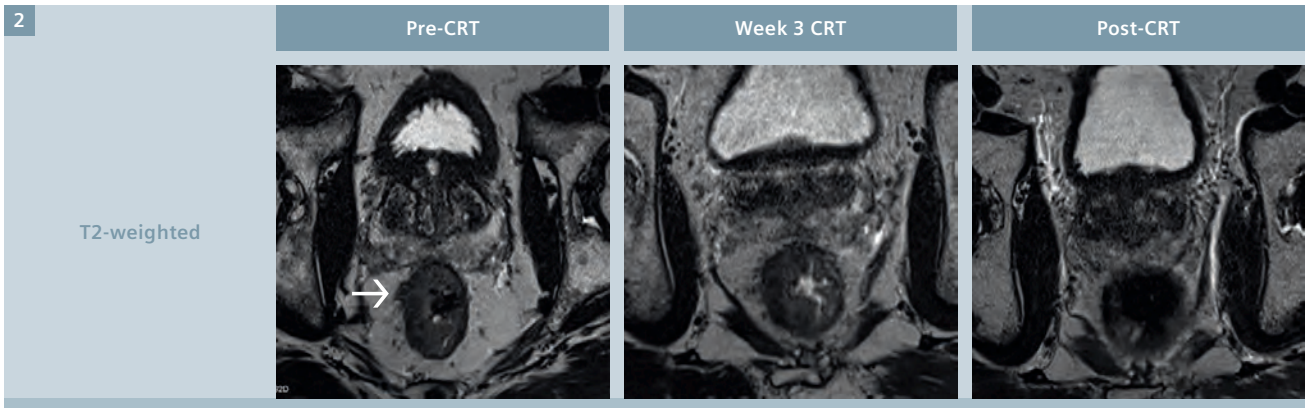

2 T2-weighted images for a rectal cancer patient at 3 time-points: pre-CRT, week 3 of CRT, and post-CRT. The rectal tumor (arrow) invades into the mesorectal fat. T2-weighted images alone cannot accurately assess treatment response, because of difficulty detecting residual tumor deposits within areas of radiation-induced necrosis or fibrosis.

3

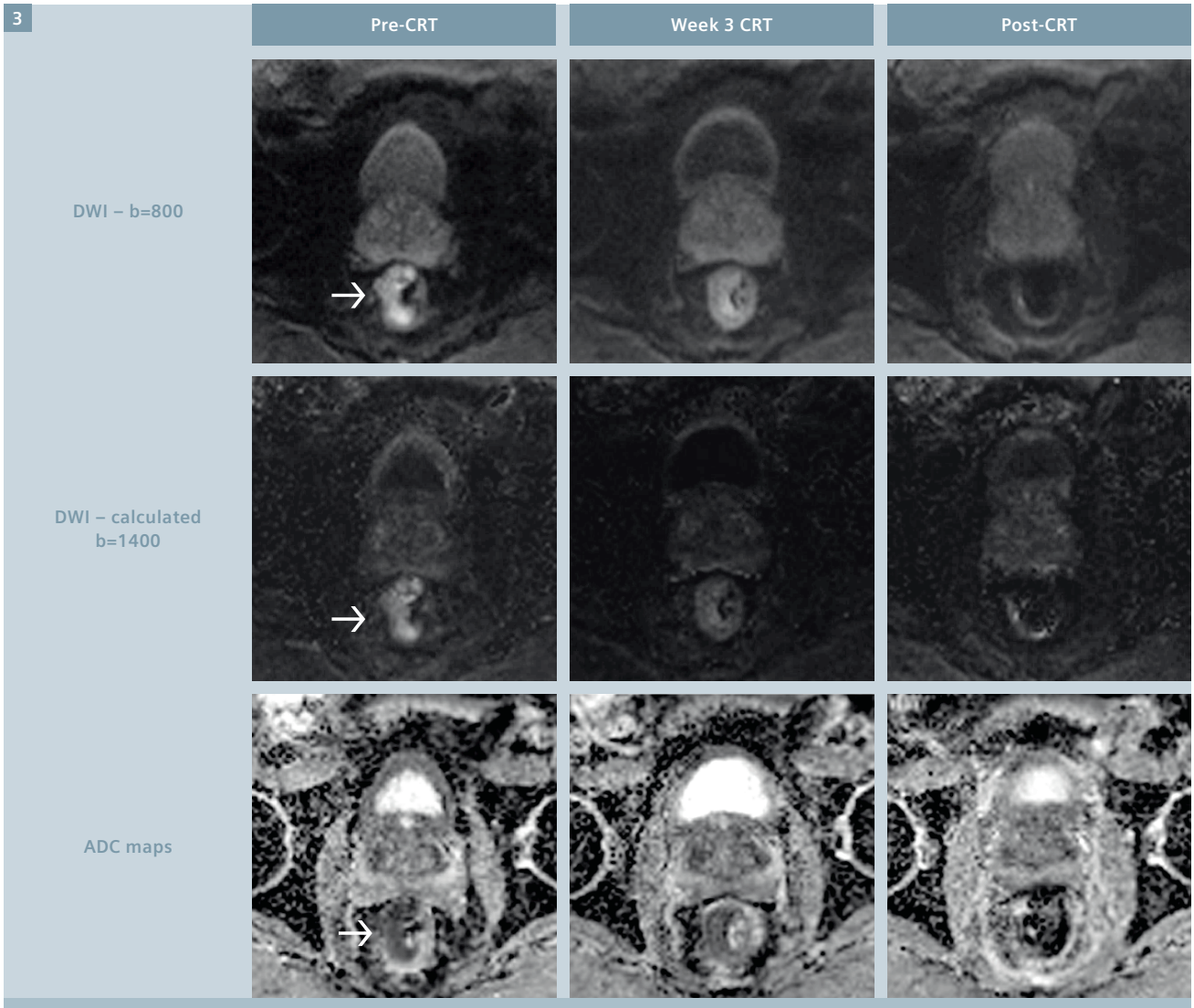

3 Diffusion-weighted RESOLVE images for the same rectal cancer patient at 3 time-points. The top panel shows the b = 800 s/mm^2 images, the middle panel shows the calculated b = 1400 s/mm^2 images and the bottom panel shows the ADC maps. Response to treatment can be seen on the diffusion images, with the level of tumor hyperintensity decreasing across the time-points. The histopathology demonstrated AJCC tumor regression grade 1 indicating a good response to preoperative CRT.

Tissue 4D. We have found this provides better results than using the available deformable registration. ADC and K^{trans} parameter maps were subsequently exported to OncoTreat where they were registered to T2-weighted images. Semi-automated segmentation was used to define the volume of interest from the hyperintense tumor on the calculated b-value = 1400 s/mm^2 images. We have found this dataset particularly useful – gaining both from the extra sensitivity and reduced noise of a calculated high b-value. A voxel-by-voxel technique was used to produce color-coded histograms of ADC and K^{trans}, as well as combined

4

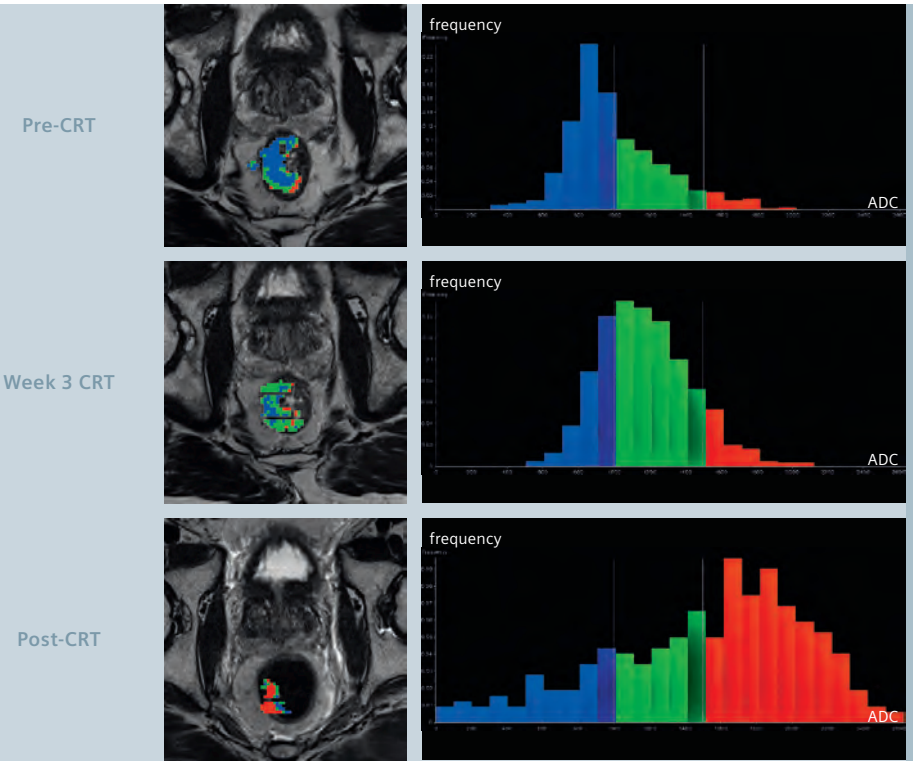

4 Example of the color-coded ADC maps and voxel-by-voxel histograms for a patient with good response to CRT. This patient had AJCC tumor regression grade 1 (moderate response, single cells or small groups of cancer cells) on histopathology. The histograms demonstrated an increase in the absolute ADC values of voxels over the time-points.

5

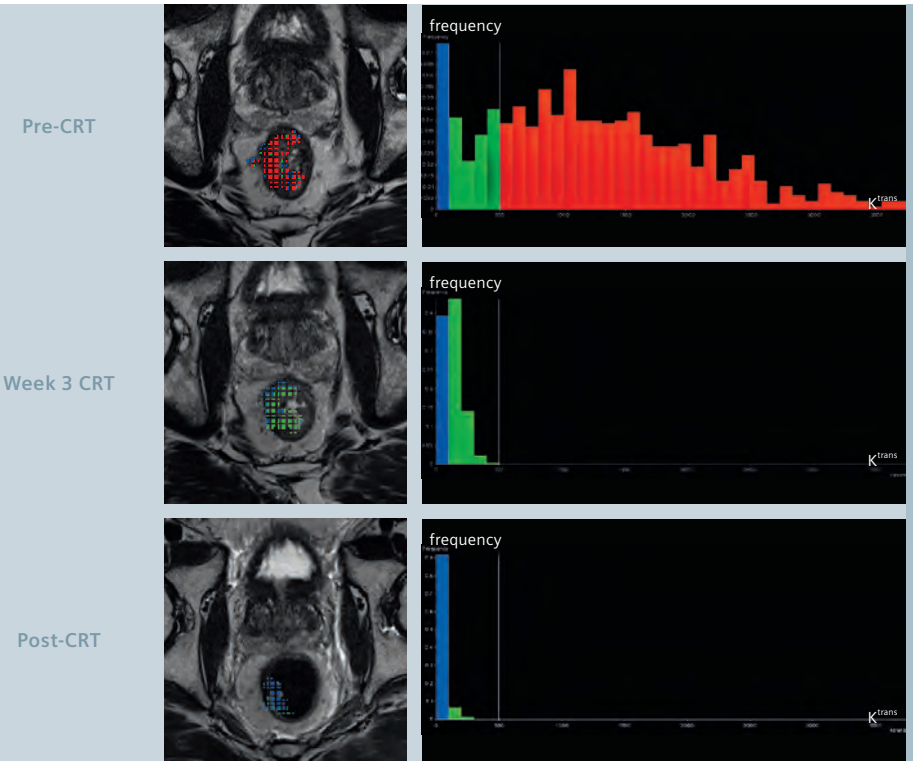

5 K^{trans} color-coded maps and voxel-by-voxel histograms for the same patient, who had a good response to CRT (AJCC TRG 1). The majority of K^{trans} voxel values were high (red) pre-CRT. A possible explanation for this is that the high K^{trans} is due to a well perfused oxic tumor, which is predictive of good radiotherapy response. By week 3-CRT the K^{trans} histogram demonstrated a marked reduction in the absolute K^{trans} values of voxels.

6 The scatterplots demonstrating changes in combined ADC and K^{trans} of voxels of segmented region over the time-points for a good responder with AJCC TRG 1 (top panel) and a poor responder with AJCC TRG2 (bottom panel). Percentages of voxels in each quadrant are shown. The scatterplots show different patterns of shift in the distribution of plots between the two patients. For Patient 1, the week 3 histograms and maps showed both a shift in distribution of ADC of voxels to higher values and K^{trans} of voxels to lower values compared to the pre-CRT histogram. In contrast, Patient 2 had low K^{trans} values pre-CRT, without much change in the values of voxels over the time-points. The low K^{trans} values in this patient may be due to poor perfusion representing a hypoxic tumor, which is predictive of a radio-resistant tumor and poor response to radiotherapy.

scatterplots for each time-point. CRT response was defined according to histopathology tumor regression grade (TRG) (AJCC 7th Edition) [4].

Conclusions

We have successfully integrated a multi-parametric MRI technique in our clinic to monitor response to treatment in patients with rectal cancer. This is a particularly challenging anatomy to image and provide robust functional datasets that can be examined in a serial manner. A voxel-by-voxel multi-parametric analysis strategy has been adopted and early results show this is important in quantitatively assessing heterogeneity within the entire tumor region, and the changes in response to CRT in rectal cancer.

Acknowledgement

This work was partially funded by the Royal Australian and New Zealand College of Radiologists (RANZCR) Withers and Peters Research Grant 2014.

References

1 van der Paardt et al. Patients who undergo preoperative chemoradiotherapy for locally advanced rectal cancer restaged by using diagnostic MR imaging: a systematic review and meta-analysis. Radiology. 2013;269:101-12.

2 Beets-Tan R and Beets G. MRI for assessing and predicting response to neoadjuvant treatment in rectal cancer. Nat Rev Gastroenterol Hepatol. 2014;11:480-88.

3 Liney G et al. Quantitative evaluation of diffusion-weighted imaging techniques for the purposes of radiotherapy planning in the prostate. Br J Radiol. 2015. DOI http://dx.doi.org/10.1259/bjr.20150034.

4 Edge S, Byrd D, Compt C et al (Eds). AJCC Cancer staging manual 7th edition. New York Springer 2010.

Contact

Dr. Trang Pham
Radiation Oncologist
Liverpool Cancer Therapy Centre
2170, 1 Campbell Dr,
Liverpool NSW 2170
Australia
Phone: +61 2 87389806
trangpham283@gmail.com

TOGETHER WE MOVE FORWARD IN THE FIGHT AGAINST CANCER

When two leading companies join forces in the fight against cancer, it broadens the realm of what's possible. That's why Varian and Siemens have partnered. Siemens' advanced diagnostic imaging capabilities coupled with Varian's powerful delivery systems and treatment planning tools give even more of an edge in the pursuit of our common goal: to **EnVision better cancer care**. Together we offer more personalized treatment and expanded care options that aid you in making the best possible decisions for your patients—with confidence. By gathering our strengths, we have the energy and vision to better help healthcare professionals detect, diagnose and treat cancer while paving the way for the future of cancer care.

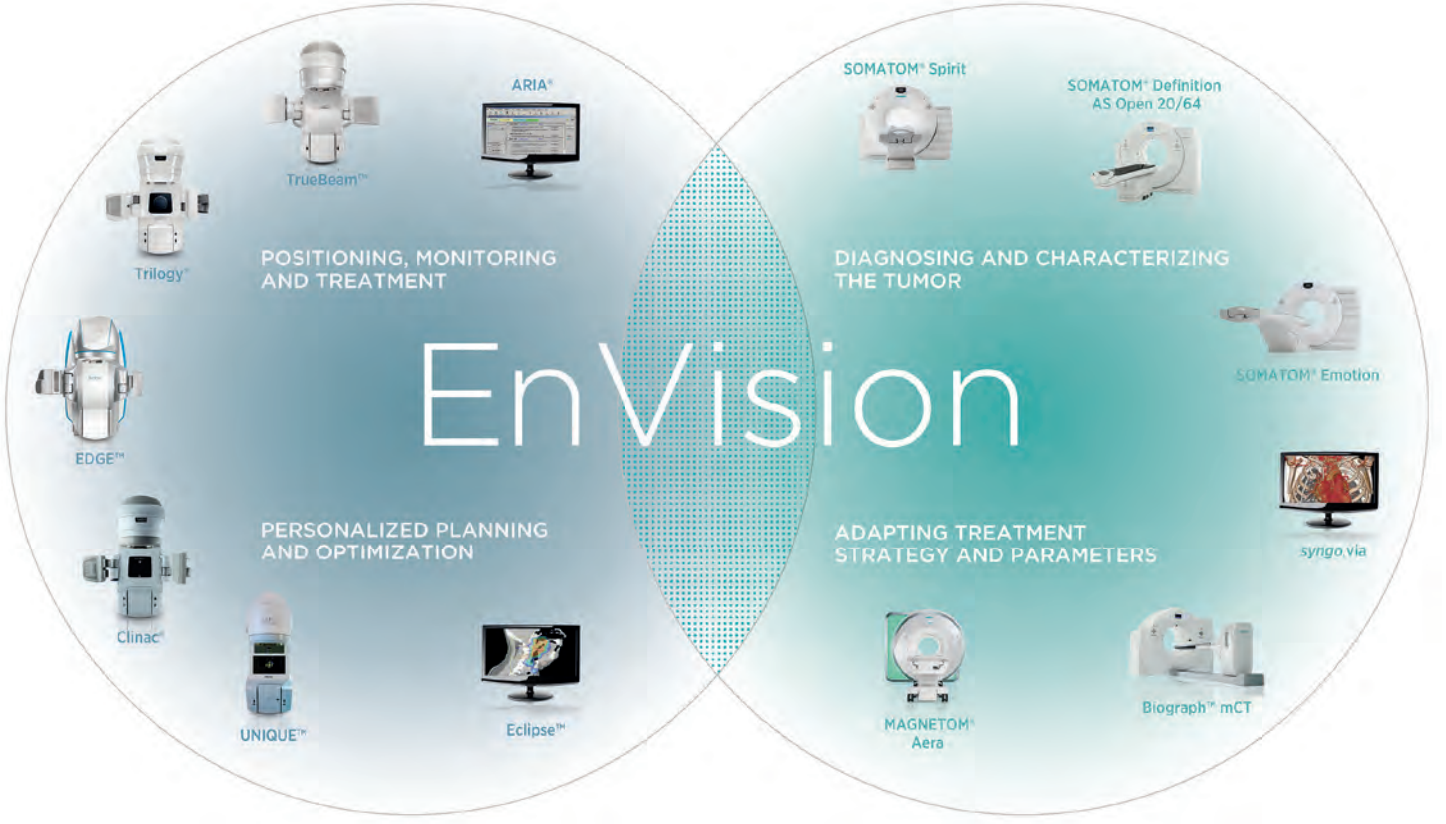

VARIAN medical systems

SIEMENS
Strategic Partner of Varian for Radiation Therapy

Varian Medical Systems
International AG
Zug, Switzerland
Tel: +41 - 41 749 88 44
Fax: +41 - 41 740 33 40
varian.com
info.europe@varian.com

Global Siemens Healthcare Headquarters
Siemens AG
Healthcare Sector
Henkestrasse 127
91052 Erlangen, Germany
Tel: +49 9131 84-0
siemens.com/healthcare

Find out more at **varian.com/envision**

Optimizing MRI for Radiation Oncology: Initial Investigations

James Balter[1]; Yue Cao[1]; Hesheng Wang[1]; Ke Huang[1]; Shu-Hui Hsu[1]; Martin Requardt[2]; Steven M. Shea[3]

[1] Department of Radiation Oncology, University of Michigan, Ann Arbor, MI, USA
[2] Siemens Healthcare, Erlangen, Germany
[3] Siemens Corporation, Corporate Technology, Baltimore, USA

Introduction

The superior soft tissue contrast, as well as potential for probing molecular composition and physiological behavior of tumors and normal tissues and their changes in response to therapy, makes MRI a tempting alternative to CT as a primary means of supporting the various processes involved in radiation therapy treatment planning and delivery. Obvious examples of the benefit of MRI over CT include target delineation of intracranial lesions, nasopharyngeal lesions, normal critical organs such as the spinal cord, tumors in the liver, and the boundaries of the prostate gland and likely cancerous regions within the prostate gland. For brachytherapy planning for cervical cancer, a recent GEC-ESTRO report directly recommends a change from traditional point-based prescriptions based primarily on applicator geometry, to volumetric treatment plans and prescriptions aided by soft tissue visualization, specifically improved by the use of MRI. MRI-based maps of diffusion and perfusion have demonstrated potential for predicting therapeutic outcome for tumors as well as normal tissues, and current clinical trials seek to validate their roles and performance as a means to individualize therapy to improve outcomes (minimize toxicity and improve local tumor control). In addition to these advantages, MRI has been initially investigated as a means to better map the movement and deformation of organs over time and due to physiological processes such as breathing.

The historically accepted challenges in using MRI for primary patient modeling in radiation oncology have included distortion, lack of electron density information, and lack of integrated optimized systems to scan patients immobilized in treatment configuration.

MRI 'simulator' system

Over the past several years, we have investigated the feasibility of MRI systems to function in the same roles that CT scanners have for the past 10–15 years, that is as primary tools for patient modeling for radiation therapy. These efforts have accelerated in the past years with the installation of a dedicated MRI 'simulator' at the University of Michigan, based on a 3T wide-bore scanner (MAGNETOM Skyra, Siemens Healthcare, Erlangen, Germany), outfitted with a laser marking system (LAP, Lueneburg, Germany) and separate detachable couch tops supporting brachytherapy and external beam radiation therapy applications.

1

MRI simulation system shows a volunteer in position for initial setup wearing a customized face mask **(1A)**. Close-up view of anterior coil setup and crosshairs from laser marking system **(1B)**.

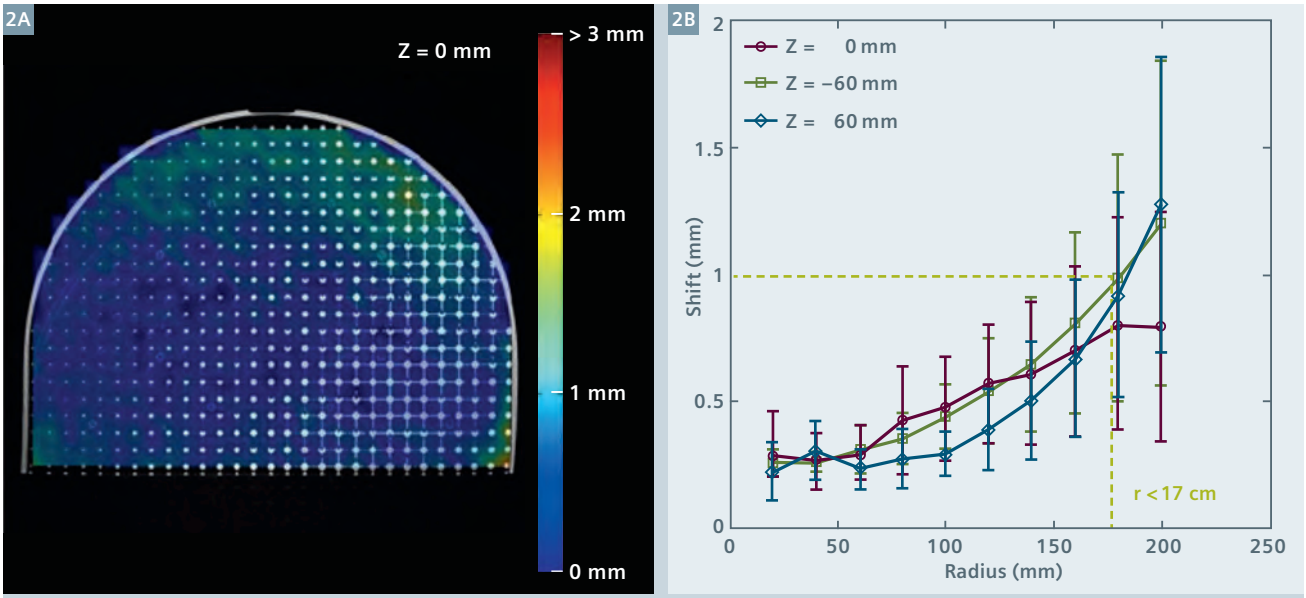

2 Colorwash of measured distortion through an axial plane of the distortion phantom **(2A)**. Magnitude of distortion-induced shifts in circles of increasing radius from the bore center in axial planes at the center and +/– 6 cm along the bore **(2B)**.

The process of integrating MRI into the standard workflow of radiation oncology requires attention be paid to a number of specific areas of system design and performance. In our instance, we chose a system that could potentially support both external beam therapy as well as brachytherapy. The brachytherapy requirement played a specific role in some of our design choices. As the high-dose-rate (HDR) brachytherapy system was housed in a room across the hall from the MRI suite, a room design was created that permitted the direct transfer of patients from MRI scanning to treatment. Typically brachytherapy treatment has involved transferring patients to and from imaging systems, a process that could potentially influence the treatment geometry and changes the dose delivered away from that planned. Treating a patient directly without moving them has significant advantages for geometric integrity as well as patient comfort. To facilitate such treatments, a detachable couch was chosen as part of the magnet specifications, and two such couches were specifically purchased to support simultaneous treatment of patients on the couch used for MRI scanning and scanning of other patients for subsequent external beam treatments.

To support external beam radiotherapy, patients need to be scanned in positions and configurations that can be reproduced at treatment. In addition to necessitating a wide bore MRI scanner, an indexed flat table top insert was purchased from a company that specializes in radiation therapy immobilization systems (Civco, Kalona, IA, USA). A number of immobilization accessories were customized for use in the MRI environment, most notably a head and neck mask attachment system. To support high quality scanning of patients in treatment position without interfering with their configuration for treatment, a series of attachments to hold surface coils (primarily 18-channel body coils) relatively close to the patient without touching are used.

Initial commissioning and tests

To commission the system, a number of tests were performed in addition to the standard processes for MRI acceptance and quality assurance. The laser system was calibrated to the scanner coordinates through imaging of a phantom with externally visible laser alignment markings and internal MRI-identifiable coordinates indicating the nominal laser intersection, and end-to-end tests were performed on phantoms and volunteers to establish the accuracy of isocenter marking using MRI scans as a source of input.

To characterize system-level distortion, a custom phantom was developed to fill the bore of the magnet (with perimeter space reserved for testing the 18-channel body coil if desired). The resulting phantom was a roughly cylindrical section with a sampling volume measuring 46.5 cm at the base, with a height of 35 cm, and a thickness of 16.8 cm. This sampling volume was embedded with a three-dimensional array of interconnected spheres, separated by 7 mm center-to-center distances. The resulting system provided a uniform grid of 4689 points to sample the local distortion. The phantom was initially scanned using a 3D, T1-weighted, spoiled gradient echo imaging sequence (VIBE, TR 4.39 ms and TE 2.03 ms, bandwidth 445 Hz/pixel) to acquire a volume with field-of-view of 500 × 500 × 170 mm with a spatial resolution of 0.98 × 0.98 × 1 mm. Standard 3D shimming was used for scanning, and 3D distortion correction was applied to the images prior

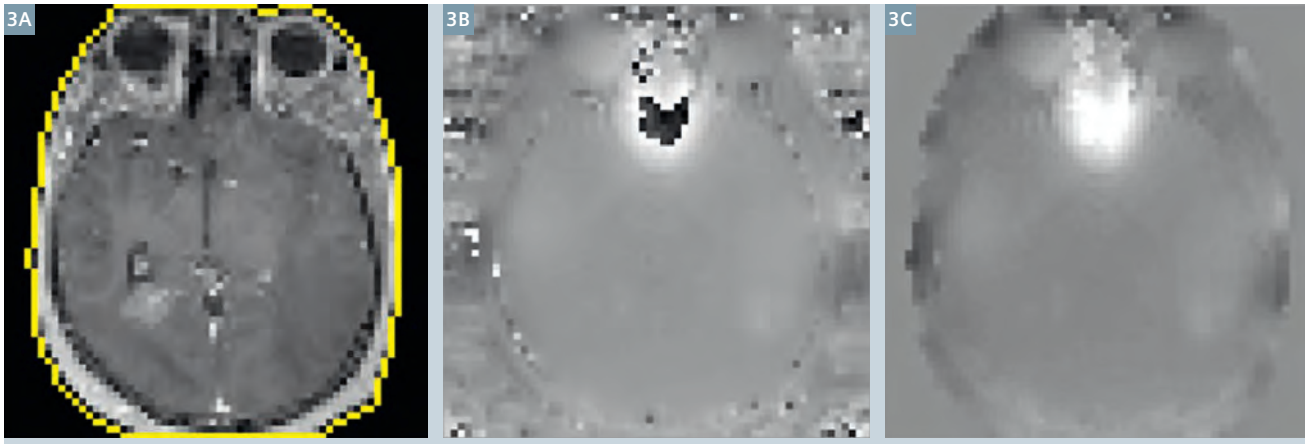

3 T1-weighted image with external contour delineated as a mask **(3A)**. The B_0 inhomogeneity map acquired from this subject **(3B)** was unwrapped within the boundaries of the mask, yielding the resulting distortion map **(3C)**.
Reprinted with permission from Wang H, Balter J, Cao Y. Patient-induced susceptibility effect on geometric distortion of clinical brain MRI for radiation treatment planning on a 3T scanner. Phys Med Biol 58(3):465-77, 2013.

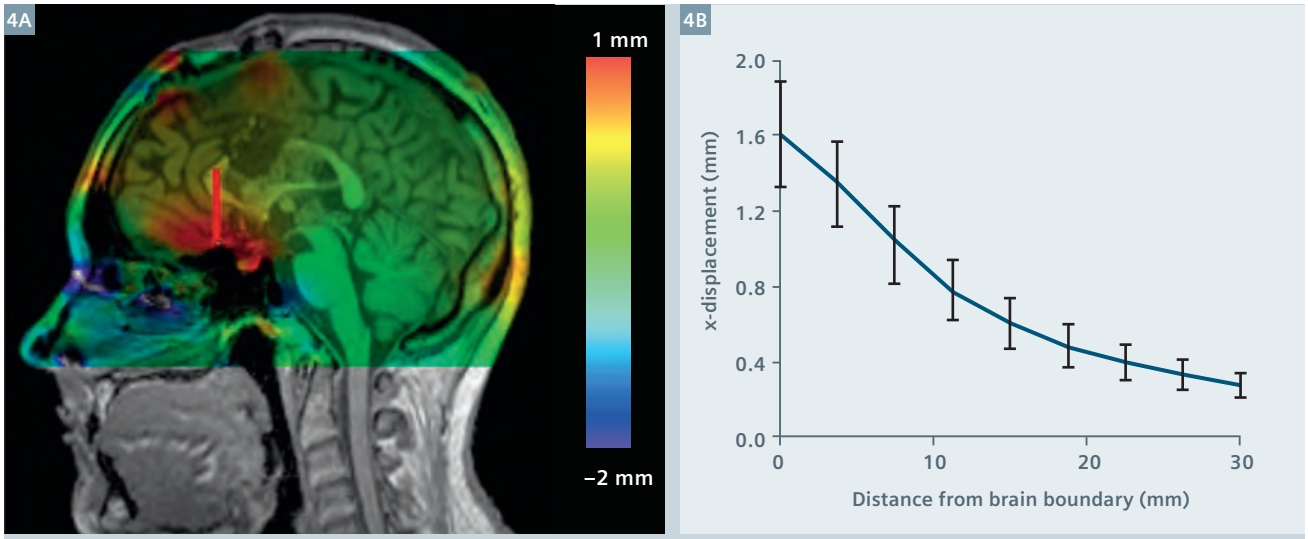

4 Colorwash of distortion-induced displacements through a sagittal plane of a subject **(4A)**. Analysis of displacements along a line moving away from the sinus (red line in fig. 4A) shows the falloff of distortion due to susceptibility differences as a function of distance from the interface **(4B)**.
Reprinted with permission from Wang H, Balter J, Cao Y. Patient-induced susceptibility effect on geometric distortion of clinical brain MRI for radiation treatment planning on a 3T scanner. Phys Med Biol 58(3):465-77, 2013.

to analysis. For this initial test, the body coil integrated into the magnet was used. Automated analysis of the images localized the sphere centers, yielding a deformation vector field that described the influence of system-level distortion on the measured sphere locations. This initial test demonstrated the accuracy of coordinate mapping via this scanning protocol, with average 3D distortions of less than 1 mm at radii of up to 17 cm in planes through the bore center as well as +/– 6 cm along the bore length. Of note, scanning was performed using the *syngo* MR D11 software version. Future tests will be performed on the *syngo* MR D13 release.

To begin to assess the impact of subject-induced susceptibility on distortions, B_0 inhomogeneity maps were acquired during routine patient scanning and analyzed (for 19 patients) under an IRB-approved protocol. These maps were acquired using a 2D, double-echo, spoiled gradient echo sequence (GRE field mapping TE_1 4.92 ms, TE_2 7.38 ms, TR 400 ms, flip angle 60 degrees, voxel size 3.5 × 3.5 × 3.75 mm), masked by the boundaries of the head acquired from T1-weighted images, and unwrapped using an algorithm from the Oxford Center for Functional Magnetic Resonance Imaging of the Brain [1]. The resulting maps showed homogeneity

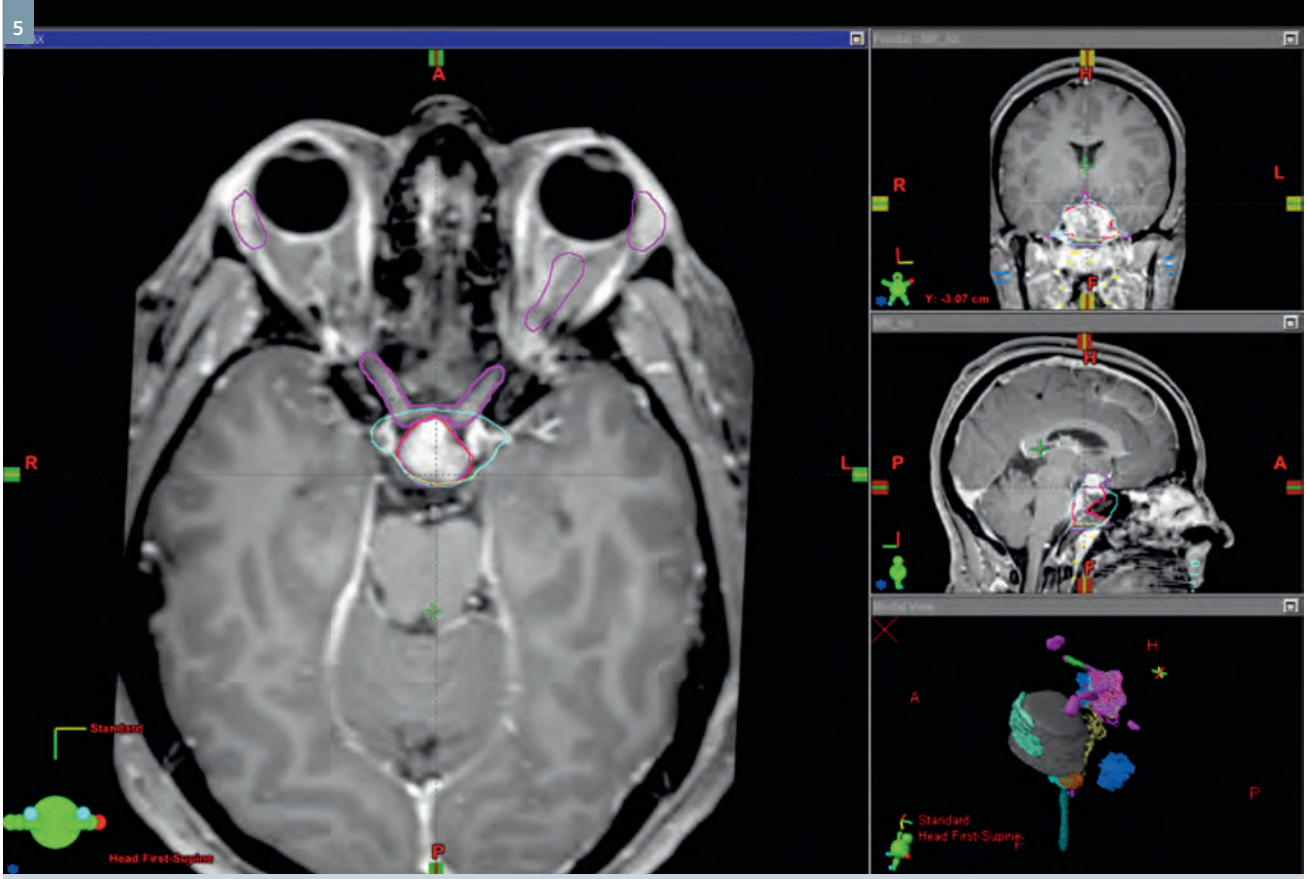

5 Post-contrast T1-weighted images of a patient scanned in an immobilization mask using an anterior 18-channel body surface coil and a posterior 4-channel small soft coil and displayed in a radiation therapy treatment planning system (Eclipse, Varian, Palo Alto, CA, USA). Various delineated structures shown are used to guide optimization of intensity-modulated radiation therapy.

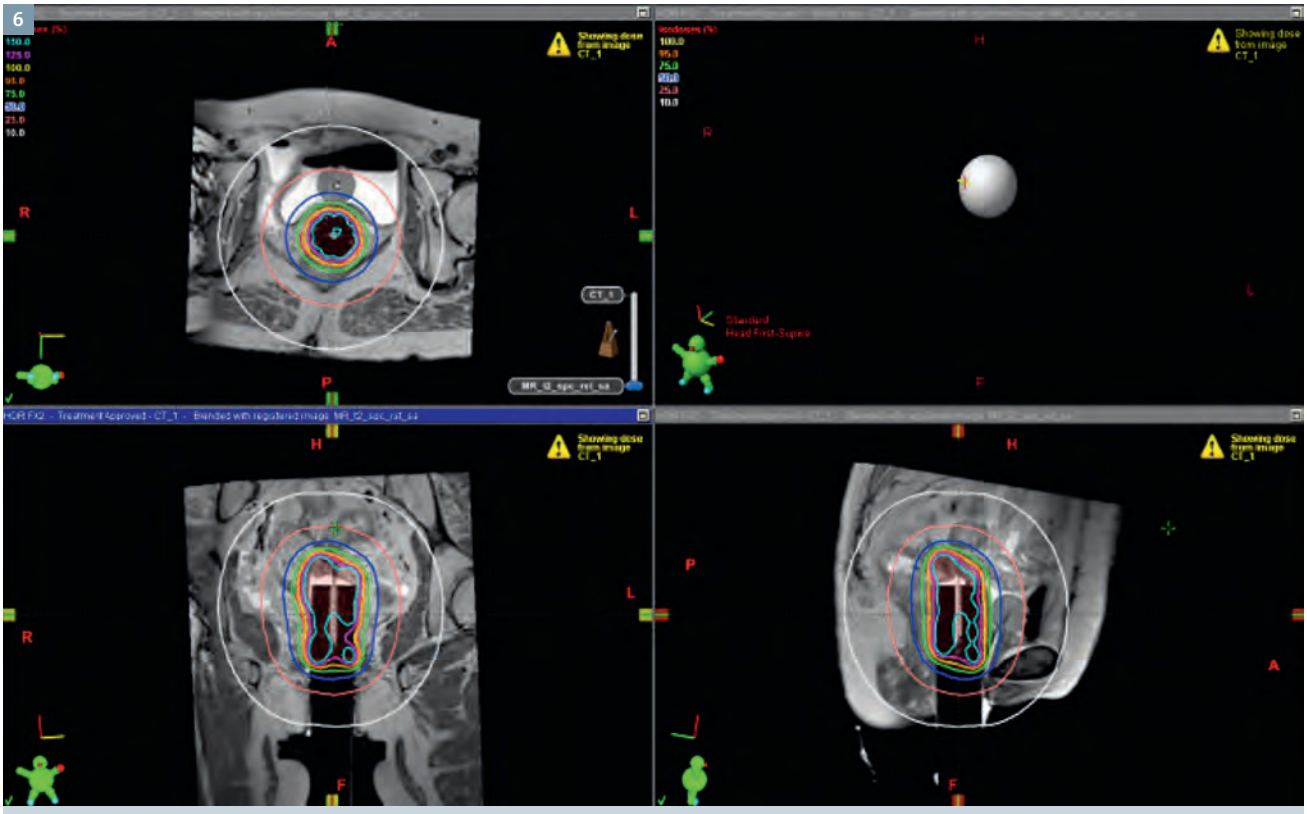

6 Display from a brachytherapy treatment planning system (Brachyvision, Varian, Palo Also, CA, USA) showing orthogonal planes through cylindrical applicator implanted in a patient. Source locations (red dashes through the center of the applicator) are shown, as well as radiation isodose lines.

of 0.035 ppm or less over 88.5% of a 22 cm diameter sphere, and 0.1 ppm or less for 100% of this volume.

These inhomogeneity maps were applied to calculate distortions from a typical clinical brain imaging sequence (3D T1-weighted MPRAGE sequence with TE 2.5 ms, Siemens TR 1900 ms, TI 900 ms, flip angle 9 degrees, voxel size 1.35 × 1.35 × 0.9 mm, frequency-encoding sampling rate of 180 Hz/pixel). On these images, 86.9% of the volume of the head was displaced less than 0.5 mm, 97.4% was displaced less than 1 mm, and 99.9% of voxels exhibited less than 2 mm displacement. The largest distortions occurred at interfaces with significant susceptibility differences, most notably those between the brain and either metal implants or (more significantly) adjacent air cavities. In the location with the largest displacement (interface with the sinus), the average displacement of 1.6 mm at the interface falls to below 1 mm approximately 7 mm away.

Examples of clinical use

We have implemented a number of scanning protocols in our first year of operation. Routine scans are performed for patients with intracranial lesions of all forms, as well as for those with nasopharyngeal tumors, hepatocellular carcinoma, and certain spinal and pelvic lesions. Routine use of the system for MRI-based brachytherapy of patients with cervical cancer using a ring and tandem system is currently pending modification of part of the applicator for safety and image quality reasons, although patients undergoing other implants (e.g. cylinders) have had MRI scans to support treatment planning.

Summary

We have implemented the initial phase of MRI-based radiation oncology simulation in our department, and have scanned over 300 patients since operations began just over one year ago. The system demonstrates sufficient geometric accuracy for supporting radiation oncology decisions for external beam radiation therapy, as well as brachytherapy. Work is ongoing in optimizing MRI scanning techniques for radiation oncology in various parts of the body and for various diseases. In addition to current and future work in optimizing MRI for use in routine radiation therapy, a variety of research protocols are underway using this system. A major current focus is on using MRI without CT for external beam radiation therapy. Results of these efforts will be presented in future articles.

References

1 Jenkinson M. Fast, automated, N-dimensional phase-unwrapping algorithm. Magn Reson Med. 2003 Jan;49(1):193-7.
2 Dimopoulos JC, Petrow P, Tanderup K, Petric P, Berger D, Kirisits C, Pedersen EM, van Limbergen E, Haie-Meder C, Pötter R. Recommendations from Gynaecological (GYN) GEC-ESTRO Working Group (IV): Basic principles and parameters for MR imaging within the frame of image based adaptive cervix cancer brachytherapy. Radiother Oncol 103(1):113-22, 2012.
3 Wang H, Balter J, Cao Y. Patient-induced susceptibility effect on geometric distortion of clinical brain MRI for radiation treatment planning on a 3T scanner. Phys Med Biol 58(3):465-77, 2013.

Contact

James M. Balter, Ph.D., FAAPM
Professor and co-director,
Physics division
Department of Radiation Oncology
University of Michigan
Ann Arbor, MI
USA
Phone: +1(734)936-9486
jbalter@umich.edu

Management of MRI Spatial Accuracy for Radiation Therapy

Teo Stanescu, Ph.D.; David Jaffray, Ph.D.

Princess Margaret Cancer Centre, University Health Network; Department of Radiation Oncology, University of Toronto, Toronto, ON, Canada

Introduction

Radiation Therapy (RT) demands tight constraints regarding the geometric accuracy of image data used in its workflows for treatment simulation and in-room treatment delivery guidance. The spatial accuracy requirements are largely driven by the ability to deliver and deposit therapeutic radiation doses to targeted anatomical sites (1-2 mm). The benefits of MRI's superior soft-tissue contrast as compared to RT's gold standard based on x-ray imaging (i.e. CT, Cone Beam CT) are somewhat overshadowed by the intrinsic MR image distortions manifested as loss of spatial accuracy and local intensity inhomogeneities.

The MR image distortions are given by a) scanner-related distortions caused by nonlinearities in the imaging gradients and inhomogeneities in the main magnetic field (B_0), and b) patient-induced distortions mainly due to variations in the magnetic susceptibility properties of neighboring tissues (and chemical shift). The scanner-related distortion field (S) is predictable, independent of the imaged subject and its spatial characteristics are static over time given optimal functionality of the MR system. S magnitude is negligible in the vicinity of the MR isocenter and gradually increases with distance, reaching about 1-2 cm for large fields of views [1-3]. In comparison, the susceptibility-induced distortion field (X) is highly dependent on the subject anatomy as they arise at the boundary between structures exhibiting local discontinuities in the susceptibility (χ) values, e.g. soft-tissue and air-filled cavities. The magnitude of χ effects is in the range of a few millimeters and depends on several factors such as magnetic field and encoding gradient strength [4, 5].

A composite distortion field (C) can be defined as the vector summation of S and X, to characterize the combined aspects of the two fields [6]. S and X

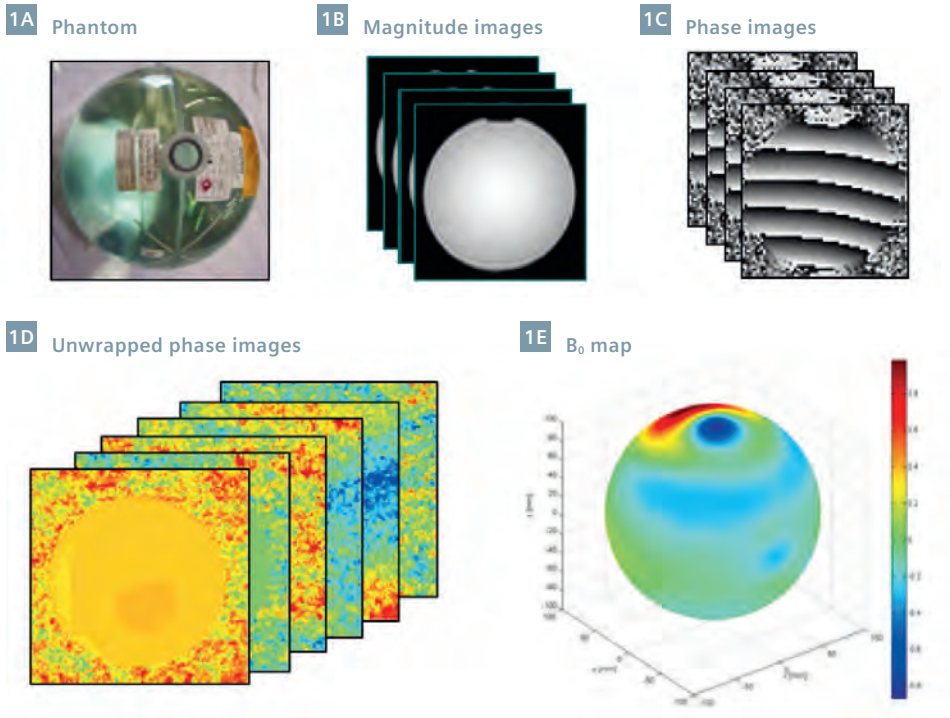

1 B_0 mapping: the magnitude images of a spherical uniformity phantom are used to facilitate the segmentation and analysis of the phase images. The 3D distribution of the magnetic field is then computed from the unwrapped phase images and B_{rms} and B_{pp} values are derived to quantify the overall field homogeneity. Visualization of the 3D map is also provided for trouble-shooting purposes.

have negligible mutual coupling and can be treated independently following dedicated methodology. When C is associated with intrafraction motion, specific to mobile anatomical structures, it becomes more complex featuring 4D characteristics, e.g. for fast imaging 2D-cine, 4D MR. The quantification of C is then particularly challenging due to real anatomical changes in the targeted structure's volume, shape and relative location within the MR imaging volume. The accurate knowledge of a tumor's true contours during the motion cycle is paramount for advanced RT planning and delivery techniques which are based on radiation field gating or tracking [7, 8].

MR manufacturers made significant progress over the past years in implementing improved hardware and algorithms to reduce the magnitude of S. However, residual distortions are still an issue for RT applications [9]. Overall, the geometric distortions need to be well-understood for each MR-based technique and appropriate mitigation implemented to safely integrate MR data in radiotherapy workflows. Our work on the management of MR image distortions is motivated by the clinical implementation of MR-guided brachytherapy and external beam RT technologies and to enable MR-based adaptive procedures [10].

Scanner-related distortions

Routine testing for monitoring the field homogeneity and its stability is recommended as a pre-requisite for good imaging. As part of our standard procedures for MR commissioning and periodic quality control (QC) of the system shim, we develop and implemented a fast B_0 mapping technique based on a) phantom data acquisition with a GRE double-echo sequence and b) an image processing algorithm for data reformatting and phase unwrapping, and c) generation of analytics and reporting. The simplified flowchart is shown in Figure 1. First, magnitude and phase images are collected with a uniformity phantom. Then phase unwrapping is performed using the PUROR method [11] and metrics such as B_{rms} (root mean square) and B_{pp} (peak-to-peak) are computed and reported in a ready to print file. The image acquisition and post-processing was optimized to match the performance of the Phantom Shim Check procedure available in the Siemens service environment (1.5T MAGNETOM Espree, with software version *syngo* MR B17A). The total time to scan and run the analysis on a mid-range PC workstation is under 100 seconds.

It is typical to quantify the gradient nonlinearities using a) a theoretical approach considering the spherical harmonics coefficients specific to each gradient set or b) via measurements with a linearity phantom. Although the theoretical approach is very appealing as it can be easily streamlined for image unwarping of live image data, it does not fully compensate for the image geometric errors [3, 9]. A phantom with a known structure, the most common being a 2D or 3D grid pattern, is desirable to measure the remainder of the distortions. In RT one of the requirements is to accurately define the anatomy for both small and large field of views, which means that the linearity phantoms should be able to provide enough spatial coverage. In particular, at large FOVs a phantom with a grid pattern needs to fill the entire volume to provide adequate sampling for S, which often translates into increased phantom weight. The manufacturing, routine preparation (positive or negative contrast) and manipulation of such a phantom may also be challenging.

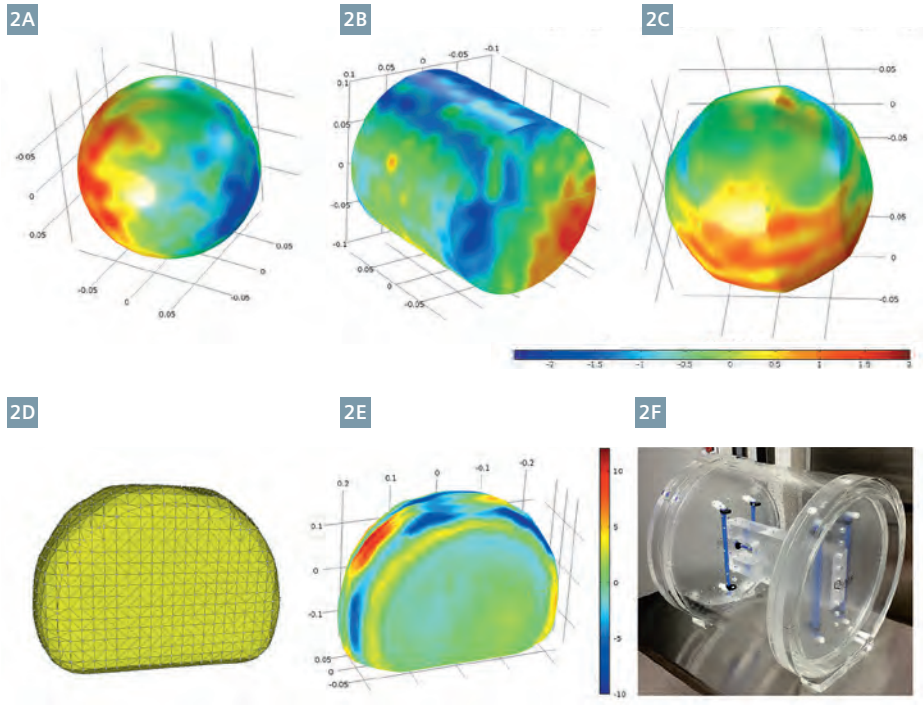

2 Harmonic analysis was applied to compute the 3D distortion vector field for an arbitrarily shaped volume from data measured on the surface. **(2A)** and **(2B)** show basic quadratic geometries; **(2C)** shows a Reuleaux 9-gon to test the method for a more complex structure; **(2D)** depicts the meshed and irregular surface of an MR imaging FOV as measured with a large phantom based on a grid design; **(2E)** the surface data corresponding to **(2D)** was used as BC in the harmonic analysis to stress-test its performance.

To address the above limitations our group focused on a design which minimized phantom material, weight and implicitly the manufacturing cost without compromising the accuracy in quantifying S. The design was driven by the ability to fully reconstruct S in a given volume solely from field data mapped on the geometry's surface [12]. This means that harmonic analysis can be applied to S, since S is natively related to the magnetic field. Specifically, the Laplace equation was solved with well-defined Dirichlet boundary conditions (BC) for functions representing the 3D geometric distortion vector field. The Dirichlet BCs were given by the measured vector field values corresponding to the domain's boundary. The method was validated for multiple quadratic and arbitrary geometries. In particular, Figure 2E depicts sample results for a general case of a highly irregular surface, which wraps the raw data measured on a grid phantom with a high density of control points. The case is challenging due to the magnitude and local gradients specific to S at large FOVs. A cylindrical shell phantom and associated software application based on the harmonic analysis was developed in collaboration with Modus Medical Devices (London, ON, Canada) as shown in Figure 2F [13].

Susceptibility-induced distortions

The field X is challenging to predict or quantify, especially when live image data is needed for the clinical decision making process. The map of tissue susceptibility-induced effects may change even for the same patient as a function of daily anatomy. Several methods were proposed in the literature to assess the χ perturbations [5, 4, 15]. Rather than measure the susceptibility, which often requires additional image data leading to longer acquisitions times, we chose to investigate the χ effects by means of numerical simulations [4, 6]. A finite difference technique iteratively solves the Maxwell equations with associated BCs for the case of a time independent and uniform magnetic field (i.e. B_0 of an MR scanner). The input data is given by 3D susceptibility maps synthetically generated by assigning bulk χ values to anatomical structures delineated on CT image data sets. CT images were used to ensure the spatially true representation of the anatomy and to dissociate the χ effects from other potential sources of geometric inconsistencies (e.g. B_0 and B_1 local inhomogeneities, S). Magnetic field maps expressed in terms of ppm values were set as the output of the numerical computations. The spatial distortions (in mm) were then easily converted by specifying the B_0 and readout gradient values ($\Delta_{mm} = ppm \cdot B_0 / G_E$). Furthermore, the Δ_{mm} values were interpolated and reported for the anatomical regions of interest. The simulation method was validated in phantom using a wide range of G_E values at 1.5T and 3T.

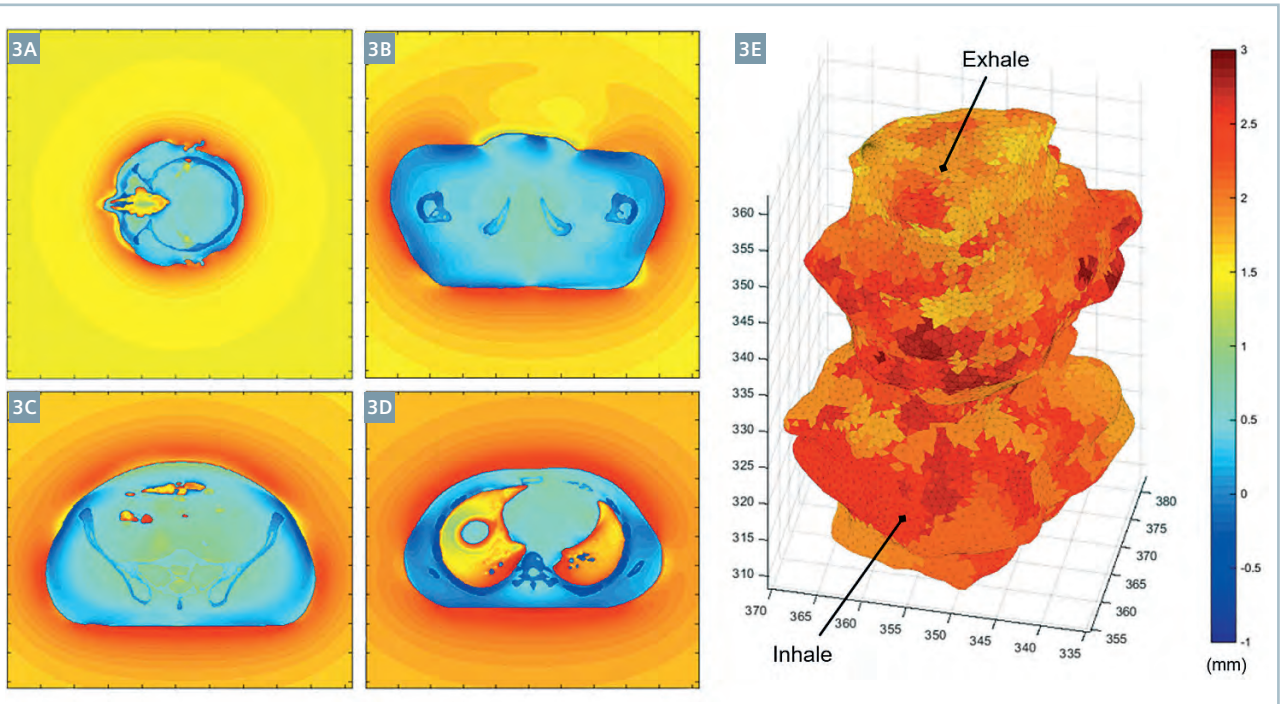

3 Sample results of the magnetic field numerical computations performed to investigate the magnitude of χ geometric effects. Multiple anatomical regions were simulated such as **(3A)** brain (whole skull), **(3B)** prostate, **(3C)** abdomen/upper GI, and **(3D)** lung. Inset **(3E)** shows the 4D composite distortion field results for a small and mobile lung tumor as estimated for the two extreme phases of the respiratory cycle, i.e. inhale and exhale.

Figure 3 shows several examples of X as modelled for specific anatomical sites. We found the data useful for at least two reasons: a) estimate the maximum boundary of the X effects for a given site and b) generate $\Delta_{mm}=f(G_E)$ curves for B_0 values of interest. The trends from b) were used to guide the optimization of clinical imaging protocols so that the geometric distortions were mitigated while the SNR penalty for increasing G_E was minimized. Therefore, our approach was to predict the X effects outcome for patient populations and compensate upfront whenever possible.

4D Composite distortion field

The raw MR images intrinsically embed the effects of both scanner-related and X-induced geometric distortions. The assessment of C for mobile tumors may be particularly non-trivial due to continuous variations in the local profile of the S and X fields as experienced by the tumors [6]. For example, S is static with respect to the MR scanner, but when seen from the mobile tumor's system of reference it becomes time-dependent as the target travels in regions with potentially different local S values. Therefore, a 4D characteristic may be associated with S. Similarly, X becomes 4D as the tumor deforms and changes location relative to surrounding anatomical landscape. To evaluate the upper boundary of the 4D composite field we combined the methodologies from above for S and X in the case of mobile lung tumors. The susceptibility simulations were performed for 10 separate 3D data sets representing individual phases of the breathing cycle as captured with 4D CT imaging. S was also derived for all tumor motion phases via vector field interpolation. Metrics such as max/mean/range and spatial perturbations in the tumor's center of mass were reported for the individual and combined fields. An example is shown in Figure 3E. The dominant contribution was from S, and it was suggested that a unique C correction (e.g. derived from one phase or a mean phase) may be applied to all tumor phases with negligible residual errors. For fast imaging, X was found largely negligible as a high BW is typically employed.

Summary

The quantification of geometric distortions is needed especially for radiation therapy applications to ensure a high degree of image data accuracy. Knowing the true location of the targeted anatomy may enable the use of tighter treatment margins expected to improved tumor control through dose escalation and increased sparing of healthy tissues. The assessment of MR image distortions is recommended to be part of the MR scanner commissioning and routine quality control. The susceptibility effects may be minimized within acceptable thresholds in certain applications whereas the scanner-related distortions may be mapped via phantoms and unwrapped on patient data when relevant.

References

1 D. Wang, W. Strgnell, G. Cowin, D.M. Doddrell, R. Slaughter, "Geometric distortion in clinical MRI systems Part II: correction using a 3D phantom," Magn. Reson. Imag. 22(9):1223-32 (2004).

2 S.F. Tanner, D.J. Finnigan, V.S. Khoo, P. Mayle, D.P. Dearnaley, M.O. Leach, "Radiotherapy planning of the pelvis using distortion corrected MR images: the removal of system distortions," Phys. Med. Biol. 45:2117-2132 (2000).

3 S.J. Doran, L. Charles-Edwards, S.A. Reinsberg, M.O. Leach, "A complete distortion correction for MR images: I. Gradient warp correction," Phys. Med. Biol. 50(7):1343-61 (2005).

4 T. Stanescu, K. Wachowicz, D.A. Jaffray, "Characterization of tissue magnetic susceptibility-induced distortions for MRIgRT," Med. Phys. 39(12):7185-93 (2012).

5 R. Bhagwandien, M.A. Moerland, C.J.G. Bakker, R. Beersma, J.J.W. Lagendijk, "Numerical analysis of the magnetic field for arbitrary magnetic susceptibility distributions in 3D," Mag. Res. Imag. 12:101-107 (1994).

6 T. Stanescu, D. Jaffray, "Investigation of the 4D composite MR image distortion field associated with tumor motion for MR-guided radiotherapy," Med. Phys. (in press).

7 M.B. Tacke, S. Nill, A. Krauss, U. Oelfke, "Real-time tumor tracking: automatic compensation of target motion using the Siemens 160 MLC," Med. Phys. 37(2):753-61 (2010).

8 A. Sawant, R.L. Smith, R.B. Venkat, L. Santanam, B. Cho, P. Poulsen, "Toward submillimeter accuracy in the management of intrafraction motion: the integration of real-time internal position monitoring and multileaf collimator target tracking," Int. J. Radiat. Oncol. Biol. Phys. 74(2): 575-82 (2009).

9 A. Walker, G. Linley, P. Metcalf, L. Holloway, "MRI distortion: considerations for MRI based radiotherapy treatment planning," Austral. Phys. Engin. Sci. Med. 37(1):103-113 (2014).

10 D. Jaffray, M. Carlone, M. Milosevic, S. Breen, T. Stanescu, "A facility for magnetic resonance-guided radiation therapy," Semin. Radiat. Oncol. 24(3):193-5 (2014).

11 J. Liu, M. Drangova, "Intervention-based multidimensional phase unwrapping using recursive orthogonal referring," Magn. Reson. Med. 68(4):1303-16 (2012).

12 T. Tadic, D. Jaffray, T. Stanescu, "Harmonic analysis for the characterization and correction of geometric distortion in MRI," Med. Phys. 41(11):112303 (2014).

13 http://modusqa.com/imaging/phantoms/mrid3d

14 H. Chang and J. Fitzpatrick, "A technique for accurate magnetic resonance imaging in the presence of field inhomogeneities," IEEE Trans. Med. Imaging 11, 319–329 (1992).

15 M. Jenkinson, J. L. Wilson, and P. Jezzard, "Perturbation method for magnetic field calculations of nonconductive objects," Magn. Reson. Med. 52(3), 471–477 (2004).

Dr. David Jaffray

Dr. Teo Stanescu

Contact

Teo Stanescu, PhD, MCCPM
Assistant Professor
Princess Margaret Cancer Centre
610 University Avenue
Toronto, ON, M5G 2M9
Canada
Phone (416) 946-4501 Ext. 5071
teodor.stanescu@rmp.uhn.ca

Comprehensive RT-Specific QA for MRI Simulation

Eric Paulson, Ph.D., DABR

Medical College of Wisconsin, Radiation Oncology, Milwaukee, WI, USA

Introduction

MRI simulation is the process of acquiring high fidelity, high contrast resolution magnetic resonance images to identify true disease extent and proximity relative to adjacent organs at risk (OAR) for the purposes of radiation treatment planning. MRI simulation can be performed using dedicated MRI scanners in radiotherapy departments [1] or using MRI scanners sited in other departments as shared resources. As more radiotherapy departments begin incorporating MRI simulation into routine treatment planning, questions often arise regarding what level of quality assurance (QA) activities are required to maintain accuracy and avoid errors. Several well-established references from the American College of Radiology (ACR) [2-3] and American Association of Physicists in Medicine (AAPM) [4-6] provide guidance regarding acceptance testing (AT), commissioning, and routine QA of MRI scanners. However, while these manuals provide procedures and tolerances for general MRI QA, no guidance documents exist that describe the unique radiotherapy-specific QA activities that need to be considered. Radiation therapy presents a new set of challenges and places additional demands on MRI compared to diagnostic radiology that, if not properly addressed, can undermine the advantages MR images offer for treatment planning. The goal of this article is to describe a comprehen-sive MRI simulation QA program to address the RT-specific QA activities required for MRI simulation.

RT-specific acceptance testing and commissioning activities for MRI simulators

Acceptance testing and commissioning of an MRI scanner often involves a series of tests from the MRI scanner vendor as well as tests recommended in ACR and AAPM guidance documents. These tests can include characterization of static magnetic field (B_0) homogeneity and drifting, radiofrequency field (B_1) gains, percent image uniformity, percent signal ghosting, slice position and thickness accuracy, and others. The majority of the latter tests are performed using the ACR MRI QA phantom [2-3]. While initial AT measurements are useful for establishing constancy benchmarks for routine MRI QA, certain tests more relevant for radiotherapy (e.g., geometrical accuracy) may not be fully characterized based on measurements of the ACR MRI QA phantom, due to the relative small size of the phantom.

Beyond the general AT and commissioning activities discussed above, RT-specific activities should also be considered. Table 1 provides a summary of the RT-specific AT and commissioning activities for MRI simulators. The fringe fields of dedicated MRI simulators sited in radiotherapy departments may affect the performance of conventional linear accelerators (LINACs) installed proximal to the MRI simulator. The strength of these fringe fields should be mapped and verified to be within the tolerance specified by the LINAC manufacturer. Residual geometric distortions that persist following three dimensional gradient nonlinearity correction should be characterized by evaluating images of a large grid phantom scanned, ideally, using a reversed gradient technique [7]. These residual distortions may affect the geometric accuracy of delineated anatomy, particularly when large field-of-view prescriptions are utilized (e.g., supine breast). In addition, optimization of RT-specific MRI simulation imaging protocols should be performed [1] utilizing thin, contiguous slices, high readout bandwidths, high order shimming, and spin echo sequences to minimize chemical shift and patient-induced distortions. The accuracy of respiratory gating and triggering windows should be assessed using dynamic motion phantoms, particularly for those institutions wishing to match the MRI acquisition to the same respiratory phases used for gated radiation therapy deliveries. For those MRI simulator suites in which external lasers are available, the longitudinal distance between the laser and MRI isocenters must be determined and configured as offsets in the MRI simulation imaging protocols. Finally,

Table 1:
RT-specific acceptance testing and commissioning activities for MRI simulators

	Acceptance Testing and Commissioning Activities
☐	Determine fringe field strength at conventional LINACs proximal to MRI simulator[1]
☐	Characterize residual distortions following 3D gradient distortion correction
☐	Optimize MRI simulation imaging protocols (FOV, slice thickness, skip, rBW, etc.)
☐	Determine the accuracy of respiratory gating windows and triggering positions
☐	Determine longitudinal offset distance between external laser and MRI isocenters[2]
☐	Perform end-to-end tests utilizing RT peripheral equipment (all orientations)[3]

[1] Required for MRI simulators sited in radiotherapy departments
[2] Required for MRI simulators equipped with external laser systems
[3] Also required following upgrades to MRI system or RT peripheral equipment

end-to-end testing utilizing ancillary RT-specific equipment, including flat table overlays, coil bridges, immobilization devices, and external lasers should be performed.

In terms of personnel, it would be most desirable if a team of MRI physicists and radiation therapy physicists performed the activities listed in Table 1. Alternatively, the activities could be performed by individuals cross-trained in both MRI and radiation therapy physics.

RT-specific daily QA activities for MRI simulators

Once AT and commissioning have been performed, a routine QA program needs to be established. Daily, monthly, and annual activities comprise our routine QA program for MRI simulators. Table 2 provides a summary of the RT-specific daily QA activities. These activities are performed during morning warm-up, similar to daily QA of other equipment in the radiotherapy department.

Minimization of geometric distortions is pivotal to the success of MRI simulation. Despite patients being screened for loose metal prior to MRI exams, it can be common to find bobby pins, earrings, and other small metal fragments lining the magnet bore. The presence of these items may affect the homogeneity of the static magnetic field and, consequently, contribute to geometric distortions. A quick daily inspection and swiping of the scanner bore for the presence of loose metal mitigates this issue. In addition, flexible phased-array receive coils are often utilized during MRI simulation exams. These coils permit the patient to be imaged in treatment position using immobilization devices. However, the repeated wrapping of the coils can lead to a higher likelihood of failure due to breakage of internal coil elements. Therefore, a short signal-to-noise ratio (SNR) and brightness check is performed daily on alternating coils used for MRI simulation exams. An alternative approach may be to extract receive coil gain information directly from log files on the MRI scanner. Finally, components involved in patient safety are also tested daily, including the intercom, panic ball, and metal detector.

Table 2: RT-specific daily QA activities for MRI simulators.

	Daily QA Activities
☐	Inspect/sweep bore for loose metal (bobby pins, earrings, fragments, etc.)
☐	Flexible RF coil inspection, SNR, brightness measurements (alternating each day)
☐	Patient safety (intercom, panic ball, metal detector)
☐	Laser alignment, isocenter agreement, couch position accuracy, end-to-end test[4]
☐	B_0 drift[4]
☐	Basic geometric accuracy[4]

[4] For sites utilizing MR-only workflows

Table 3: RT-specific monthly QA activities for MRI simulators.

	Monthly QA Activities
☐	Laser adjustment, isocenter agreement, couch position accuracy, end-to-end test[5]

[5] Required for MRI simulators equipped with external laser systems

For institutions utilizing MRI-only[6] workflows (i.e., MRI-derived images used for both delineation and dose calculation), it is essential to verify the accuracy of the laser-MRI coordinate systems on a daily basis. This includes verifying laser alignment, external laser to MRI isocenter constancy, and couch position accuracy. In addition, a quick end-to-end test should be performed to ensure the lasers used for marking patients are driven to the isocenter location prescribed on the MR images. Daily B_0 drift and basic geometric accuracy can also be evaluated using the same MR images obtained for the end-to-end test.

The RT-specific daily QA activities listed in Table 2 would ideally be performed by radiation therapists who have received additional cross-training in MRI. For sites utilizing MR-only workflows, the activities could alternatively be performed by diagnostic MRI technologists who have received cross-training in radiotherapy software used for isocenter placement.

RT-specific monthly QA activities for MRI simulators

For radiotherapy departments that utilize MRI scanners sited in other departments as shared resources, or sites that perform diagnostic MRI exams in addition to MRI simulation exams on dedicated MRI scanners sited in radiotherapy departments, weekly QA is often performed by diagnostic MRI technologists to maintain ACR accreditation. Commercial or open source [8] software is available to automate image quality analysis of the weekly QA images based on guidelines and action limits established by the ACR [2]. In these scenarios, in which the monitoring of MRI simulator performance can occur jointly across departments, reducing the workload for radiotherapy personnel.

Beyond general image quality activities recommended for MRI, the only RT-specific monthly QA activity for MRI simulators (see Table 3) involves laser adjustment for those MRI simulator suites equipped with external laser systems [9]. Ideally, these adjustments would be made by radiation therapy physicists.

RT-specific annual QA activities for MRI simulators

Annual MRI QA activities (including SNR and brightness tests of dedicated coils used for diagnostic imaging, magnetic field homogeneity, etc.) are performed by MRI physicists to maintain ACR accreditation [2]. Beyond these general QA activities recommended for MRI, no additional RT-specific QA activities are performed for MRI simulators on an annual basis.

[6] Radiotherapy Planning where MR data is the only imaging information is ongoing research. The concepts and information presented in this article are based on research and are not commercially available. Its future availability cannot be ensured.

RT-specific patient QA checklist for MRI simulation

Although conceptually, the process of virtual simulation using MRI parallels that of CT, there are several additional steps that must be performed before, during, and after an MRI simulation exam in order to maintain the high accuracy required for radiation treatment planning. To protect against human performance failures, a checklist of patient-specific QA activities (see sample checklist in Table 4) was designed similar to the safe surgery checklists [10] derived from the airline industry. The checklist items would ideally be performed during an MRI simulation exam by a radiation therapist who has received additional cross-training in MRI.

Summary

A comprehensive MRI simulation QA program consists of unique RT-specific QA activities that supplement established, general MRI QA activities. For many institutions, QA activities can be split between radiotherapy and diagnostic radiology departments. With the move toward MR-only treatment planning, comprehensive QA programs will be essential to protect against machine and human performance failures and maintain the high levels of accuracy required for radiation therapy.

*The MRI restrictions (if any) of the metal implant must be considered prior to patient undergoing MRI exam. MR imaging of patients with metallic implants brings specific risks. However, certain implants are approved by the governing regulatory bodies to be MR conditionally safe. For such implants, the previously mentioned warning may not be applicable. Please contact the implant manufacturer for the specific conditional information. The conditions for MR safety are the responsibility of the implant manufacturer, not of Siemens.

Table 4: RT-specific patient QA checklist for MRI simulation exams

Yes	N/A	Task
☐	☐	Patient orientation (Cervix brachy: FFS; otherwise use treatment orientation)
☐	☐	Abdomen/Chest/Pelvis: Large RF flexible receive coils supported by coil bridges
☐	☐	Esophagus: ECG leads placed on patient
☐	☐	Cholangiocarcinoma: Nasal cannula placed on patient with oxygen at 2-3 liter/min
☐	☐	Cholangiocarcinoma: Injector loaded with Eovist (Bayer HealthCare, Whippany, USA)
☐	☐	Cervix brachy/Abdomen: 0.5 mg glucagon IV at start, midway of exam
☐	☐	Prostate: Bladder, rectum fill check
☐	☐	High order shim volume optimized and copied to each series
☐	☐	B_0 map acquired with body coil; magnitude and phase images reconstructed successfully
☐	☐	Additional diagnostic sequences added for MR Sim with interpretation
☐	☐	High bandwidths or Advanced WARP used for metal* (hip replacements, spine hardware)
☐	☐	Cervix brachy: 3D images acquired as straight axials
☐	☐	Abdomen/Esophagus: Breath holds at end expiration
☐	☐	Coverage sufficient (check order for directives and special instructions)
☐	☐	Images screened for artifacts. Did fatsat, Dixon separation work? (re-run if necessary)
☐	☐	Spine/Sarcoma: Upper+lower groups combined in 3D viewer or composer
☐	☐	Brain: rCBF mosaic separated into individual images (Application → Mosaic → Split)
☐	☐	3D distortion correction applied to all images
☐	☐	3D distortion-corrected images (DIS3D suffix) sent to treatment planning systems

Contact

Eric Paulson, Ph.D., DABR
Assistant Professor and Senior Medical Physicist
Radiation Oncology, Radiology, and Biophysics
Medical College of Wisconsin
Radiation Oncology
8701 Watertown Plank Road
Milwaukee, WI 53223
USA
epaulson@mcw.edu

References

1 Paulson ES, Erickson B, Schultz C, Li XA. Comprehensive MRI simulation methodology using a dedicated MRI scanner in radiation oncology for external beam radiation treatment planning. Med Phys 2015; 42:28-39.
2 American College of Radiology (ACR). Magnetic resonance imaging quality control manual. 2015.
3 American College of Radiology (ACR). MR accreditation program phantom test guidance. 2005.
4 American Association of Physicists in Medicine (AAPM). AAPM Report 28: Quality assurance methods and phantoms for magnetic resonance imaging. 1990.
5 American Association of Physicists in Medicine (AAPM). AAPM Report 34: Acceptance testing of magnetic resonance imaging systems. 1992.
6 American Association of Physicists in Medicine (AAPM). AAPM Report 100: Acceptance testing and quality assurance procedures for magnetic resonance imaging facilities. 2010.
7 Baldwin LN, Wachowicz K, Fallone BG. A two-step scheme for distortion rectification of magnetic resonance images. Med Phys 2009; 36:3917-3926.
8 Sun J, Barnes M, Dowling J, Menk F, Stanwell P, Greer PB. An open source automatic quality assurance (OSAQA) tool for the ACR MRI phantom. Australas Phys Eng Sci Med 2015; 38:39-46.
9 Mutic S, Palta JR, Butker EK, Das IJ, et al. Quality assurance for computed-tomography simulators and the computed-tomography-simulation process: Report of the AAPM radiation therapy committee task group No. 66. Med Phys 2003; 30:2762-2792.
10 Haynes A, Gawande A. A surgical safety checklist to reduce morbidity and mortality in a global population. New Eng J Med 2009; 360:491-499.

Advance your clinical capabilities with the MAGNETOM RT Pro edition

For more information please visit us at: siemens.com/mri

Go to: MRI in Therapy > MAGNETOM RT Pro edition

MRI in Clinical Radiation Oncology: Dosimetry and Patient-Specific Plan Verification

Niko Papanikolaou, Ph.D.[1]; Geoffrey D. Clarke, Ph.D.[1]; Lora T. Watts, Ph.D.[1]; Thomas G. Maris, Ph.D.[2,4]; Evangelos Pappas, Ph.D.[3,4]

[1] University of Texas Health Science Center, San Antonio, Texas, USA
[2] University of Crete, Medical School, Heraklion, Crete, Greece
[3] Technological Educational Institute, Athens, Greece
[4] R&D department at RTsafe S.A., Athens, Greece

Introduction

The role of MRI in radiation oncology has been continuously evolving over the past decade. Radiation treatment planning, delivery and patient monitoring have been enriched through the increased use of MRI in radiotherapy clinical practice. Although MRI was originally introduced and continues to be a superb imaging modality for soft tissue characterization it has so far been used exclusively for imaging studies in humans and animals. There is however a novel application of MRI in the evaluation of radiation dose delivered to a phantom using dosimetry gels. Although the idea of gel-based dosimetry was introduced over two decades ago, its application in patient specific clones, with the explicit purpose of performing patient specific plan verification, is less than a year old.

Polymer gel MRI dosimetry was first introduced in 1993 and a large number of scientific publications exists on this topic, including a review by Baldock et al. [1]. The essence of this dosimetric method is that the local polymerization induced to a polymer gel after it has been irradiated, can be detected and quantified by MRI. The higher the dose absorbed within an elementary voxel of a polymer gel, the higher the amount of polymerization within that voxel and therefore the slower the water molecules motion within it, resulting in a lower T2 spin-spin relaxation time. Therefore, absorbed dose and T2 are directly and monotonically related. Accurate and quick measurements of T2 values can thus be converted to dose measurements. Moreover, given the 3D nature of MR scanning, polymer gel MRI dosimetry is inherently a 3D-dosimetry method.

Polymer gel MRI dosimetry has not entered radiotherapy clinical practice, mainly because of the practical issues of access to an MRI scanner, but more importantly because there was no demonstrable need for accurate 3D dosimetry in stylized phantoms. Consequently, polymer gel MRI dosimetry was until recently a research topic rather than a clinical tool. However, in early 2015 a novel application of gel dosimetry was introduced, whereby polymer gels were used as an end-to-end quality assurance and patient-specific plan verification process in radiotherapy [2-4]. An increasing number of radiotherapy centers world-wide have already started to adopt this novel clinical tool which has now been commercialized by RTsafe S.A. (Athens, Greece).

Gel dosimetry provides a new opportunity and a challenge for MRI scanners in the arena of clinical radiotherapy: how to obtain quick and accurate measurements of T2 relaxation times in three dimensions with minimal spatial distortions. We have found that the 2D HASTE multi echo Carr-Purcell-Meiboom-Gill (CPMG) sequence addresses this challenge.

The challenges with MRI T2 relaxometry in polymer gel dosimetry and the way by which the HASTE pulse sequence addresses these challenges are described below. A clinical example of the use of an MRI scanner with gel dosimetry for patient-specific dosimetric and geometric plan verification is also presented for a clinical case of a multiple metastases SRS treatment.

MRI HASTE T2 relaxometry in polymer gel dosimetry

In polymer gel MRI dosimetry, the R2 spin-spin relaxation rates (R2=1/T2) are linearly related with the absorbed radiation doses. This is the basic relationship present on the radiation induced polymerization phenomenon which shortens the T2 values which in turn, are measured by MRI techniques in polymer gel dosimetry. Their relationship (R2 vs. Dose) serves a linear calibration curve dependent on the chemical composition and the fabrication conditions of the gel material. A plethora of chemical formularies and fabrication procedures exist in the literature, all being suitable for gel dosimetry [1]. The purpose of this analysis is twofold. Firstly, to present the clinical MRI T2 relaxation measurement sequences available on all commercial Siemens MRI scanners that are used for the measurement of

the Vinylpyrrolidone (VPL) based polymer gel dosimeters [5-8], and secondly, to present the solution of the HASTE sequences for the T2 relaxation measurements in polymer gel dosimetry.

The basic rationale is that all of the T2 measurements can be performed by utilizing sequences that exist on all Siemens commercial clinical MRI systems. There are four distinct technical challenges.

Challenge 1: To accurately measure with MR imaging T2 values ranging from approximately 1000 ms to 200 ms, for pre and post irradiation respectively of a VPL polymer gel receiving a dose of 30 Gy.

Challenge 2: To obtain the best possible in-plane and cross-plane spatial resolution. An ideal resolution would be an MR image with a voxel size of 1 x 1 x 1 mm^3.

Challenge 3: To achieve the best possible geometrical representation of true physical volumes throughout the total depicted imaging volume by eliminating any geometrical distortions.

Challenge 4: To limit the total examination time to a minimum while maximizing the measured signal-to-noise-ratio (SNR).

The quest is to produce an MRI sequence that satisfactorily addresses all four challenges.

Addressing challenge 1:

We need an accurate and fast multi-echo sequence designed for T2 relaxometry, covering a range of T2 measurements between 200 and 1000 ms. The existing MR sequences on a Siemens clinical MRI system are:

a. The 2D SE multi echo PHAPS sequence

This sequence is implemented on a 2D mode. Its advantages and disadvantages for multi-echo T2 relaxometry are:

Advantages: 32 equidistant echoes, use of high receiver bandwidths, same receiver bandwidth on each echo

Disadvantages: No 3D mode, no physical space filling on the 2D mode, no possibility of choosing asymmetric echoes in time, no use of RF restore pulses, long imaging time for either single or multi slice acquisition

b. The 2D TSE (RARE) multi echo CPMG sequence

This sequence is implemented on a 2D mode. Its advantages and disadvantages for multi-echo T2 relaxometry are:

Advantages: Physical space filling on the 2D mode, use of high receiver bandwidths, same receiver bandwidth on each echo, use of RF restore pulses, imaging time is reduced by increasing the Echo Train Length (ETL) factor and is independent from the chosen number of slices

Disadvantages: Only 3 echoes, no 3D mode, no possibility of choosing asymmetric echoes

c. The 2D HASTE multi echo CPMG sequence

This sequence is implemented on a 2D mode. Its advantages and disadvantages for multi-echo T2 relaxometry are:

Advantages: Physical space filling on the 2D mode, use of high bandwidths, same bandwidth on each echo, choice of asymmetric echoes, use of restore pulses, imaging time is only related to the number of slices. It is reduced by minimizing the number of slices and is kept minimum, due to the use of the highest possible ETL factor

Disadvantages: Only 4 echoes, no 3D mode

Addressing challenge 2:

The highest possible in-plane and cross-plane spatial resolution is required. Spatial resolution can be expressed by the MR image voxel physical dimensions and is mainly dependent on the gradient strength of the MR system. In-plane spatial resolution is fundamentally related to the physical dimensions of the selected field-of-view (FOV) and the raw data reconstruction matrix.

Cross-plane spatial resolution (slice thickness) depends on the slice selection gradient strength. In cranial T2 relaxometry, where an FOV of 250-300 mm is used, an in-plane spatial resolution of 1 x 1 mm^2 and a cross-plane spatial resolution of 2 mm could be easily achieved. This spatial resolution of 1 x 1 x 2 mm^3 is the practical limit, when using all of the above MR relaxometry sequences on most of the Siemens clinical MR systems. Spatial resolution can be improved by using software spatial interpolation to 0.5 x 0.5 x 1 mm^3.

Addressing challenge 3:

Appropriately designed MR sequences and methods are needed to eliminate MRI geometrical distortions, related either to the system's hardware problems like gradient non-linearities or B_0 inhomogeneities, or to distortions induced by the scanned objects themselves. Geometric distortions related to systems' hardware problems can be eliminated either by extensive gradient calibration and Eddy current compensation procedures or by post-processing distortion correction software tools. Software distortion correction data can be obtained from the use of special MRI phantoms covering large imaging volumes.

Geometrical distortions of scanned objects can originate either by chemical shift spatial miss-registrations or by magnetic susceptibility artifacts which in turn distort the local magnetic field homogeneity. Fortunately, both types of such object-related geometric distortions can be eliminated by the use of the highest possible receiver bandwidths embedded on special MR sequences. Receiver bandwidths strongly depend on the MR systems' gradients. The higher the gradients used the higher the receiver's bandwidths.

In cranial T2 relaxometry, a typical receiver bandwidth of 500 Hz/pixel or greater is a prerequisite when using Siemens MRI systems with gradient strengths at the range of 30 mT/m. Such a high bandwidth is capable of eliminating to a large

extent most of scan object induced geometric distortions.

Addressing challenge 4:

Fast MR sequences are necessary to reduce examination time and maintain SNR to an acceptable practical level (SNR > 80, at a field strength of 1T, for a standard 2-channel Head CP coil). However, we also have to keep spatial resolution to the above-mentioned practical limit of 1 x 1 x 2 mm³. HASTE sequences are by definition the fastest MR sequences available on the Rapid Acquisition with Relaxation Enhancement (RARE) regime. They were developed specifically to minimize the patient scan time.

In cranial T2 relaxometry, HASTE sequences can be modified by utilizing a multi-echo pattern of 4 non time equidistant echoes for the goals of relaxometry. SNR is maintained to more than the practical acceptable level for a spatial resolution of 1 x 1 x 2 mm³. Therefore, HASTE sequences are the solution to challenge 4. For the Siemens clinical MR systems, equipped with the standard 8-channel phased array head coil, a standard cranial HASTE T2 relaxometry examination time is in the range of 10-15 minutes.

By summarizing all the above challenges and respective solutions we can confidently conclude that HASTE sequences address all four challenges and as such are ideal for the T2 relaxometry methods applied for MRI gel dosimetry. Polymer gels suitable for MRI gel dosimetry purposes have T2 relaxation times that practically mimic soft tissues and human body fluids. HASTE sequences were designed to image soft tissues and human body fluids in the shortest possible examination times. Clinical HASTE sequences can therefore be easily modified by incorporating multi-echo trains in order to measure T2 relaxation times of dosimetric gel materials. In our implementation, we are using 4 echoes in a single echo train for T2 value measurements.

HASTE sequences can accommodate an RF restore pulse in order to restore longitudinal magnetization back to its equilibrium state prior to the following excitation. This technique is of paramount importance because it allows the users to keep TR (repetition time) as low as 2000 ms while accurately measuring T2 values. This feature has an important effect on the reduction of imaging time. Moreover, the possibility of using non-equidistant echoes is also one of the great advantages of the HASTE sequences, because it increases T2 measurement sensitivities for the chosen measurement range of T2 values in MRI gel dosimetry.

The last but not least advantage of the HASTE sequences is their time dependence on the number of anatomical slices. The fewer the slices obtained, the less the acquisition time. HASTE sequences are designed to operate in a sequential rather than an interleaved way. This means that each slice is acquired in one TR. This is not the case in all the other relaxometric sequences where parts of each slice are obtained in each TR. Acquisition time is linearly related to the TR factor. The main advantage therefore is that we can have a predefined set of slices covering a specific irradiated volume or multiple volumes, without having to cover the entire brain anatomy for the scan. This feature can dramatically reduce imaging time to the order of seconds, while maintaining high sensitivity for measuring T2 values.

Clinical example: Patient-specific pre-treatment plan verification of a single isocenter multiple-metastases SRS treatment

A single-isocenter 6-metastases SRS treatment plan has been implemented for a selected patient (details regarding the software and hardware used for the implementation of the treatment plan and the SRS treatment itself are out of the scope of this brief clinical example). The patient planning CT scans were used for the production of a 3D-replica of the selected patient that was printed with sub-millimeter accuracy (Fig. 1). This 3D-printed replica was then filled with a VPL polymer gel. The final product was a patient-specific dosimetry phantom that was used for patient-specific plan verification (this service is commercially available and marketed by RTsafe S.A.). This patient-specific phantom was then irradiated as if it was the actual patient, i.e. set-up, image guidance and irradiation were applied to this patient-specific phantom as would have been done to the real patient (the 3D printed bone structures of the phantom simulate accurately the real patient bones in terms of its interaction with radiation. Moreover, the polymer gel that fills the phantom simulates soft tissue in terms of its interaction with radiation). A 2D HASTE multi echo CPMG sequence was used for MRI scanning of the irradiated phantom.

This patient-specific dosimetry phantom was scanned on a 3T superconducting MR imager (MAGNETOM Trio, A Tim System, Siemens Healthcare, Erlangen, Germany. Gradient strength: 45 mT/m, slew rate: 200 mT/m/s). A standard quadrature RF body coil was used with all measurements and a standard 8-channel phased array head coil was used for signal detection. The phantom was placed in the supine position and entered the magnet cradle using the head-first configuration, by exactly mimicking the real patient positioning for a standard MRI head examination. A conventional gradient echo (GRE) 2D multi slice multi plane turbo Fast Low Angle Shot (turboFLASH) T1-weighted imaging sequence was initially applied in axial, sagittal and coronal planes for the localization of the phantom head anatomy.

Once localized, a series of a 2D, multi slice, multi echo, Half fourier Single Shot Turbo Spin Echo (HASTE) PD to T2-weighted sequence was utilized sequentially with no interslice delay time. The HASTE sequence was applied using 4 asymmetric spin echoes. The first TE was 36 ms and the rest 3 TEs were obtained thereafter approximately every 400 ms. With the above chosen parameters a sensitive multi-echo sequence for T2 measurements ranging from 1000 ms down to 200 ms was obtained. The relative HASTE sequence contrast related

1 Photographs of the 3D-printed patient-specific phantom just before its filling with VPL based polymer gel.

parameters were therefore: (TR/TE1/TE2/TE3/TE4/FA: infinite/36 ms/436 ms/835 ms/1230 ms/90°). An effective TR of 2000 ms was used. A standard RF restore pulse was used prior to next excitation in order to minimize examination time.

77 contiguous space filling oblique axial slices of 2 mm slice thickness were used. A FOV image area of 350 x 219 mm² was covered from each slice. The image reconstruction matrix was 256 x 160 pixels respectively to the FOV dimensions, corresponding to a square pixel matrix with pixel dimensions 1.4 X 1.4 mm² (in-plane spatial resolution). The cross-plane spatial resolution was equal to the slice thickness (2 mm). The overall spatial resolution expressed in raw data voxel dimension was 1.4 x 1.4 x 2 mm³. The total space filling imaging dimension on the cross-plane direction was 154 mm, covering the entire cranial anatomy.

The longer anatomical axis (anterior to posterior direction for the axial oblique slices) was chosen each time as the frequency encoding axis. The highest possible receiver bandwidth (781 Hz/pixel) was used in order to eliminate geometric distortions due to susceptibility artifacts. Geometric distortion filtering was also applied in order to eliminate geometric distortions due to inherent gradient field imperfections. The ETL factor for the specific HASTE sequence was 160 and the echo spacing was 4.54 ms. The overall SNR measured on the first echo proton density image was 280. 14 signal averages were used and the total examination time was approximately 20 minutes.

T2 measurements were obtained by utilizing the T2 HASTE quantitative MRI (T2-HASTE-QMRI) multi slice protocol, applied in reference to all 77 space filling slices. As a final result 77 space filling T2 calculated parametric maps were obtained, which were consequently transformed to 77 space filling relative dose maps. The minimum sensitive dosimetric volume was determined simply by the raw data voxel dimensions and was 1.4 x 1.4 x 2 mm³.

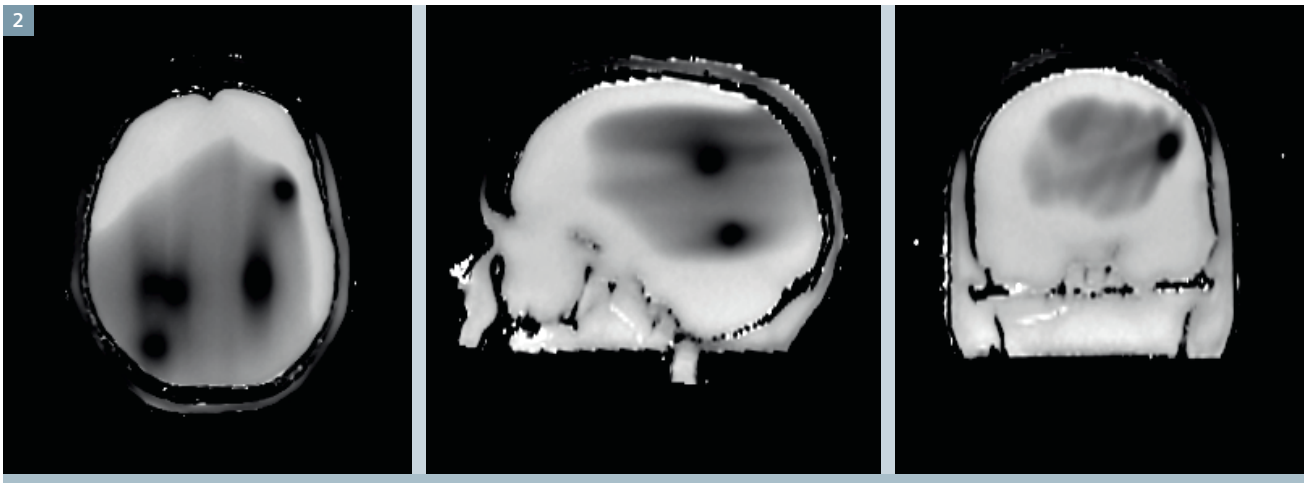

2 MRI T2 maps of the irradiated patient-specific phantom, derived using the 2D HASTE pulse sequence. Dark areas are the **low** T2 and therefore **high dose** areas. Brightness and contrast are adjusted so that high and low dose areas are depicted.

The MRI scans were used for the calculation of 3D-T2 maps. These T2 maps include the 3D dose information. The dark areas (low T2) are the high dose areas (Fig. 2) and the dose to (1/T2) linear relationship was measured using a calibration process.

The 3D-printing sub-millimeter accuracy of the patient-specific dosimetry phantom, allows a co-registration between the real patient planning CT scans (that also include the RTstructures and RTdose data in the same reference space) with the T2 maps of the irradiated phantom (Fig. 3). A first qualitative analysis reveals that the delivered dose (MRI scans) satisfactorily matches with the calculated dose (Treatment Planning System (TPS) RTdose data). The T2 maps correlate to the full 3D dose of the treatment that has been delivered. From the dose to (1/T2) calibration curve, the 3D T2 map was converted to a 3D dose map. Comparisons between the TPS RTdose calculations and the experimental 3D dose data are now possible. Therefore, quantitative data can be derived (Fig. 4).

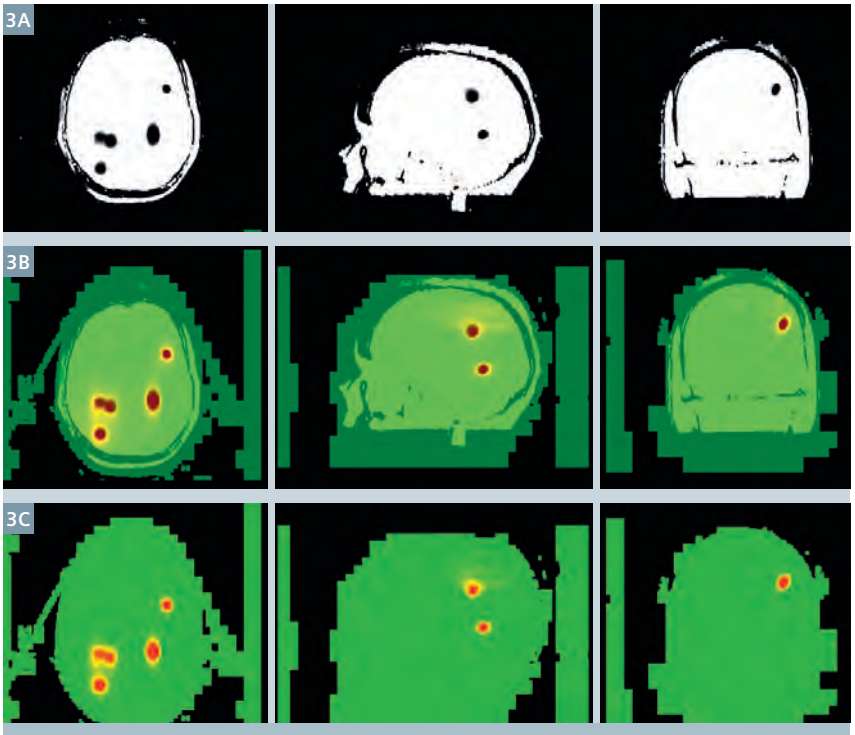

3 MRI T2 maps of the irradiated patient-specific phantom depicting the **actually** delivered dose, blended with 'RTdose' corresponding TPS **calculated** dose. **(3A)** MRI 100% – TPS 0%, **(3B)** MRI 50% – TPS 50%, **(3C)** MRI 0% – TPS 100%. Brightness and contrast adjusted so that only high dose areas are depicted. The T2 maps are co-registered to the real patient planning-CT scans. Therefore, a direct qualitative comparison with the TPS derived 'RTdose' data is feasible. A first qualitative inspection shows a satisfying spatial accuracy of dose delivery.

A significant number of radiotherapy centers, including University of Texas Health Science Center (San Antonio, TX, USA), The Royal Marsden NHS Foundation Trust (London, UK), the Institut Sainte Catherine (Avignon, France), Ichilov and Assuta Medical Centers (Tel Aviv, Israel) and the University of Freiburg (Freiburg, Germany) have started to implement end-to-end quality assurance tests and/or patient-specific plan verification procedures using this novel technique and their Siemens MRI scanners. Conclusively, a significant amount of data exists that supports the use of gel dosimetry for patient treatment QA and the claim that the HASTE pulse sequence is ideally suited to perform such 3D dosimetry measurements.

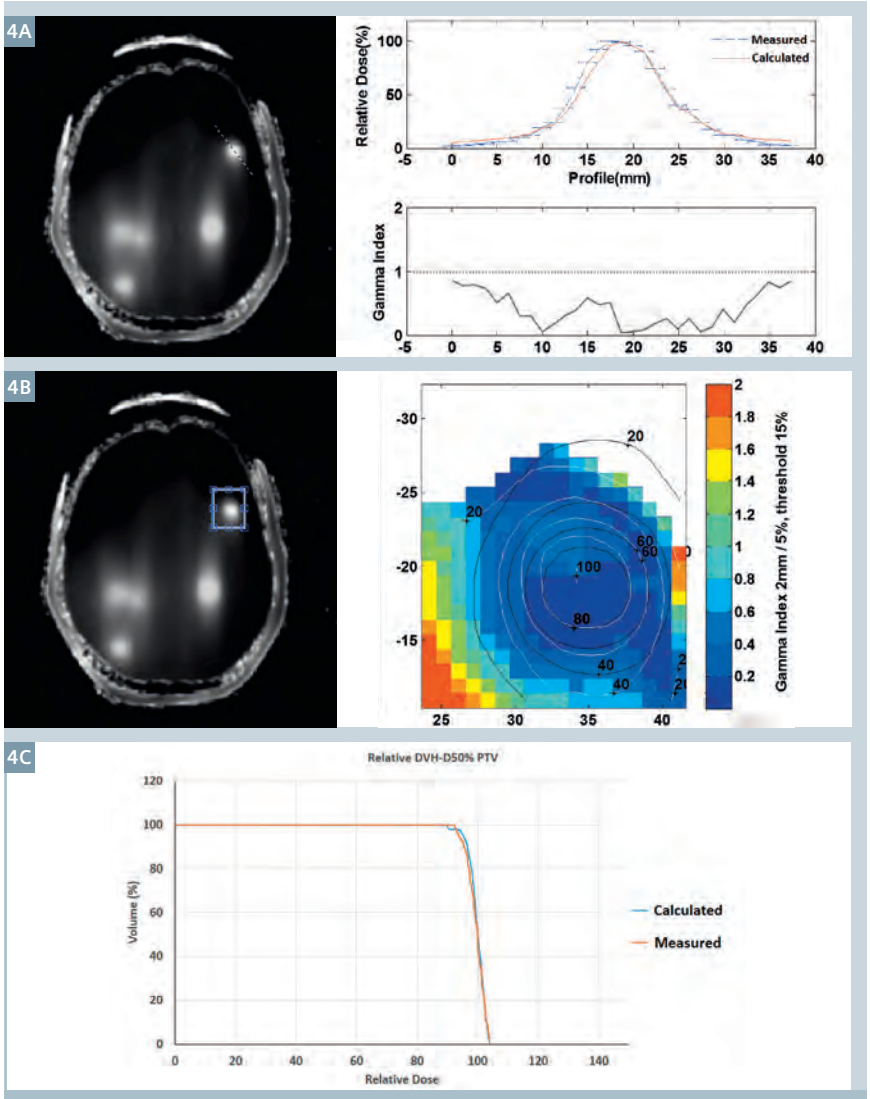

4 Quantitative dosimetric information derived by MRI T2 relaxometry performed using 2D HASTE pulse sequence. **(4A)** 1-D dose profile comparison. MRI measured dose profile vs. TPS calculated dose profile. 1-D gamma index (2 mm DTA / 5% dose difference). The profile corresponds to the line superimposed on the MRI-derived dose measurements depicted in the image on the left. **(4B)** 2D gamma index map and relative isodose lines comparison between the measured (MRI derived) and calculated (TPS derived) doses. The area where the 2D gamma index was calculated is superimposed on the MRI-derived dose measurements depicted in the image on the left. **(4C)** Dose Volume Histogram (DVH) inter-comparison for one of the six metastasis treated. MRI-derived measured DVH versus TPS-derived calculated corresponding DVH.

References

1 Baldock C, De Deene Y, Doran S, et al. 'Polymer gel dosimetry', Phys Med Biol. 2010, Mar 7;55(5):R1-63.

2 Papanikolaou N., Pappas E., Maris T.G., Teboh Forbang R., Stojadinovic S., Stathakis S., Gutierrez A.N. 'Stereotactic Treatment of Multiple Brain Metastasis: Pseudo In Vivo Evaluation of Three Different Techniques', International Journal of Radiation Oncology * Biology * Physics, 2015,93(3):E572.

3 Pappas E., Maris T.G. , Kalaitzakis G., Boursianis T., Makris D., Maravelakis E. 'Innovative QA methodology for true patient-specific Dose Volume Histograms (DVHs) measurements', Radiotherapy and Oncology, 2015, Vol.115, S704-S705.

4 Pappas E., Maris T.G., et al. "An innovative method for patient-specific pre-treatment plan-verification (PTPV) in head & neck radiotherapy treatments: preliminary results" International Journal of Radiation Oncology * Biology * Physics 2013, Vol. 87, Issue 2, Supplement, Page S756-7.

5 Papoutsaki MV, Maris TG, Pappas E, et al. "Dosimetric characteristics of a new polymer gel and their dependence on post-preparation and post-irradiation time: Effect on X-ray beam profile measurements. Phys Med. 2013, S1120-1797(13).

6 Pappas E., Maris T.G., Manolopoulos S., Zacharopoulou F., et al. "Small SRS photon field profile dosimetry performed using a PinPoint air ion chamber, a diamond detector, a novel silicon-diode array (DOSI) and polymer gel dosimetry. Analysis and intercomparison" Med. Phys. 2008, 35(10), p.4640-4648.

7 Papadakis A.E., Maris T.G., Zacharopoulou F., Pappas E. et al. An evaluation of the dosimetric performance characteristics of N-vinylpyrrolidone-based polymer gels. Phys. Med. Biol. 2007, 52, p.5069-5083.

8 Pappas E., Maris T.G., Papadakis A., et al. Experimental determination of the effect of detector size on profile measurements in narrow photon beams. Med. Phys. 2005, 33(10), p.3700-3710.

Contact

Niko Papanikolaou, Ph.D.
University of Texas
Health Science Center
7703 Floyd Curl Dr
San Antonio, TX 78229
USA
Phone: +1 (210) 450-5664
papanikolaou@uthscsa.edu

Contact

Evangelos Pappas, Ph.D.
TEI
RTsafe, www.rt-safe.com
48 Artotinis Str.
116 33 Athens
Greece
Phone: +30 2107563691
epappas@rt-safe.com

Development of MR-only Planning for Prostate Radiation Therapy Using Synthetic CT

Peter Greer, Ph.D.[1]; Jason Dowling, Ph.D.[2]; Peter Pichler, M.P.H.[3]; Jidi Sun, M.Sc.[3]; Haylea Richardson, B.Med.Rad.Sc.[3]; David Rivest-Henault, Ph.D.[2]; Soumya Ghose, Ph.D.[2]; Jarad Martin, M.D.[1]; Chris Wratten, FRANZCR[1]; Jameen Arm, MSc[4]; Leah Best, MSc[4]; Jim Denham, M.D.[1]; Peter Lau, FRANZCR[4]

[1] Calvary Mater Newcastle, Newcastle, New South Wales, Australia and University of Newcastle, Newcastle, New South Wales, Australia
[2] CSIRO, Australian e-Health Research Centre, Brisbane, Queensland, Australia
[3] Calvary Mater Newcastle, Newcastle, New South Wales, Australia

Introduction

The department of Radiation Oncology at Calvary Mater Newcastle, treats approximately 1,800 new patients per year. When it comes to prostate treatments, MR scans are used in addition to CT for treatment planning. Having to undergo two scans however is a burden both to patients as well as the health system. We have looked into addressing this by replacing the CT by an MR-only[1] workflow when treating patients with prostate cancer.

Description of the current treatment process

In the conventional CT based workflow the patient undergoes two imaging sessions, an MR imaging session and a CT imaging session. The MR dataset with its high soft tissue contrast enables precise visualisation of the prostate target and adjacent rectum and bladder organs at risk, while the CT dataset provides electron density information for dose calculations. The two image sets are registered in the Varian Eclipse™ treatment planning system (TPS) and the anatomical target and normal tissue contours delineated on the MR scan are transferred to the CT scan. Dose calculation and beam definition are then performed on the CT scan. Virtual or digitally reconstructed radiographs (DRRs) are also generated from the CT scan which shows the location of implanted fiducial gold markers in the prostate relative to the beam isocenter. These are used as reference images to align the patient using orthogonal X-rays before treatment in one of our five Varian (Trilogy™ and TrueBeam™) linear accelerators.

MR-only workflow[1]

The MR-only workflow differs in that the only imaging session is the MR and a synthetic CT scan is produced for dose calculations and DRR generation [1]. This workflow reduces the patient and health system burden and reduces systematic errors in treatment planning introduced by image registration uncertainties. This project is a collaboration between the clinical/academic site the Department of Radiation Oncology, Calvary Mater Newcastle and the Biomedical Imaging Research Group of the Commonwealth Scientific and Industrial Research Organisation (CSIRO).

[1] Radiotherapy Planning where MR data is the only imaging information is ongoing research. The concepts and information presented in this article are based on research and are not commercially available. Its future availability cannot be ensured.

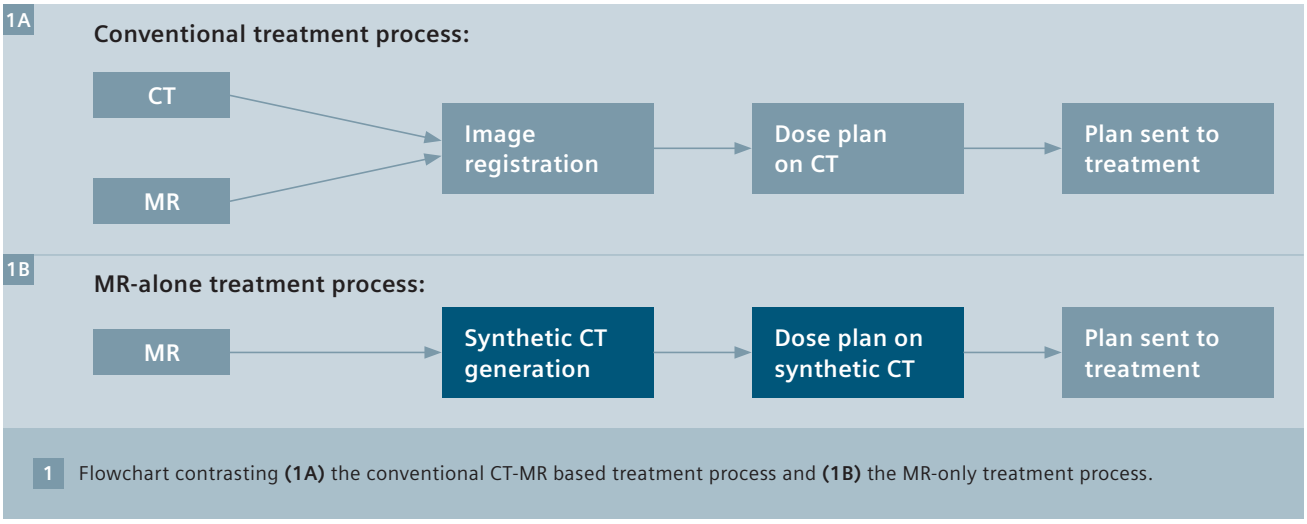

1 Flowchart contrasting **(1A)** the conventional CT-MR based treatment process and **(1B)** the MR-only treatment process.

The major technical steps in the treatment process are setup and imaging of the patient in the 3T MAGNETOM Skyra suite, production of synthetic CT scans; contouring of relevant organs; beam definition and dose calculation in Eclipse; setup, image-guided positioning and treatment at the Linac.

To date 40 men with ages ranging from 58 to 78, undergoing prostate cancer radiation therapy treatment have been scanned under a research protocol. All prostate patients undergoing long fractionation treatment were eligible except that patients with hip prostheses were excluded due to distortions induced by metallic implants*. Synthetic CT scans were produced for treatment planning comparisons to conventional CT based dose calculations.

Conventional MR scanning sequences are currently used for the MR-only workflow. Three sequences are used. The planning MR is a 3D, T2-weighted 1.6 mm isotropic voxel SPACE sequence with field-of-view (FOV) to cover the entire pelvis (ranging from 380-450 mm²). The prostate delineation sequence is a 2D axial T2-weighted sequence with FOV approximately 200 × 200 mm². A further T1-weighted gradient echo sequence with flip angle 80 degrees is used to image the implanted prostate fiducial markers (gold seeds 1 × 3 mm). These sequences were acquired in 12-15 minutes total with 340 s for the planning MR, 235 s for the small FOV T2 scan and 186 s for the T1 flip 80 scan. Patients were MR imaged prior to treatment as close as possible to the acquisition of the conventional planning CT scan so that dose comparisons on synthetic CT and conventional CT could be made. Although not necessary for treatment planning a further set of weekly MR scans was obtained for each patient to examine patient anatomical and dose variations. Therefore the data set consists of one MR session of three sequences for RT planning and seven MR scanning sessions of three sequences throughout the duration of treatment.

Seven field intensity modulated treatment delivery is used at our Center for prostate treatments. The treatments are delivered in 39 fractions of 2 Gy per fraction. Typical margins are 7 mm with 5 mm posteriorly.

Simulation at the MR

The patient is positioned at MR in the treatment position. This is achieved with an MR compatible laser bridge for patient rotation alignment, a radiation therapy specific couch top and coil mounts (CIVCO, Rotterdam, The Netherlands) which hold the coils away from the patient surface so they do not disturb the patient position. The 3T images are utilized for both delineation of the target and normal tissues using the MR patient model and for the production of the synthetic CT for dose calculation and DRRs for image-guidance at treatment.

2 Patient positioning for MR scanning showing the coil bridges.

The synthetic CT scans are created using an enhancement of our previous single atlas method [2] that combines multi-atlas deformable registration to the patient MR scan and local weighted voting to assign a CT value to each voxel of the MR planning scan. Firstly an atlas database is created in two steps:

1. A set of matching patient MR and CT planning scans are acquired;
2. The patient CT scan is deformably registered to the corresponding patient MR scan to form conjugate MR-CT pairs with matching geometry.

Then to create synthetic CT scans from a subsequent patient planning MR scan the following steps are used:

1. Each atlas MR scan is deformably registered to the patient planning MR scan;
2. For each small region of the patient planning MR, the intensity is compared to the same region in all the registered atlas MR scans;
3. Each atlas scan is assigned a weighting according to the similarity of the region values with the most similar having the highest weighting (all assigned weights sum to 1);
4. The CT values from the corresponding region of the conjugate CT atlas scans are added together using the previously determined weightings to provide the CT intensity value of that region of the synthetic CT scan. Methods to automatically segment both prostate and normal tissues are also being developed which will further increase treatment planning efficiency [3, 4]. The bone contours on the MR scans can be segmented very accurately with the deformable image registration method.

*The MRI restrictions (if any) of the metal implant must be considered prior to patient undergoing MRI exam. MR imaging of patients with metallic implants brings specific risks. However, certain implants are approved by the governing regulatory bodies to be MR conditionally safe. For such implants, the previously mentioned warning may not be applicable. Please contact the implant manufacturer for the specific conditional information. The conditions for MR safety are the responsibility of the implant manufacturer, not of Siemens.

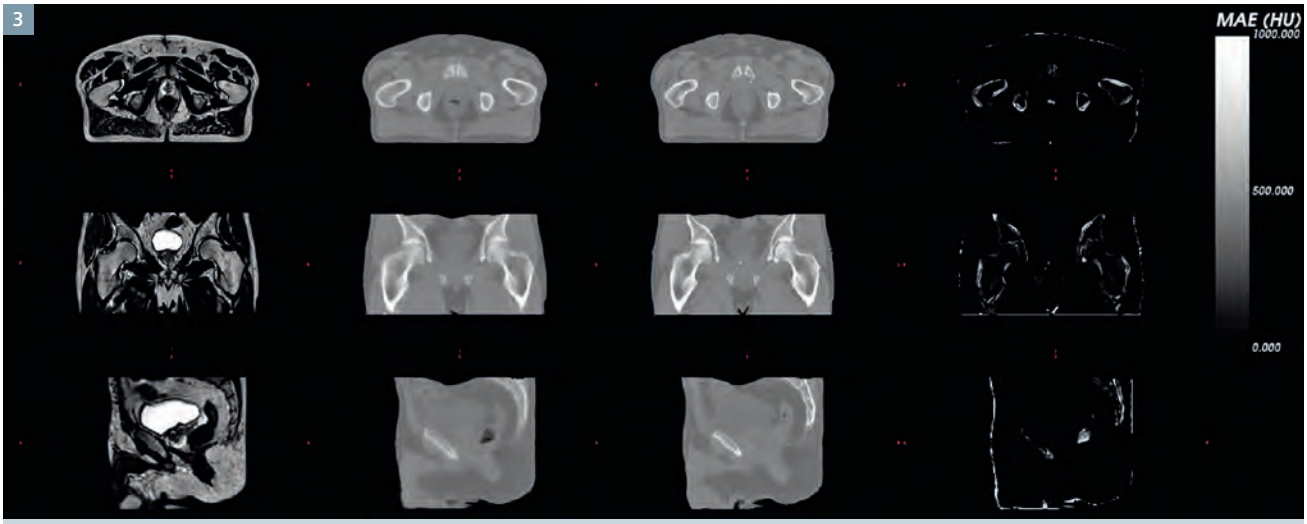

3 Shows axial, coronal and sagittal views from an original MR image of a 67-year-old study participant. The second column shows the automatically generated synthetic CT (sCT) with the original patient CT shown in the third column. The final column shows the difference between the synthetic and actual CT.

Treatment planning

The synthetic CT and MR images are imported to the Eclipse TPS with the AAA algorithm. The synthetic CT is first written to DICOM format with the header details written so that Eclipse interprets this as a CT scan for the patient. As the synthetic CT is created from the MR image data the scans are inherently registered. Target and normal tissue anatomy are delineated by the radiation oncologist on the MR scans. A treatment plan and dose calculation is then developed by the radiation therapist using the synthetic CT scan. The dose is then displayed for the radiation oncologist on the MR scan. The image guidance is performed using the Varian On-Board-Imager® and the treatment plan is delivered using the Varian Trilogy Linac.

Doses calculated on the synthetic CT scans were compared to gold standard doses calculated on the conventional CT scan with an average difference of 0.3% on average. A major advantage of the technique is that it does not require specialized sequences such as ultra-short echo time sequences. Only the single 3D SPACE sequence is required for synthetic CT generation which reduces the potential for patient motion compared with multi-sequence methods of generating synthetic CT that have been proposed [5, 6].

Conclusion

This study has shown that synthetic CT scans can be generated from MR scans using conventional T2-weighted sequences and that dose calculations are comparable to conventional CT scan dose calculations. Investigations of MR image distortion were also performed using test phantoms. Distortions in the region of the prostate were found to be sub-mm and distortions at the periphery were a maximum of 1.7 mm with the MAGNETOM Skyra 3D distortion correction applied. The MR-only workflow is efficient and only requires one imaging session for the patient. The next stage of our work is a prospective study where treatment will be performed using the MR-based treatment plan for a group of patients. MR-only prostate treatment planning is feasible and represents an improved process in radiation therapy planning.

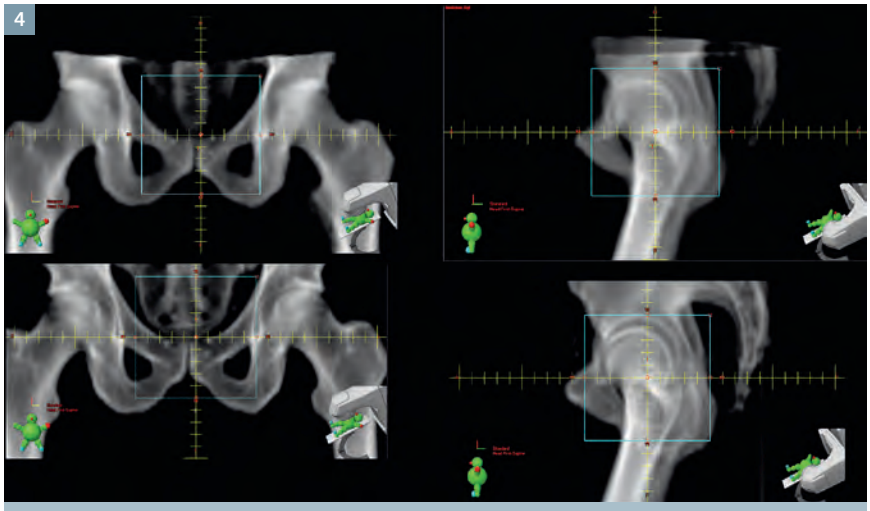

4 Anterior-posterior (AP) (left) and lateral (right) Digitally Reconstructed Radiographs (DRRs) generated from the MRI derived synthetic CT volume (top row) and actual planning CT (bottom row) for the same patient as in figure 3.

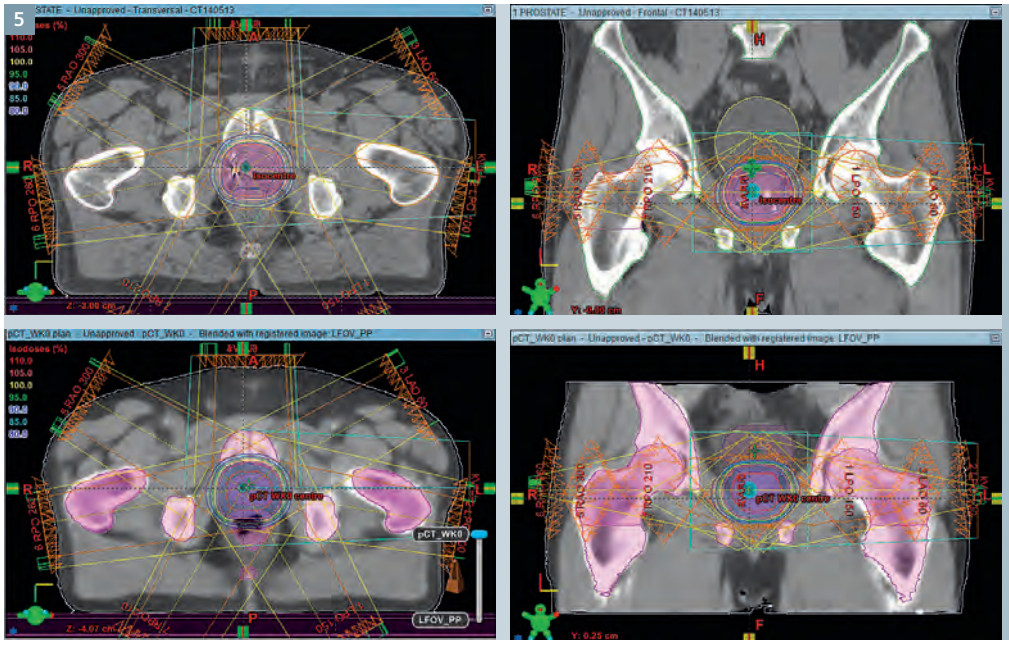

5 Screenshots from Eclipse TPS for the same patient as in figures 3, 4 showing comparison of dose calculation on conventional CT (top) and on synthetic CT (bottom). Contours displayed on the synthetic CT are the MR defined contours.

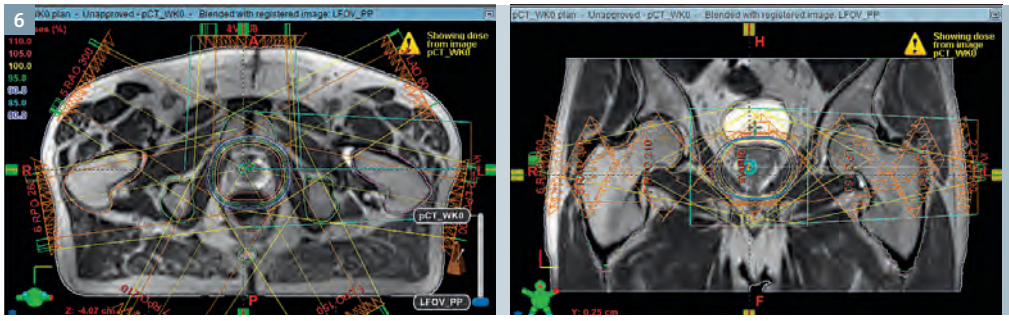

6 Screenshot from Eclipse TPS showing dose calculated on the synthetic CT scan displayed on the MRI scan.

Acknowledgments

This work was supported by Cancer Council New South Wales research grant RG11-05, the Prostate Cancer Foundation of Australia (Movember Young Investigator Grant YI2011) and Cure Cancer Australia.

References

1 Greer P, Dowling J, Lambert J, Fripp J, Parker J, Denham J, et al. A magnetic resonance imaging-based workflow for planning radiation therapy for prostate cancer. Med. J. Aust. 2011;194:S24.

2 Dowling JA, Lambert J, Parker J, Salvado O, Fripp J, Capp A, et al. An atlas-based electron density mapping method for magnetic resonance imaging (MRI)-alone treatment planning and adaptive MRI-based prostate radiation therapy. Int. J. Radiat. Oncol. Biol. Phys. 2012;83:e5–11.

3 Dowling JA, Fripp J, Chandra S, Pluim JPW, Lambert J, Parker J, et al. Fast automatic multi-atlas segmentation of the prostate from 3D MR images. Prostate Cancer Imaging. Image Analysis and Image-Guided Interventions. Springer; 2011. p. 10–21.

4 Chandra S, Dowling J, Shen K, Raniga P, Pluim J, Greer P, et al. Patient Specific Prostate Segmentation in 3D Magnetic Resonance Images. IEEE Transactions on Medical Imaging. 2012 Aug 2;31.

5 Johansson A, Karlsson M and Nyholm T, CT substitute derived from MRI sequences with ultrashort echo time, Med. Phys. 2011;2708-2714

6 Hsu, S-H, Cao Y, Huang K, Feng M, Balter JM, Investigation of a method for generating synthetic CTmodels from MRI scans of the head and neck for radiation therapy, Phys. Med. Biol. 2013;8419-8435.

Contact

Peter Greer
Principal Physicist
Calvary Mater Newcastle
Corner of Edith & Platt Streets
Waratah, NSW, 2298 Australia
Phone: +61 2 4014 3689
peter.greer@newcastle.edu.au

Contact

Jason Dowling
Research Scientist
CSIRO, Australian e-Health Research Centre
Level 5 – UQ Health Sciences Building
Royal Brisbane and Women's Hospital
Herston, QLD, 4029 Australia
Phone: +61 7 3253 3634
Jason.Dowling@csiro.au

Technical Aspects of MR-only Radiotherapy

Tufve Nyholm, Joakim Jonsson

Umeå University, Sweden

Introduction

Magnetic resonance imaging (MRI) has emerged as a key component in modern radiotherapy. The superior soft tissue contrast compared to computed tomography (CT) allows for increased accuracy in the definition of both target and organs at risk [7] using commonplace sequences [29]. Functional imaging techniques, primarily diffusion-weighted imaging and dynamic contrast enhanced imaging, are currently studied as a means of identifying areas within a tumor that require a higher dose in dose-painting trials [41]. Several current studies also aim to evaluate the possibilities of early treatment response assessment using MRI [25], which could enable treatment adaptation. At present, the main rationale of integrating MRI into the radiotherapy workflow is the gain in accuracy in target volume definitions. For several major patient groups, MR imaging is preferable from a medical point of view, i.e. for tumor definition [5, 27, 30]. CT or CT equivalent information is still, however, required for the technical aspects of treatment planning such as:

- accurate dose calculations, which depend on knowledge of the attenuation properties of the tissue measured in a CT exam and
- generation of reference images which are used for patient positioning based on in-room X-ray imaging.

Therefore, it is common practice to acquire both CT and MR data and align these image series in the same coordinate system, or frame of reference, through image registration. The MR data is used to define the target volume and the CT data to plan the treatment and serve as a reference for patient positioning. This workflow is, however, not optimal for several reasons. Besides the increase in cost and workload when using multiple imaging modalities, there is also an introduction of additional geometrical uncertainty due to the image registration.

Image registration is commonly performed at many clinics in order to align two image sets within a common frame of reference. Depending on the purpose of the image registration and the properties of the available image data, the registration can be performed in several ways. Mutual information rigid registration, based either on the full image volume or a smaller sub-volume, is available in most clinical treatment planning systems. For prostate cancer cases, where gold fiducial markers are commonly used, landmark registration methods can be employed in order to co-register MRI data to the planning CT. Manual registration, which is a robust but time-consuming method, is also an option. Regardless of method, image registration is a tricky business for several reasons. First off, for clinical cases we never know the correct alignment of two images, which makes it difficult to assess the uncertainties of a specific method. Phantom studies and purely digital experiments are unlikely to reflect the full complexity of the clinical case. Secondly, and related to the aforementioned problem, is the lack of robust quality measures for individual registrations. Finally, the task may actually be close to impossible, regardless of registration method. An example could be a prostate case without implanted fiducial markers. MRI is the imaging modality of choice for target definition, due to the greater soft tissue contrast. The prostate behaves much in the same way as other soft tissue tumors, i.e. its position in the body is not fixed and the spatial relation to surrounding bony anatomy may vary. This implies that a sub-volume based registration algorithm would be suitable in order to avoid any negative influence the surrounding anatomy may have on the registration. Although there are limited references regarding the matter, it is reasonable to assume that the limited soft tissue contrast in, and in close proximity to, the prostate gland in the CT image set would degrade the quality of a multi-modal sub-volume

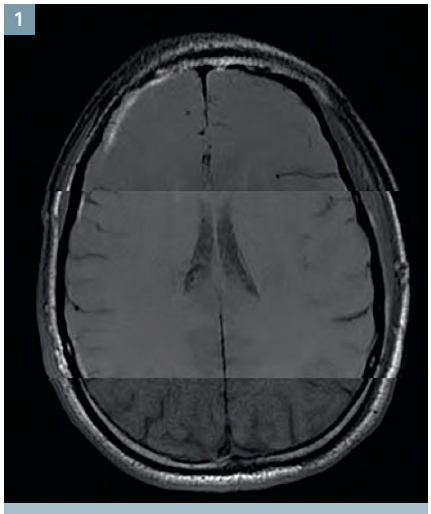

1 Top 40 Hz/pixel, mid 100 Hz/pixel, bottom 400 Hz/pixel. Notice differences in signal-to-noise but especially geometrical differences.

registration. In other words, the reason that soft tissue registrations between MR and CT images will be associated with substantial uncertainties is exactly the same reason why we need MR image data to begin with; we lack sufficient anatomical information on soft tissue in the CT images. For the sake of balance, it should be said that for some indications, such as intracranial lesions, including larger volumes in the registration is not associated with any added uncertainty since the soft tissue is relatively fixed with respect to the bony anatomy. Even in those cases, however, image registration uncertainty is still a factor to consider. Ulin et al. [42] investigated the clinical variability of MR-CT registrations for one patient with an intracranial lesion for 45 clinics. The analysis revealed a standard deviation of 2.2 mm, which only accounts for the variability among the observers. There may still be a systematic component on top of this.

In summary, MR imaging has been shown to increase the geometrical accuracy in the definition of target volume. The challenge today is to make sure that we can radiate this target volume in an accurate and precise manner. This problem can be reduced into several sub-problems, e.g. control over geometrical distortions in the MR images; differences in the patient setup in the MR scanner compared to treatment; and registration uncertainties introduced when MR and CT data is placed in the same coordinate system. In this article we provide a brief overview of the current knowledge regarding geometrical distortions and patient setup in the radiotherapy context and describe the problems and proposed solutions for MR only radiotherapy.

MR image distortions

Geometric distortions in MR images can be caused by the system itself, from nonlinearities in the magnetic gradients or inhomogeneities in the static magnetic field. Nonlinearities in the gradients can be characterized and corrected using spherical harmonics expansions of the fields generated by the gradient coils and can be accurately corrected using software supplied by the MR vendors.

Distortions can also be caused by the imaged object in the form of chemical shift or magnetic susceptibility artefacts. Image distortions due to susceptibility effects and chemical shift in conventional MR imaging are inversely proportional to the gradient field strength, so that stronger gradients will minimize such distortions at a cost of more image noise. Phantom studies have shown the residual distortion for clinical sequences to be within 1 mm [18, 31]. Object-induced distortion effects have also been investigated in clinical data and the effect proved to be small for internal structures relevant for prostate treatments [28]. In general, anatomical imaging sequences using relatively high bandwidths reduce distortions caused by susceptibility effects and chemical shift to an acceptable level for radiotherapy [26, 40]. Methods using post-processing corrections [35] or special modes of acquisition [6] have also been studied.

Some MR protocols are more sensitive to geometric distortions, echo planar imaging being one example. Such sequences can display significant geometric distortions due to susceptibility effects, and must be handled with care when used for radiotherapy purposes.

MR imaging using immobilization equipment

Planning CT scans are normally acquired using flat table tops to match the flat treatment couch used at the accelerator. The standard patient support is concave in most MRI scanners, although some have flat couches. The problem of concave patient supports is easily surmounted, either by manufacturing a flat table top insert at the hospital or by purchasing a commercial solution. Flat table tops are necessary if patient immobilization is to be used at the MRI scanner.

A more intricate problem is MRI compatibility of the immobilization equipment, both in material properties and size. MR safe materials must be used for base-plates, nuts, bolts and other fittings. A traditional plastic face mask for head and neck immobilization is normally constructed in MR safe materials; however, a standard MRI head coil will not be able to accommodate it. By using surface coils (i.e. flex coils) instead, imaging of the immobilized head and neck is possible, although a dedicated head coil still provide higher quality images [10]. When using surface coils for radiotherapy planning, care must be taken not to place the coils directly on the skin of the patient since the external anatomy may be distorted. Instead, the coils should be placed either hanging from a frame or on top of a holder close to the patient surface, without touching it. Nowadays, MRI compatible immobilization equipment and coil holders are commercially available.

MR-only radiotherapy[1]

In this article, we define MR-only radiotherapy as external beam radiotherapy where MR data is the only imaging information that is used for the planning and preparation of the treatment. Arguments for an MR-only workflow commonly include the avoidance of image registration in the planning stage of the treatment [1, 4, 8, 15, 18, 19, 20, 23, 31, 33, 39], reduced costs due to less imaging or a simplified workflow [1, 4, 8, 24, 39], and reduced exposure to unspecifically aimed radiation [4, 18, 39].

[1] Radiotherapy Planning where MR data is the only imaging information is ongoing research. The concepts and information presented in this article are based on research and are not commercially available. Its future availability cannot be ensured.

2

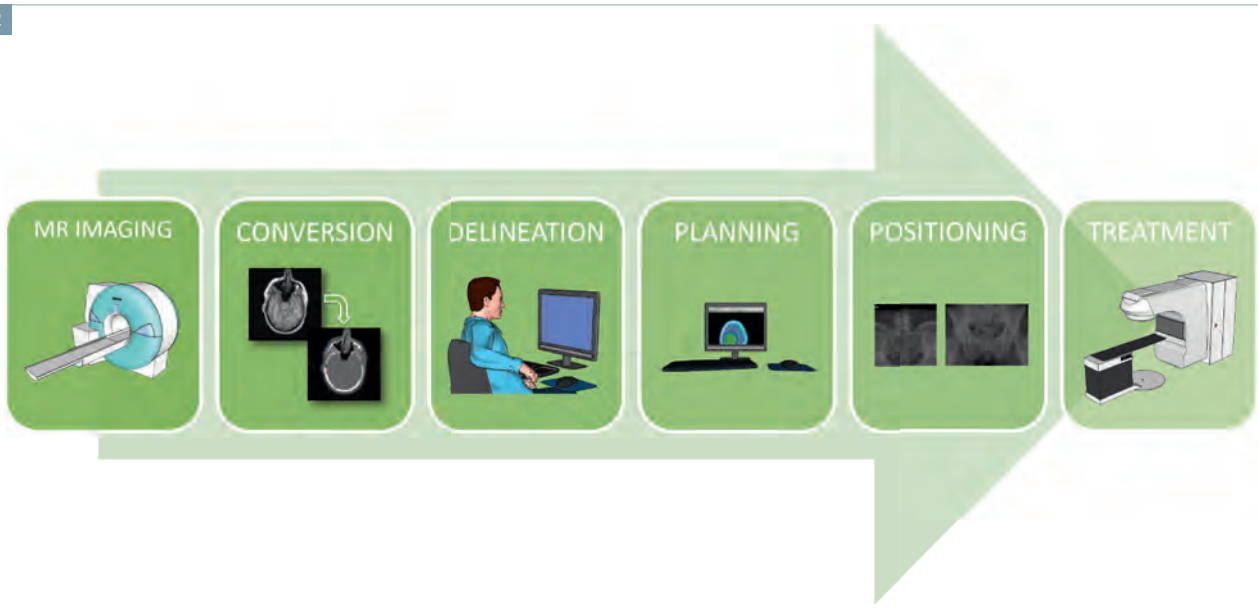

2 Simple schematic displaying the MR-only radiotherapy workflow. The difference from the traditional radiotherapy workflow is mainly the exclusion of CT imaging and registration and the addition of the conversion step.

Current methods of accurate dose calculations rely heavily on CT (or CT equivalent) information due to the relationship between Hounsfield units and electron density, and will probably continue to do so for the foreseeable future. Therefore, a reliable conversion method from MR information to CT equivalent information will be necessary for an MR-only workflow in radiotherapy. Several methods have been investigated by multiple research teams.

Manual bulk density assignment

A method that has been researched extensively is segmentation, i.e. dividing the image into classes with different attenuation properties. The simplest form of segmentation is to only use one tissue class and assign a bulk density to the entire patient, typically that of water or a mixture of adipose tissue and muscle. Even though this is an extremely simplified version of reality, it yields acceptable dosimetric results. Typical dosimetric differences from inhomogeneity corrected CT based dose calculations using this approach have been reported to be within 2-3% for prostate and intracranial target volumes [9, 17, 22, 23, 32, 33, 38]. A significant problem with this approach is that the traditional method of patient positioning at treatment depends on anatomical reference images that visualize bony anatomy. To overcome this issue, the number of tissue classes can be increased to include e.g. bone, soft tissue, lung tissue and air, and assign each tissue class an appropriate bulk density. In addition to making the creation of anatomical reference images possible, this also increases the dosimetric accuracy to around 1% for intracranial targets volumes [17, 22, 38] and between 1-2% for prostate treatments [17, 23].

Although the dosimetric results are relatively accurate, the method of manual density assignment has problems – the method relies on the precision of the operator that defines the anatomy in the MR images. This is of limited importance in the dosimetric aspect, but may have substantial impact on the subsequently generated positioning references. Also, the method is so labor intensive and time consuming that it is not feasible for widespread clinical implementation. In order to accomplish such a development, automated conversion methods from MR to s-CT data are needed.

Atlas methods

One method for automatically generating s-CT data is the combined MR-label image atlas. By deformably registering the atlas MR image to a new patient MR image and applying the resulting deformation field to the corresponding label image, a new image can be created based on the data in the label image. The label image can contain any information, e.g. CT or attenuation data. This approach has been used for attenuation correction applications in PET/MRI [37] as well as for dose calculation purposes in radiotherapy [8]. Atlas methods do not normally rely on tissue segmentation; instead, the full complexity atlas label image is warped onto the patient shape. Dosimetric results indicate accuracy comparable to bulk density assignment; for the radiotherapy application, Dowling et al [8] reported point dose differences between atlas label image and CT based calculations of about

2%. Atlas based methods are normally sensitive to atypical anatomy; e.g. in the study by Dowling et al., 2 out of 39 patients had to be excluded for this reason. Although atlas based methods are fairly robust and automatic, an argument can be made that the deformable image registration is associated with a considerable geometric uncertainty. This uncertainty is introduced into the treatment if the deformed label image is used to create the positing reference image and not solely for dose calculations.

Direct conversion

With the advent of ultra-short echo time imaging (UTE), interest has increased for direct conversion of MR image intensities to Hounsfield units. Since cortical bone appears as a signal void in traditional MR imaging, it has been impossible to distinguish it from air. UTE imaging samples the signal during the free induction decay, before the signal from cortical bone and other tissues with short T2 relaxation times has vanished [36], making it possible to discriminate such tissues from air. Even though UTE images renders signal from bone, it is not presently possible to find any single MR sequence which is directly convertible to Hounsfield units – more information is necessary. Several researchers have suggested using UTE sequences with several different echo-times to segment soft-tissue, air and bone [2, 3, 21]. This technique is fully automatic and preserves the geometric integrity of the input image. UTE images suffer from the same system related distortions as traditional MR sequences; however, the fast radial sampling makes it less sensitive to common object related distortions such as chemical shift and susceptibility effects. An alternative to the previously mentioned segmentation approach is to build a statistical model that relates MR voxel intensities to Hounsfield units [12, 34]. Such an approach yields an s-CT image with a continuous Hounsfield unit distribution, as well as making it possible to estimate the uncertainties in the conversion [13]. Recent studies

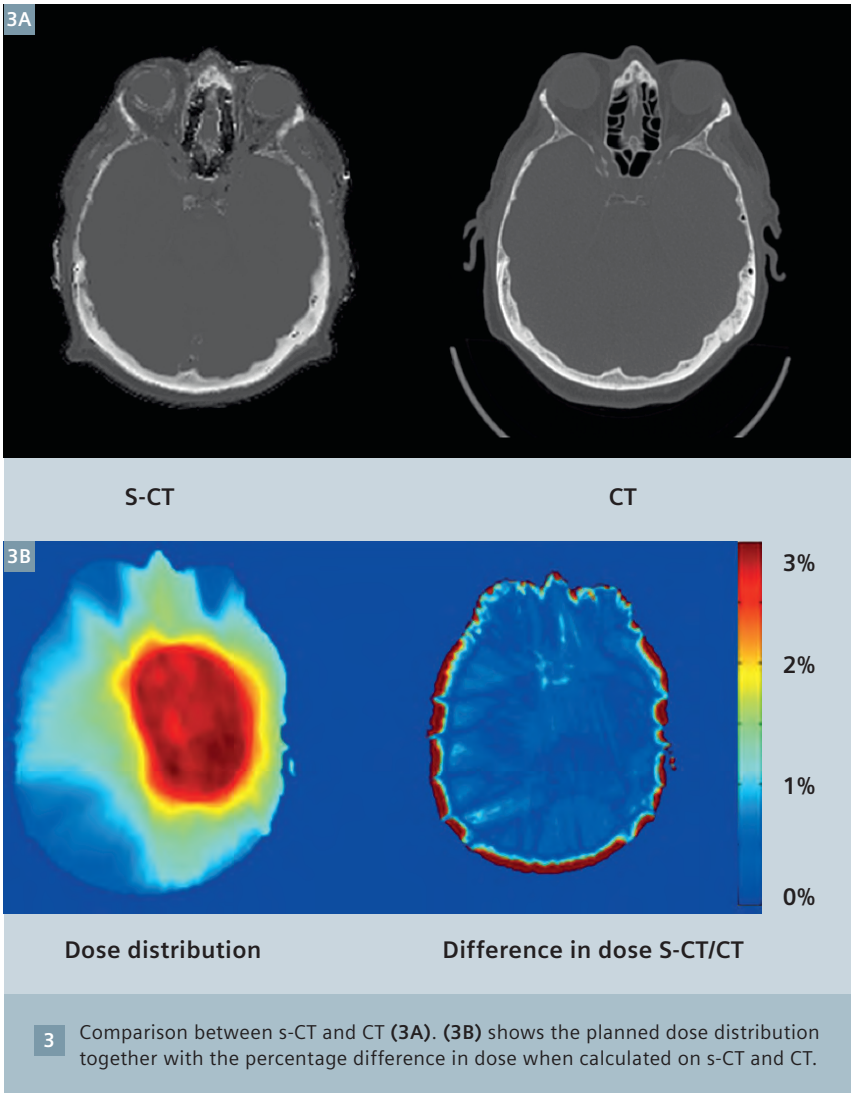

3 Comparison between s-CT and CT **(3A)**. **(3B)** shows the planned dose distribution together with the percentage difference in dose when calculated on s-CT and CT.

compared dose calculations on s-CT data with CT data, and found statistically insignificant dose differences of less than ±0.5% for intracranial targets [14, 16].

It is also possible to combine segmentation methods with direct conversion. A recent study [19] investigated the accuracy of a conversion method were the pelvic bone structures were first delineated manually. These delineations then served as input for a direct conversion method which could successfully convert the image intensities from standard MRI sequences to Hounsfield units. When the entire remaining anatomy was set to a bulk density, all points within the prostate PTV were within ±1.3% of the dose calculated on the standard CT input data.

The atlas registration approach can also produce segmentations that can serve as input for a later stage direct conversion. Hoffman et al. [11], which employed this approach for attenuation correction of PET/MR images, demonstrated that the method could accurately predict the attenuation map of a patient from MR input data. No systematic differences were found between PET images corrected with s-CT data and actual CT data. These combined methods ease the demand on the local accuracy of the segmentation, since the final conversion is performed using direct voxel wise conversion.

Summary

Radiotherapy is a local treatment modality that is highly dependent on image guidance. Over the last decade there has been an increased clinical use of both MRI and PET to enable accurate delineation of the target volume. However, the radiotherapy workflow does still depend on CT information as the treatment planning softwares require attenuation data to be able to perform accurate dose calculation and to generate reference images for positioning. It has been shown that it is possible to generate CT equivalent information based on MR data, and with this technology it will be possible to abandon the CT in the future for those diagnoses where MR is the modality of choice for target delineation. Imaging in treatment position and risk of geometrical distortions are two other areas that need to be addressed when introducing an MR scanner in the radiotherapy environment.

Contact

Tufve Nyholm
Department of Radiation Sciences
Umeå University
Umeå
Sweden
Phone: +46 90 785 8432
tufve.nyholm@umu.se

References

1 Beavis, A W, P Gibbs, R A Dealey, and V J Whitton. 1998. "Radiotherapy Treatment Planning of Brain Tumours Using MRI Alone." The British Journal of Radiology 71 (845): 544–48.

2 Berker, Yannick, Jochen Franke, André Salomon, Moritz Palmowski, Henk C W Donker, Yavuz Temur, Felix M Mottaghy, et al. 2012. "MRI-Based Attenuation Correction for Hybrid PET/MRI Systems: A 4-Class Tissue Segmentation Technique Using a Combined Ultrashort-Echo-time/Dixon MRI Sequence." Journal of Nuclear Medicine 53 (5): 796–804. doi:10.2967/jnumed.111.092577.

3 Catana, Ciprian, Andre van der Kouwe, Thomas Benner, Christian J Michel, Michael Hamm, Matthias Fenchel, Bruce Fischl, Bruce Rosen, Matthias Schmand, and A Gregory Sorensen. 2010. "Toward Implementing an MRI-Based PET Attenuation-Correction Method for Neurologic Studies on the MR-PET Brain Prototype." Journal of Nuclear Medicine 51 (9): 1431–38. doi:10.2967/jnumed.109.069112.

4 Chen, Lili, Robert a Price, Lu Wang, Jinsheng Li, Lihong Qin, Shawn McNeeley, C-M Charlie Ma, Gary M Freedman, and Alan Pollack. 2004. "MRI-Based Treatment Planning for Radiotherapy: Dosimetric Verification for Prostate IMRT." Int J Radiat Oncol Biol Phys 60 (2): 636–47. doi:10.1016/j.ijrobp.2004.05.068.

5 Chung, Na Na, Lai Lei Ting, Wei Chung Hsu, Louis Tak Lui, and Po Ming Wang. 2004. "Impact of Magnetic Resonance Imaging versus CT on Nasopharyngeal Carcinoma: Primary Tumor Target Delineation for Radiotherapy." Head & Neck 26 (3): 241–46. doi:10.1002/hed.10378.

6 Crijns, S P M, C J G Bakker, P R Seevinck, H de Leeuw, J J W Lagendijk, and B W Raaymakers. 2012. "Towards Inherently Distortion-Free MR Images for Image-Guided Radiotherapy on an MRI Accelerator." Physics in Medicine and Biology 57 (5): 1349–58. doi:10.1088/0031-9155/57/5/1349.

7 Dirix, Piet, Karin Haustermans, and Vincent Vandecaveye. 2014. "The Value of Magnetic Resonance Imaging for Radiotherapy Planning." Seminars in Radiation Oncology 24 (3). Elsevier: 151–59. doi:10.1016/j.semradonc.2014.02.003.

8 Dowling, Jason A, Jonathan Lambert, Joel Parker, Olivier Salvado, Jurgen Fripp, Anne Capp, Chris Wratten, James W Denham, and Peter B Greer. 2012. "An Atlas-Based Electron Density Mapping Method for Magnetic Resonance Imaging (MRI)-Alone Treatment Planning and Adaptive MRI-Based Prostate Radiation Therapy." Int J Radiat Oncol Biol Phys 83 (1). Elsevier Inc: e5–11. doi:10.1016/j.ijrobp.2011.11.056.

9 Eilertsen, Karsten, Line Nilsen Tor Arne Vestad, Oliver Geier, and Arne Skretting. 2008. "A Simulation of MRI Based Dose Calculations on the Basis of Radiotherapy Planning CT Images." Acta Oncologica 47 (7): 1294–1302. doi:10.1080/02841860802256426.

10 Hanvey, S, M Glegg, and J Foster. 2009. "Magnetic Resonance Imaging for Radiotherapy Planning of Brain Cancer Patients Using Immobilization and Surface Coils." Physics in Medicine and Biology 54 (18): 5381–94. doi:10.1088/0031-9155/54/18/002.

11 Hofmann, Matthias, Florian Steinke, Verena Scheel, Guillaume Charpiat, Jason Farquhar, Philip Aschoff, Michael Brady, Bernhard Schölkopf, and Bernd J Pichler. 2008. "MRI-Based Attenuation Correction for PET/MRI: A Novel Approach Combining Pattern Recognition and Atlas Registration." Journal of Nuclear Medicine 49 (11): 1875–83. doi:10.2967/jnumed.107.049353.

12 Johansson, Adam, Mikael Karlsson, and Tufve Nyholm. 2011. "CT Substitute Derived from MRI Sequences with Ultrashort Echo Time." Medical Physics 38 (5): 2708. doi:10.1118/1.3578928.

13 Johansson, Adam, Yu Yun, Thomas Asklund, Mikael Karlsson, and Tufve Nyholm. 2012. "Voxel-Wise Uncertainty in CT Substitute Derived from MRI." Medical Physics 39 (6): 3283–90. doi:10.1118/1.4711807.

14 Jonsson, Joakim H, Mohammad M Akhtari, Magnus G Karlsson, Adam Johansson, Thomas Asklund, and Tufve Nyholm. 2015. "Accuracy of Inverse Treatment Planning on Substitute CT Images Derived from MR Data for Brain Lesions." Radiation Oncology (London, England) 10 (1): 13. doi:10.1186/s13014-014-0308-1.

15 Jonsson, Joakim H, Anders Garpebring, Magnus G Karlsson, and Tufve Nyholm. 2012. "Internal Fiducial Markers and Susceptibility Effects in MRI-Simulation and Measurement of Spatial Accuracy." Int J Radiat Oncol Biol Phys 82 (5): 1612–18. doi:10.1016/j.ijrobp.2011.01.046.

16 Jonsson, Joakim H, Adam Johansson, Karin Söderström, Thomas Asklund, and Tufve Nyholm. 2013. "Treatment Planning of Intracranial Targets on MRI Derived Substitute CT Data." Radiotherapy and Oncology 108: 118–22.

17 Jonsson, Joakim H, Magnus G Karlsson, Mikael Karlsson, and Tufve Nyholm. 2010. "Treatment Planning Using MRI Data: An Analysis of the Dose Calculation Accuracy for Different Treatment Regions." Radiation Oncology 5 (1): 62. doi:10.1186/1748-717X-5-62.

18 Kapanen, Mika, Juhani Collan, Annette Beule, Tiina Seppälä, Kauko Saarilahti, and Mikko Tenhunen. 2013. "Commissioning of MRI-Only Based Treatment Planning Procedure for External Beam Radiotherapy of Prostate." Magnetic Resonance in Medicine 70 (1): 127–35. doi:10.1002/mrm.24459.

19 Kapanen, Mika, and Mikko Tenhunen. 2013. "T1/T2*-Weighted MRI Provides Clinically Relevant Pseudo-CT Density Data for the Pelvic Bones in MRI-Only Based Radiotherapy Treatment Planning." Acta Oncologica (Stockholm, Sweden) 52 (3): 612–18. doi:10.3109/0284186X.2012.692883.

20 Karlsson, Mikael, Magnus G Karlsson, Tufve Nyholm, Christopher Amies, and Björn Zackrisson. 2009. "Dedicated Magnetic Resonance Imaging in the Radiotherapy Clinic." Int J Radiat Oncol Biol Phys 74 (2): 644–51. doi:10.1016/j.ijrobp.2009.01.065.

21 Keereman, Vincent, Yves Fierens, Tom Broux, Yves De Deene, Max Lonneux, and Stefaan Vandenberghe. 2010. "MRI-Based Attenuation Correction for PET/MRI Using Ultrashort Echo Time Sequences." Journal of Nuclear Medicine 51 (5): 812–18. doi:10.2967/jnumed.109.065425.

22 Kristensen, Brian Holch, Finn Jørgen Laursen, Vibeke Løgager, Poul Flemming Geertsen, and Anders Krarup-Hansen. 2008. "Dosimetric and Geometric Evaluation of an Open Low-Field Magnetic Resonance Simulator for Radiotherapy Treatment Planning of Brain Tumours." Radiotherapy and Oncology 87 (1): 100–109. doi:10.1016/j.radonc.2008.01.014.

23 Lambert, Jonathan, Peter B Greer, Fred Menk, Jackie Patterson, Joel Parker, Kara Dahl, Sanjiv Gupta, et al. 2011. "MRI-Guided Prostate Radiation Therapy Planning: Investigation of Dosimetric Accuracy of MRI-Based Dose Planning." Radiotherapy and Oncology : Journal of the European Society for Therapeutic Radiology and Oncology 98 (3). Elsevier Ireland Ltd: 330–34. doi:10.1016/j.radonc.2011.01.012.

24 Lee, Young K, Marc Bollet, Geoffrey Charles-Edwards, Maggie A Flower, Martin O Leach, Helen McNair, Elizabeth Moore, Carl Rowbottom, and Steve Webb. 2003. "Radiotherapy Treatment Planning of Prostate Cancer Using Magnetic Resonance Imaging Alone." Radiotherapy and Oncology 66 (2): 203–16. doi:10.1016/S0. doi:10.1088/0031-9155/57/5/1349.

25 Li, Sonia P, and Anwar R Padhani. 2012. "Tumor Response Assessments with Diffusion and Perfusion MRI." Journal of Magnetic Resonance Imaging 35 (4): 745–63. doi:10.1002/jmri.22838.

26 Liney, Gary P, and Marinus a Moerland. 2014. "Magnetic Resonance Imaging Acquisition Techniques for Radiotherapy Planning." Seminars in Radiation Oncology 24 (3). Elsevier: 160–68. doi:10.1016/j.semradonc.2014.02.014.

27 Milosevic, M, S Voruganti, R Blend, H Alasti, P Warde, M McLean, P Catton, C Catton, and M Gospodarowicz. 1998. "Magnetic Resonance Imaging (MRI) for Localization of the Prostatic Apex: Comparison to Computed Tomography (CT) and Urethrography." Radiotherapy and Oncology 47 (3): 277–84.

28 Pasquier, D, N Betrouni, M Vermandel, T Lacornerie, E Lartigau, and J Rousseau. 2006. "MRI Alone Simulation for Conformal Radiation Therapy of Prostate Cancer: Technical Aspects." IEEE EMBS, January, 160–63. doi:10.1109/IEMBS.2006.260341.

29 Paulson, Eric S., Beth Erickson, Chris Schultz, and X. Allen Li. 2015. "Comprehensive MRI Simulation Methodology Using a Dedicated MRI Scanner in Radiation Oncology for External Beam Radiation Treatment Planning." Medical Physics 42 (1): 28–39. doi:10.1118/1.4896096.

30 Prabhakar, R, K P Haresh, T Ganesh, R C Joshi, P K Julka, and G K Rath. 2007. "Comparison of Computed Tomography and Magnetic Resonance Based Target Volume in Brain Tumors." Journal of Cancer Research and Therapeutics 3 (2): 121–23.

31 Prabhakar, R, P K Julka, T Ganesh, a Munshi, R C Joshi, and G K Rath. 2007a. "Feasibility of Using MRI Alone for 3D Radiation Treatment Planning in Brain Tumors." Japanese Journal of Clinical Oncology 37 (6): 405–11. doi:10.1093/jjco/hym050.

32 Prabhakar, R, P K Julka, T Ganesh, A Munshi, R C Joshi, and G K Rath. 2007b. "Feasibility of Using MRI Alone for 3D Radiation Treatment Planning in Brain Tumors." Japanese Journal of Clinical Oncology 37 (6): 405–11. doi:10.1093/jjco/hym050.

33 Ramsey, C R, and A L Oliver. 1998. "Magnetic Resonance Imaging Based Digitally Reconstructed Radiographs, Virtual Simulation, and Three-Dimensional Treatment Planning for Brain Neoplasms." Medical Physics 25 (10): 1928–34.

34 Rank, Christopher M, Christoph Tremmel, Nora Hünemohr, Armin M Nagel, Oliver Jäkel, and Steffen Greilich. 2013. "MRI-Based Treatment Plan Simulation and Adaptation for Ion Radiotherapy Using a Classification-Based Approach." Radiation Oncology 8 (1): 51. doi:10.1186/1748-717X-8-51.

35 Reinsberg, Stefan a, Simon J Doran, Elizabeth M Charles-Edwards, and Martin O Leach. 2005. "A Complete Distortion Correction for MR Images: II. Rectification of Static-Field Inhomogeneities by Similarity-Based Profile Mapping." Physics in Medicine and Biology 50 (11): 2651–61. doi:10.1088/0031-9155/50/11/014.

36 Robson, Matthew D, Peter D Gatehouse, Mark Bydder, and Graeme M Bydder. 2003. "Magnetic Resonance: An Introduction to Ultrashort TE (UTE) Imaging." Journal of Computer Assisted Tomography 27 (6): 825–46.

37 Schreibmann, Eduard, Jonathon a. Nye, David M. Schuster, Diego R. Martin, John Votaw, and Tim Fox. 2010. "MR-Based Attenuation Correction for Hybrid PET-MR Brain Imaging Systems Using Deformable Image Registration." Medical Physics 37 (5): 2101–9. doi:10.1118/1.3377774.

38 Stanescu, T, H-S Jans, N Pervez, P Stavrev, and B G Fallone. 2008. "A Study on the Magnetic Resonance Imaging (MRI)-Based Radiation Treatment Planning of Intracranial Lesions." Physics in Medicine and Biology 53 (13): 3579–93. doi:10.1088/0031-9155/53/13/013.

39 Stanescu, Teodor, Jans Hans-sonke, Pavel Stavrev, and B Gino Fallone. 2006. "3T MR-Based Treatment Planning for Radiotherapy of Brain Lesions." Radiology and Oncology 40 (2): 125–32.

40 Walker, Amy, Gary Liney, Peter Metcalfe, and Lois Holloway. 2014. "MRI Distortion: Considerations for MRI Based Radiotherapy Treatment Planning." Australasian Physical & Engineering Sciences in Medicine / Supported by the Australasian College of Physical Scientists in Medicine and the Australasian Association of Physical Sciences in Medicine, February. doi:10.1007/s13246-014-0252-2.

41 Van der Heide, Uulke A, Antonetta C Houweling, Greetje Groenendaal, Regina G H Beets-Tan, and Philippe Lambin. 2012. "Functional MRI for Radiotherapy Dose Painting." Magnetic Resonance Imaging 30 (9). Elsevier Inc.: 1216–23. doi:10.1016/j.mri.2012.04.010.

42 Kenneth Ulin, Marcia Urie, Joel Cherlow. 2010. "Results of a Multi-Institutional Benchmark Test for Cranial CT/MR Image Registration" Int. J. Radiation Oncology Biol. Phys. 77 (5): 1584-1589.

The Potential Role of Ultrashort Echo Time Sequences in MRI Guided Radiotherapy

Soumya Ghose[3]; Robba Rai[1]; Jason Dowling[3]; Sankar Arumugam[1]; Benjamin Schmitt[4]; Gary Liney[1,2]

[1] Liverpool Cancer Therapy Centre, Liverpool Hospital, Sydney, Australia
[2] Ingham Institute for Applied Medical Research, Sydney, Australia
[3] CSIRO, The Australian e-Health & Research Centre, Brisbane, Queensland
[4] Siemens Healthcare, Australia

Introduction

An increasing number of Oncology Centers are implementing MRI into the planning and monitoring of radiation treated patients so that the benefits of improved soft-tissue contrast can be utilized in both the tumor target and organs-at-risk. The effects of geometric distortion both from the system and the patient are well documented and can be mitigated to acceptable levels of accuracy. However CT is still required to provide the electron density correction that is needed in the dose calculation. The current treatment workflow therefore involves the patient undergoing both a CT and MRI examination and the state-of-the art solution is to acquire both of these in the same treatment position to facilitate registration in a treatment planning system. Nevertheless there are inherent differences between CT and MRI contrast that makes registration of certain structures and materials difficult. Furthermore, the requirement of a CT each time a plan is calculated, means that the potential of MRI for informing and adapting treatment at any point is never fully exploited.

One of the key attractions of MRI for Oncologists is the variety of imaging techniques that can be acquired in a single examination. Ultrashort echo time (UTE) sequences[1] [1] are now being added to the list and finding new clinical applications with their ability to image at tens of microseconds. Recently developed sequences are able to achieve the shortest possible TEs limited only by transmit/receive switching times and gradient performance and requiring no hardware upgrades. These have the potential to generate signal in previously invisible structures and/or reduce susceptibility artefacts both of which could hold advantages for radiotherapy (RT) planning; either providing better registration between the two modalities or moving towards replacing CT altogether.

This commentary describes two phantom studies that were performed to explore the potential application of UTE sequences for RT planning. All imaging was undertaken on our current 3 Tesla wide-bore MAGNETOM Skyra system, which is used as a dedicated 'MR-simulator' at Liverpool Cancer Therapy Centre in South West Sydney.

[1] The product is still under development and not commercially available yet. Its future availability cannot be ensured.

MR-CT registration: a gold marker study

Fiducial marker insertion is a common clinical practice for radiotherapy (RT) to improve target localization in the prostate. Marker position on the planning CT can be aligned with daily cone beam CT (CBCT) image by table shifts prior to RT treatment. Fiducial marker appearance on CT can include areas of streak artefacts due to their

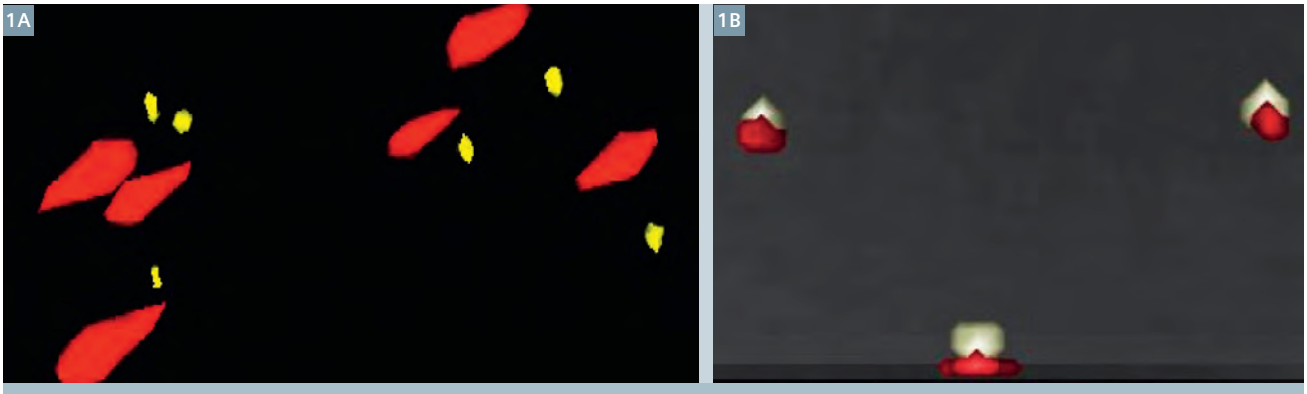

1 **(1A)** 3D rendering of artefacts in the 6 seeds for the FLASH (red) and UTE (yellow) sequences which show a 15 fold difference in volume. **(1B)** Seeds imaged with UTE show an excellent agreement compared to positions in CT.

high electron density and large Hounsfield units (HU). On MRI, these markers produce no signal but due to the difference in magnetic susceptibility, they can create signal voids and distortions that are not truly representative of the marker dimension [2]. In the prostate, these markers can be hard to visualize on anatomical T2-weighted images which are used in RT planning. An additional gradient-echo sequence such as fast low angle shot (FLASH) is currently used to increase the conspicuity of markers due to the enhanced susceptibility artifact however this is at the cost of accuracy of the marker size and location. Susceptibility artifacts are known to depend on material, orientation to the magnetic field, imaging sequence as well as echo time (TE). With the increased use of MRI for target localization and soft tissue delineation, the MRI appearance of these markers needs to be carefully characterized, particularly for new pulse sequences which may be beneficial for imaging markers. The purpose of the first study was to evaluate the appearance of two commercial fiducial markers using the current departmental protocol and compare it to various types of imaging sequences not currently used in our clinic. Five sequences were performed including the current clinical gradient echo sequence (FLASH), T2-weighted turbo spin echo (TSE), turbo gradient spin echo (TGSE), and two versions of ultra short echo time imaging (UTE and PETRA [3]). The final two sequences enabled a comparison of two minimum TEs of 0.04 ms and 0.06 ms respectively.

To evaluate these effects in a controlled manner, an in-house gelatine phantom was constructed containing three gold soft tissue markers (CIVCO Medical Solutions, Coralville, IA, USA) and 3 polymer markers (Polymark™, Portland, OR, USA). The gold marker dimensions are 1.2 x 3 mm. The Polymark™ dimensions are 1 x 3 mm and made of a PEEK-Optima polymer and medical grade stainless steel core. The fiducial markers were positioned parallel to each other and the phantom was imaged both with CT and MRI with the latter repeated so that the markers were aligned both perpendicular and parallel to the B_0 field. Results showed that the marker-induced susceptibility artifacts in the FLASH sequence were 15 times greater in total volume compared to the UTE sequence which produced the smallest artifacts (Fig. 1A). The susceptibility artifacts of the (steel cored) polymer markers were larger in dimension compared to gold markers in all cases. The FLASH sequence increased the apparent size of the polymer marker to 5.5 x 10 mm (diameter x length) perpendicular and 4.5 x 10 mm parallel to the main magnetic field. As expected, the TSE sequence reduced susceptibility artifacts compared to the FLASH for both gold and polymer in the perpendicular direction, to 2 x 5.5 mm and 2.5 x 7 mm respectively. The TGSE sequence showed a further reduction in marker artefacts to 3 x 5 mm (gold/perpendicular orientation) and 3.5 x 6.5 mm (polymer/perpendicular). PETRA demonstrated reduced artefacts of 2.5 x 3.5 mm for gold and 2.5 x 4.5 mm for polymer in the perpendicular directions. Overall the UTE images exhibited the smallest dimensions (2 x 3 mm for gold/parallel and 3 x 3 mm for polymer/perpendicular) and was comparable to the actual marker size. The Euclidean distance between the centroids of each automatically contoured UTE gold marker were sub-voxel (mean distance 1.2 mm) when compared to the CT (Fig. 1B).

Direct MR to CT conversion: validation in animal tissue

The necessity of a CT scan in the patient workflow has often hindered the flexibility and usefulness of MRI and led to many research centers turning towards MR-only planning[2] solutions – where the need for CT in the process is replaced altogether with the generation of a substitute (sCT) CT dataset from the MRI. The methods for the generation of substitute CT images to date may be broadly categorized into and atlas-based methods [4] and direct conversion or regression-based methods [5].

Atlas based methods have received most attention thus far and have been shown to produce accurate results. They work by first acquiring a representative set of co-registered patient CT and MR images. Registering these atlas MR images to a new patient MRI enables the co-registered CT Hounsfield Units to be mapped (and combined) into an MRI-based substitute CT. However atlas methods can fail in extreme cases not represented by the atlas population. The goal of regression based methods is to establish a relationship between CT and MR signal generated from one or more contrast weightings. In this next study we describe a regression-based approach to generate substitute CT images from just a single PETRA sequence[2]. Whereas soft tissue is easily seen on MRI, cortical bone which is highly electron dense is invisible on routine imaging; at ultrashort echo times signal can be detected with the potential ability to provide a tissue classification model of soft tissue, air and bone. Compared to a purely atlas-based method, the model is computationally efficient and fast.

MRI and CT scans of a porcine leg were used to validate the proposed method – this provides us with cortical bone, fat and muscle in a convenient phantom. The approach may be broadly divided into two parts: (a) an expectation maximization (EM) based clustering of the soft tissues, bone and the air class followed by (b) random forest regression based prediction of CT intensities for every voxels from class probabilities.

A 3D PETRA sequence (TE/TR 0.07/10 ms; 0.93 mm isotropic pixels) was co-registered to the corresponding CT image [6] (1.17 x 1.17 x 2 mm) to build tissue specific regression models. The MRI signal intensity was normalized between zero mean and

[2] Radiotherapy Planning where MR data is the only imaging information is ongoing research. The concepts and information presented in this article are based on research and are not commercially available. Its future availability cannot be ensured.

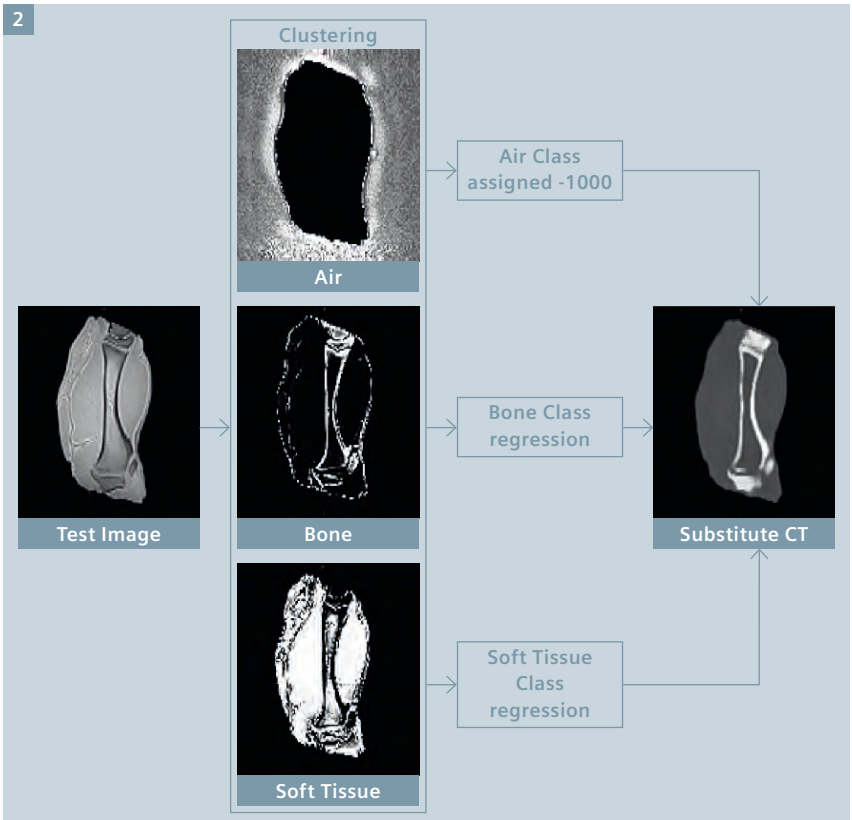

2 Overall framework of sCT generation from single PETRA dataset.

unit variance for faster convergence of the EM algorithm. A 3 class EM based clustering was performed on the co-registered PETRA image to identify the soft tissues, dense bone and air class. Unlike T2-weighted MRI the PETRA sequence is useful in separating the bone and the air classes. For each of the tissue classes (soft tissue, air and bone) the class probabilities and corresponding CT intensities were sampled from the co-registered CT/PETRA images to build tissue-specific regression models. Thus we model separate random forest regression models for soft tissue and bone. Unlike other regression models used for HU prediction we do not use signal intensities for building the regression model but instead use class probabilities (bone, soft tissues and air probabilities) for a voxel in the random forest regression model to predict the corresponding HU. The proposed approach is intuitive as there may not be any direct relationship between CT HU and MRI intensities. There is, however, a direct relationship between class probabilities of air, bone and soft tissues and corresponding HU maps. In our model we propose to exploit this relation. Air identified from the EM model is directly assigned a value of -1000 HU.
Further the degree of the regression curve is directly learnt from the class probability distribution.

For validation, an EM based clustering identified the soft tissue, the bone and the air in the phantom. Tissue specific regression models of the soft tissues and the bone were generated from half of the image to predict the other half of the image. The three classes (air, soft tissue and bone) were combined to generate the sCT. Use of half of the bone information during the training stage ensures that the training and the testing voxels were segregated. The entire substitute CT is reconstructed in less than 180 seconds. The entire framework of substitute CT image generation is illustrated in Figure 2. Chequerboard images of the CT and the substitute CT are presented in Figure 3A. The CT and the substitute CT were both thresholded at 500 HU to segment cortical bone. The surface distance difference map of the bone in mm is presented in Figure 3B. Results showed the desired level of accuracy for dosimetry calculations with a mean HU error of 15.6 HU (within the phantom skin boundary) when com-

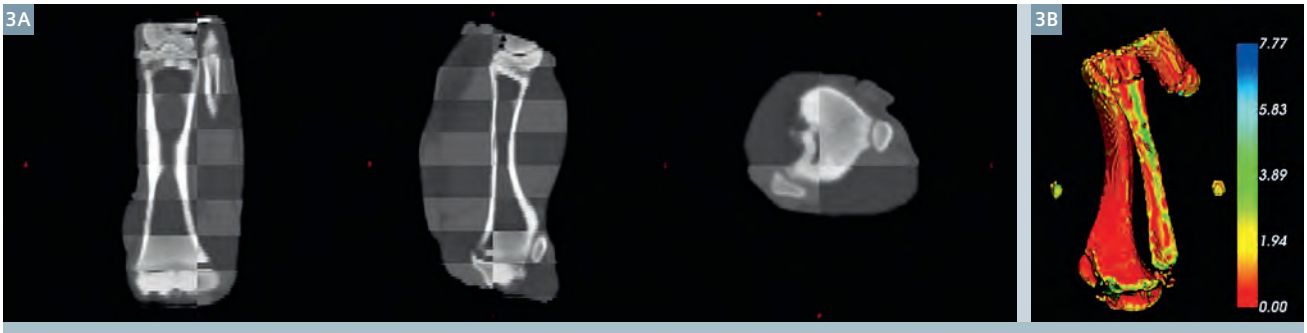

3 **(3A)** Checkerboard overlay between the actual CT and PETRA-derived sCT shows good approximation of the CT.
(3B) The surface distance error map between bone segmented from CT and sCT.

pared to CT. The proposed approach also achieves a 1.3 mm bone surface reconstruction error when compared to CT bone.

Summary

This very early work shows the potential of ultra-short TE sequences to play an important role in MR guided Radiotherapy. Acquiring signal intensity at this vastly reduced echo time opens up new imaging contrasts and many possibilities. In this report two investigations were performed; Firstly ultrashort TE was used to reduce susceptibility artifacts from fiducial marker seeds. This showed a much closer agreement with known dimension and demonstrated an improved localization accuracy compared to currently used clinical sequences. In the second example, a single ultra-short sequence was used to generate the substitute CT data directly using a novel modelling approach. This method of generating sCT shows great promise for the generation of fast MRI based sCT radiation therapy planning and PET attenuation correction. Both these methods will need further investigation *in vivo*.

References

1 Robson MD, Gatehouse PD, Bydder M, Bydder GM. Magnetic Resonance: An Introduction to Ultrashort TE (UTE) Imaging. Journal of Computer Assisted Tomography. 2003;27:825-46.

2 Wachowicz K, Thomas SD, Fallone BG. Characterization of the susceptibility artifact around a prostate brachytherapy seed in MRI. Medical Physics. 2006;33:4459-67.

3 Grodzki DM, Jakob PM, Heismann B. Ultra short echo time imaging using pointwise encoding time reduction with radial acquistion (PETRA), Proc ISMRM (2011):2815.

4 Jason A. Dowling et al. (2015). Automatic substitute CT generation and contouring for MRI-alone external beam radiation therapy from standard MRI sequences, Int. J. Radiat. Oncol. Biol. Phys., DOI: http://dx.doi.org/10.1016/j.ijrobp.2015.08.045.

5 Hsu et al. (2013). Investigation of a method for generating synthetic CT models from MRI scans of the head and the neck for radiation therapy. Phy. Med. Biol., 58(23), 8419-35.

6 David Rivest-Hénault et al. (2015). Robust inverse-consistent affine CT-MR registration in MRI-assisted and MRI-alone prostate radiation therapy. Med Image Anal. 2015 Jul;23(1):56-69.

Soumya Ghose

Robba Rai

Gary Liney

Contact

Associate Professor Gary Liney (UNSW)
Hon Principal Fellow, University of Wollongong
Ingham Institute for Applied Medical Research & Radiation Oncology
Liverpool Hospital, 1 Campbell Street
Liverpool NSW 2170, Australia
Phone: +61 2 8738 9221
gary.liney@sswahs.nsw.gov.au

Benefits of Time-Correlated and Breath-Triggered MR Acquisition in Treatment Position for Accurate Liver Lesion Contouring in Stereotactic Body Radiotherapy

Soléakhéna Ken, Ph.D.[1]; Richard Aziza, M.D.[3]; Aurélie Tournier, MSc[1]; Michel Rives, M.D.[2]; Françoise Izar, M.D.[2]; Younès Sekkal, BSc[3]; Nicolas Morel, BSc[3]; Laure Parent, Ph.D.[1]

[1] Institut Universitaire du Cancer Toulouse Oncopôle, Engineering and medical physics department, Toulouse, France
[2] Institut Universitaire du Cancer Toulouse Oncopôle, Radiotherapy department, Toulouse, France
[3] Institut Universitaire du Cancer Toulouse Oncopôle, Imaging department, Toulouse, France

Introduction

In stereotactic body radiotherapy (SBRT), high-gradient dose is delivered and target volumes have to be delineated precisely in order to avoid irradiation of healthy tissue. Liver lesions are not always visible on planning CT imaging, even after injection of contrast agent. MR images are therefore necessary for a precise lesion contouring. Accurate registration is thus a crucial step for SBRT planning in order to perform relevant delineation of target volumes.

Prior to imaging, gold fiducials are implanted under echo or CT guidance inside or in the vicinity of the lesions. These fiducials are used both as surrogate to pinpoint the lesion in order to precisely position the patient on the treatment machine, and also as markers to register planning CT and MR images.

Liver imaging is challenging because of movement caused by breathing. This movement has been reported to be up to 2 cm in free breathing [1]. Our institution uses audio coaching for a better breathing pattern reproducibility [2].

In order to account for breathing motion, planning CT is performed on a 4D CT. The planning and treatment are generally made on exhale images as these are more reproducible [3]. MR sequences were thus optimized to match CT images in exhale phase.

MR imaging

With the aim of improving registration accuracy, MR images were acquired in the same position as for CT planning images using Orfit (Orfit Industries, Wijnegem, Belgium) dedicated thermo-plastic nets, table, supports and cushions and Civco (Civco Medical Solutions, Coralville, Iowa, USA) knee cushion (Figs. 1A, 1B).

MR imaging series of the liver were acquired at the 1.5T MAGNETOM Aera (Siemens Healthcare, Erlangen, Germany) using the 18-channel body flex coil (Fig. 1C). The optimized MR sequences were able to take into account the support table and immobilization devices, which neither interfered with, nor degraded the images.

A total of three sequences were systematically acquired:

- For T2 lesion visualization, axial series of Single Shot Fast Spin Echo T2-weighted with fat saturation (T2) were used. Image acquisition is triggered on exhale and allows motion artifact reduction. TR and TE are 5248 ms and 73 ms respectively.

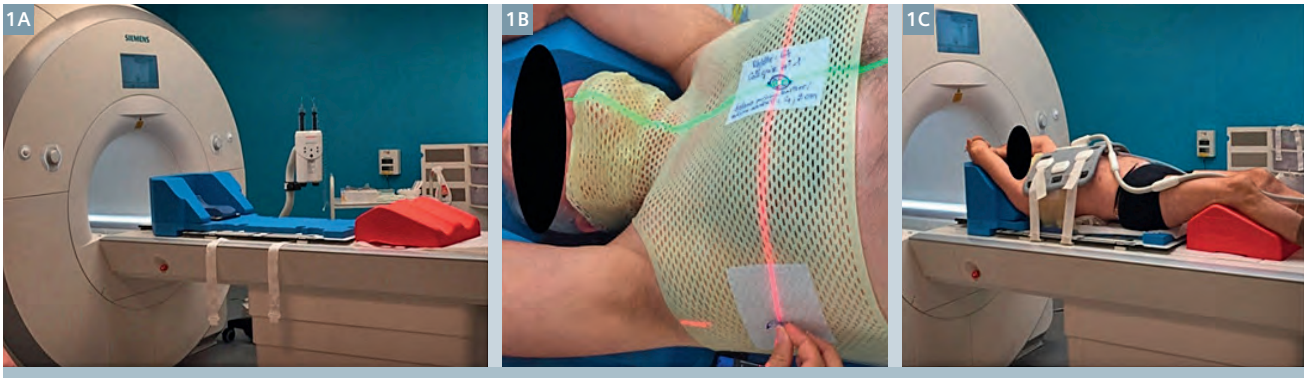

1 Dedicated table, supports and cushions for patient's immobilization and positioning at the MR 1.5T Aera scan **(1A)**; patient's thermo-plastic net with laser alignment **(1B)** and final setting with body coil ready for MR acquisitions **(1C)**.

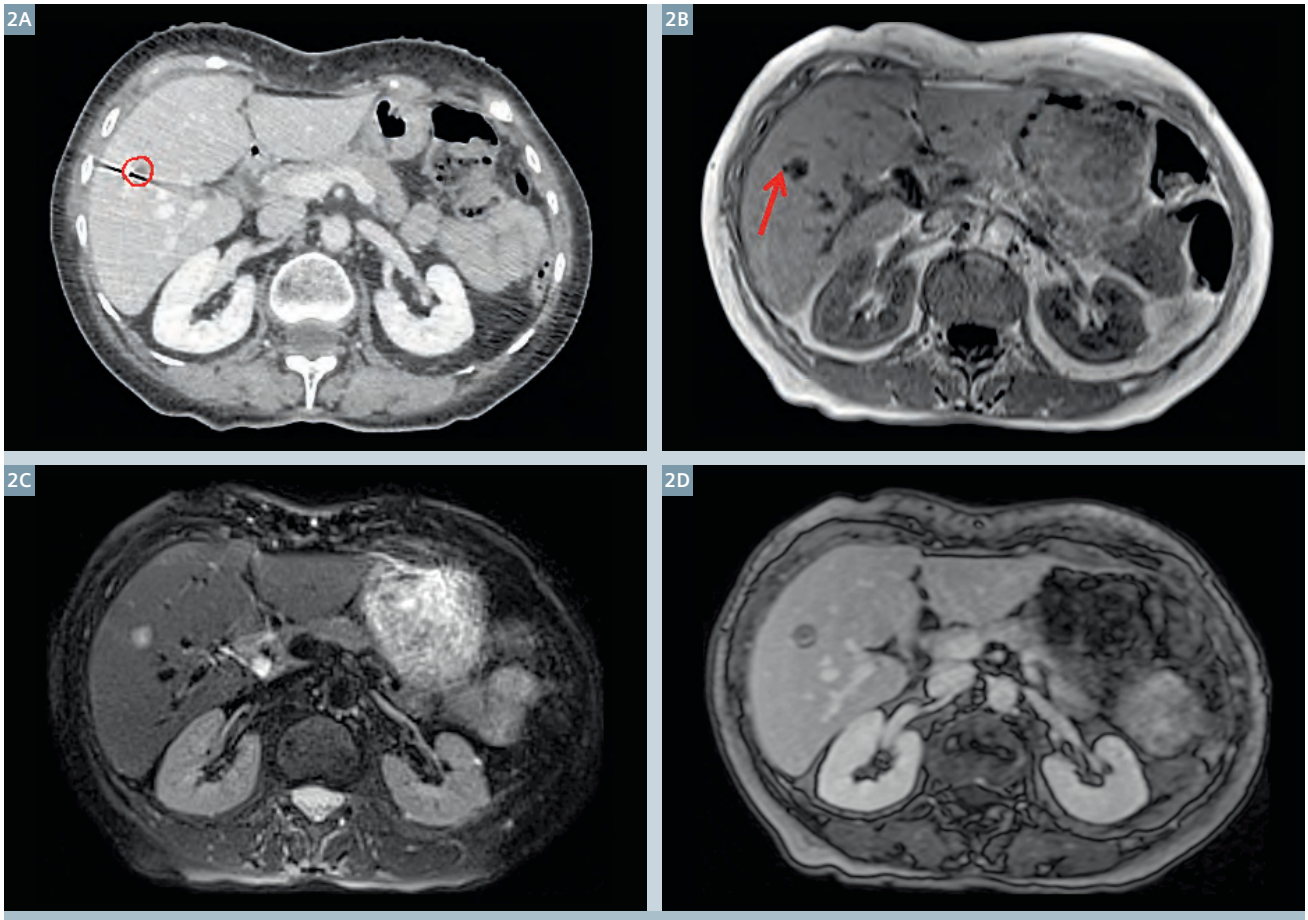

2 Example of registered image for a breast metastasis in liver segment V. Injected CT50 with target contour delineated in red thanks to the MR sequences **(2A)**, T1 Dixon with red arrow identifying fiducial **(2B)**, T2 showing hyper intense lesion **(2C)** and injected T1 TFL **(2D)**.

- The combination of Dixon and ultra-fast gradient echo T1-weighted images with CAIPIRINHA (Controlled Aliasing in Parallel Imaging Results in Higher Acceleration) technique allows performing the acquisition in one exhale breath-hold. Fiducials are visible on Dixon water separation images (T1 Dixon). TR and TE are 6.78 ms and 2.39 ms respectively.
- After injection of gadolinium-based contrast agent, lesion visualization was obtained with a T1-weighted Fast Low Angle Shot imaging sequence (T1 TFL) acquired using GRAPPA (Generalized Autocalibrating Partially Parallel Acquisitions) technique and with breath triggering on expiration phase. Gold fiducials are also visible on this sequence. TR and TE are 835 ms and 2.32 ms respectively.

Slice thickness was set to 2 mm for all series and pixel size was 1.48 x 1.48 mm² for T2 and T1 TFL; and 1.18 x 1.18 mm² for T1 Dixon. All sequences were acquired in the same plane and with the same slice positions in order to ease image registration in the treatment planning software.

The entire MR imaging protocol lasts generally between 15 and 20 minutes, depending on the regularity of the patient's breathing pattern.

Image registration for treatment planning

Radiotherapy planning is based on a 4D CT reconstructed in six phases across the respiratory cycle, CT0 and CT50 corresponding to inhale and exhale phases respectively. The CT50 expiration phase is the image set used for MR image registration.

As the three MR image sets are registered, the T1 Dixon water-only image set is used to register to CT50 images using the gold fiducials and the two other sequences are automatically registered. T1 Dixon is useful to register water separation MR images based on fiducials' position, as they are the most visible on this sequence (see red arrow on Figure 2B). The two breath-triggered (expiration phase) sequences (T2 and injected T1 TFL) provide a motion artifact-free image necessary to accurately delineate the lesion (Figs. 2C, D). An example of lesion delineation is given in Figure 2A.

Target motion range is assessed based on fiducials' displacement. Treatment planning is most frequently performed on expiration phases, but when lesion movement caused by breathing is small, target contouring is done on all breathing

phases based on fiducial movements, and treatment planning is achieved in free breathing.

Conclusion

CT and MRI acquisitions in treatment position are performed with the same table and immobilization device. The use of MR imaging sequences optimized to account not only for the dedicated table and immobilization devices but also for fiducial visualization and tumor delineation allow high precision target delineation for treatment planning. The increasing number of patient cases eligible for SBRT and proof of its benefit have stimulated the effort to set up and improve new imaging protocols at our institute for a personalized and optimal SBRT treatment.

Recent developments in 4D MRI have demonstrated the possibility to sort and reconstruct the images according to the different phases of the respiratory cycle [4–7]. The use of 4D MRI acquisition would allow better registration with 4D CT planning over the entire breathing cycle. Delineation accuracy will benefit from significant improvements if the same respiratory phases are registered from both MR and CT modalities.

Acknowledgments

The authors are thankful to Karen Mkhitaryan (Siemens Healthcare) for his help in setting up the MR image acquisition sequences.

References

1 R. B. Case, J. J. Sonke, D. J. Moseley, J. Kim, K. K. Brock, L. A. Dawson, "Inter- and Intrafraction variability in liver position in non-breath-hold stereotactic body radiotherapy," Int. J. Radiat. Oncol. Biol. Phys., vol. 75, no. 1, pp. 302–308, 2009.

2 C. J. Haasbeek, F. O. Spoelstra, F. J. Lagerwaard, J. R. van Sörnsen de Koste, J. P. Cuijpers, B. J. Slotman, S. Senan, "Impact of Audio-Coaching on the Position of Lung Tumors," Int. J. Radiat. Oncol. Biol. Phys., vol. 71, no. 4, pp. 1118–1123, 2008.

3 Y. Seppenwoolde, H. Shirato, K. Katamura, S. Shimizu, M. van Herk, J. V. Lebesque, K. Miyasaka, "Precise and real-time measurement of 3D tumor motion in lung due to breathing and heartbeat, measured during radiotherapy," Int. J. Radiat. Oncol. Biol. Phys, vol. 53, no. 4, pp. 822–834, 2002.

4 M. von Siebenthal, G. Székely, U. Gamper, P. Boesiger, A. Lomax, P. Cattin, "4D MR imaging of respiratory organ motion and its variability," Phys. Med. Biol., vol. 52, no. 6, pp. 1547–1564, 2007.

5 C. Paganelli, P. Summers, M. Bellomi, G. Baroni, M. Riboldi, "Liver 4DMRI: A retrospective image-based sorting method.," Med. Phys., vol. 42, no. 8, pp. 4814–21, 2015.

6 K. B. Bernatowicz, R. L. Perrin, M. Peroni, D. C. Weber, A. J. Lomax, "4D-MRI: Future of Radiotherapy of Moving Targets?," MAGNETOM Flash, 62, vol. 2, pp. 74–76, 2015.

7 Z. Celicanin, O. Bieri, F. Preiswerk, P. Cattin, K. Scheffler, F. Santini, "Simultaneous acquisition of image and navigator slices using CAIPIRINHA for 4D MRI." Magn Reson Med. 2015 Feb;73(2):669-76.

Contact

Soléakhéna Ken
Institut Universitaire du Cancer
Toulouse Oncopôle
1 avenue Irène Joliot-Curie
31059 Toulouse
France
ken.soleakhena@iuct-oncopole.fr

Relevant clinical information at your fingertips

From technology to tips and tricks, you will find the news on all aspects of MRI in Radiation Therapy at

www.siemens.com/magnetom-world-rt

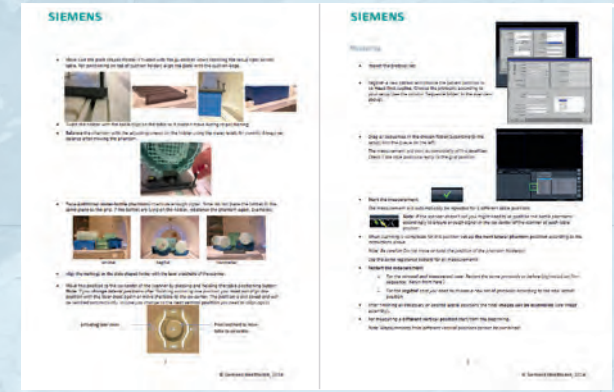

Just a mouse click away you will find application tips allowing you to optimize your daily work.

MRI Geometric Distortion QA

Using the ACR MRI Accreditation Phantom

Nina Niebuhr
Siemens Healthcare

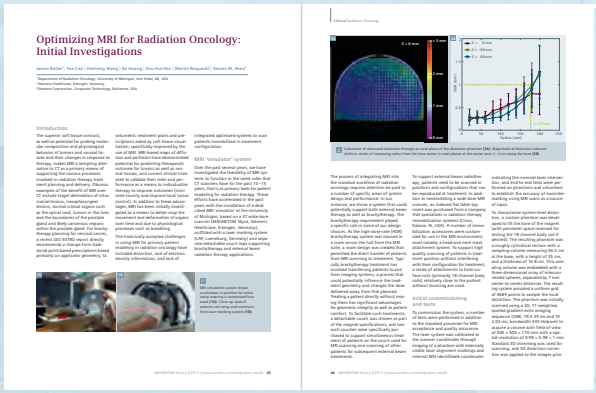

The centerpiece of the MAGNETOM World Internet platform consists of our users' clinical results. Here you will find case reports, review articles and clinical methods.

Optimizing MRI for Radiation Oncology

James Balter
Dept. of Radiation Oncology, University of Michigan

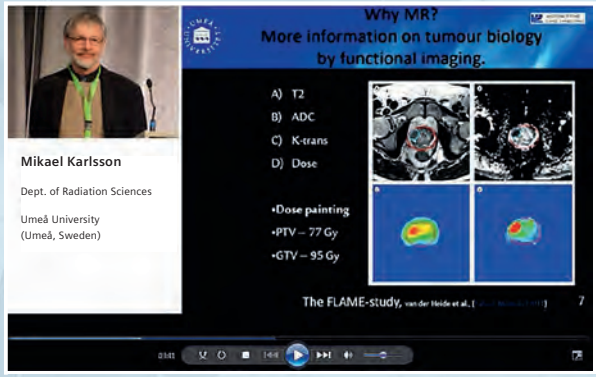

Don't miss the talks of international and renowned experts on MRI in RT.

MRI in the Radiotherapy Process. Now and in the Future

Mikael Karlsson
Umeå University Hospital (Umeå, Sweden)

Visit us at

www.siemens.com/magnetom-world-rt

4D-MRI: Future of Radiotherapy of Moving Targets?

Kinga Barbara Bernatowicz; Rosalind Lucy Perrin; Marta Peroni; Damien Charles Weber; Antony John Lomax

Center for Proton Therapy (CPT), Paul Scherrer Institut, Villigen PSI, Switzerland

Background

4D-CT imaging is widely used in radiotherapy planning of moving tumors to account for motion, and to provide the physical properties of tissue for dose calculations, e.g. electron density for conventional radiation therapy or proton stopping power for proton therapy. However, it is limited to representing only a single, averaged breathing cycle, often contains imaging artifacts, and contributes a substantial dose exposure for the patient. To overcome these issues, a 4D-MRI imaging protocol applied to evaluating respiratory motion of the liver was proposed by von Siebenthal et al. [1].

This approach is capable of resolving irregular respiratory motion, with the added benefit of delivering no imaging dose to the patient. Unfortunately, whilst being a promising technique, MR imaging alone does not provide the physical properties of tissue required for accurate dose calculations. However, by combining the motion information provided by 4D-MRI, with the density data provided by single phase CT data, the advantages of motion imaging with 4D-MRI can now be applied to radiotherapy applications.

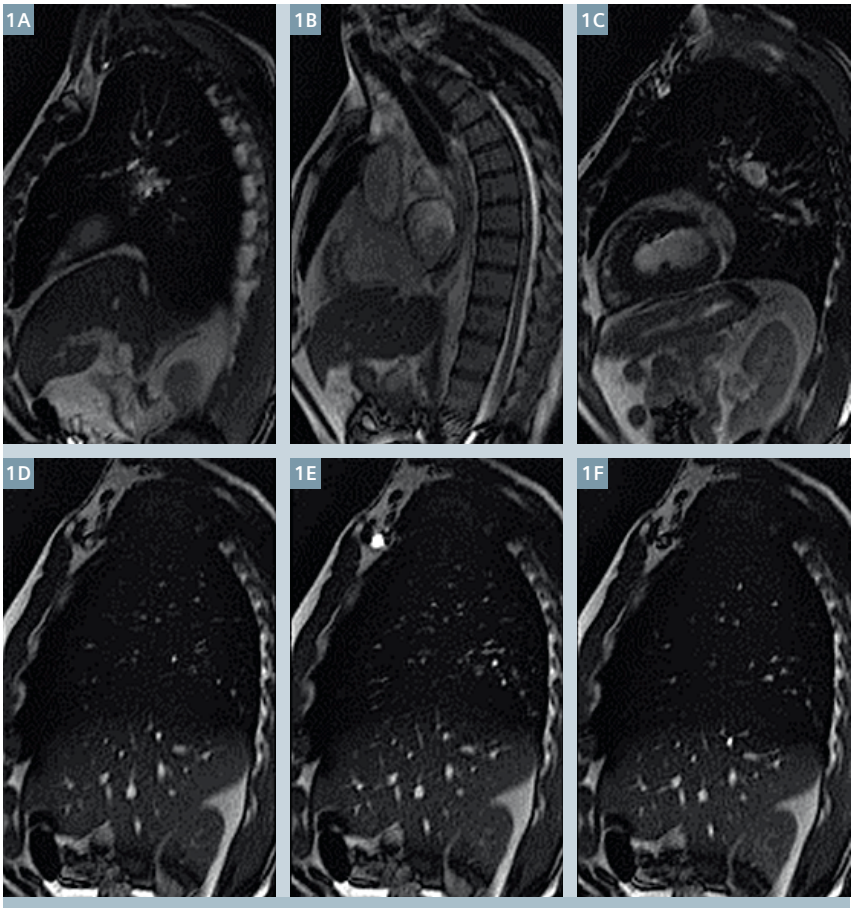

1 Sagittal slices through the thorax and upper abdomen, showing image slices **(1A–C)** and navigator slices **(1D–F)** acquired with the experimental 4D-MRI protocol*.

4D-MRI acquisition

The 4D-MRI protocol relies on the interleaved acquisition of a 'navigator' and different image slices in the sagittal plane (Fig. 1). The navigator is fixed at a single position throughout the acquisition time, and describes the motion state of the volume of interest at any instant during the acquisition. The actual 2D image slice is then scanned through the planned field-of-view (FOV).

This experimental sequence* does not make any assumptions about the breathing amplitude, its regularity, or the number of reconstructed phases. In contrast, commonly used methods for 4D imaging use a one-dimensional respiratory signal for sorting the 2D images, whereas 4D-MRI images can be retrospectively sorted based directly on the acquired navigator frames. The correspondence of the imaging slices is then established by comparing the two temporally embracing navigator frames (see Fig. 2). If these navigator frames are similar, the image slices can be stacked into a (3D) volume with the same time stamp and therefore, a complete 4D image data set with the same temporal resolution as the navigator frames can be reconstructed.

This approach has now been implemented on a 1.5T MAGNETOM Aera MR system (Siemens Healthcare, Erlangen, Germany) using an experimental version of the balanced steady state

*Work in progress, the product is still under development and not commercially available yet. Its future availability cannot be ensured.

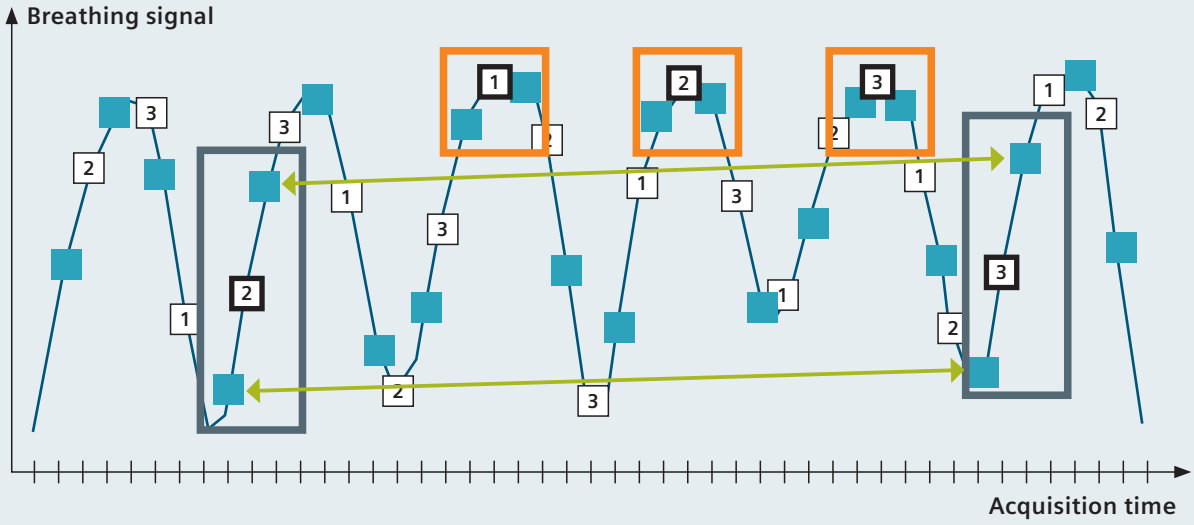

2 Acquisition of slices (white boxes) and embracing navigator frames (blue boxes). Slices associated with the same volume are matched by comparing navigator pairs (green arrows) [2].

free precession sequence (TrueFISP)*. Images are acquired in batches of 3-5 minute duration, with up to one hour of total acquisition time and with image slice thicknesses of 4 to 6 mm. Recent advances in the field are now looking at the simultaneous acquisition of navigator and data slices, with use of other advanced sequences, for example CAIPIRINHA [3].

Applications

- **Intra- and inter-fraction motion studies**
  Since MRI involves no radiation dose to patients or volunteers, 4D-MRI protocols allow for repeated studies on the same subject and/or for longer time period acquisitions in order to capture breathing variability (Fig. 3). Motion deformation fields can also be extracted using deformable image registration.
- **Mapping motion from MRI-CT**
  The 4D-CT (MRI) method has now been developed within our group for simulating many 4D-CT data sets from a single, static reference CT and a data-base of motion deformation fields extracted from 4D-MRI studies [4]. The mapping of motion information from 4D-MRI onto CT images is thereby achieved using subject-specific or population-based models, based on the establishment of mechanical correspondences between structures of interest (e.g. the liver). The resulting 4D-CT (MRI) images are of good quality when compared to 4D-CT (Fig. 4), and now represent the tissue properties necessary for dose calculations, whilst incorporating the motion information provided by 4D-MRI.
- **4D dose calculations in radiotherapy**
  Including the realistic, variable respiratory motion in provided by 4D-CT (MRI) data into 4D dose calculations, opens the door to novel future applications. Based on such data sets, advanced imaging and delivery methods, such as beam tracking (Fig. 5), can now be evaluated and comprehensive 4D planning studies and robustness evaluations performed.

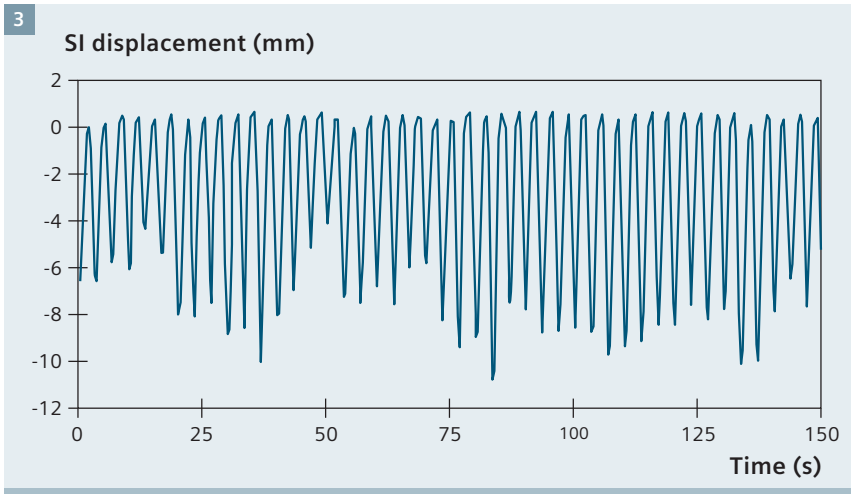

3 Example of extracted 2.5 minute trace of the average liver SI motion [2].

*Work in progress, the product is still under development and not commercially available yet. Its future availability cannot be ensured.

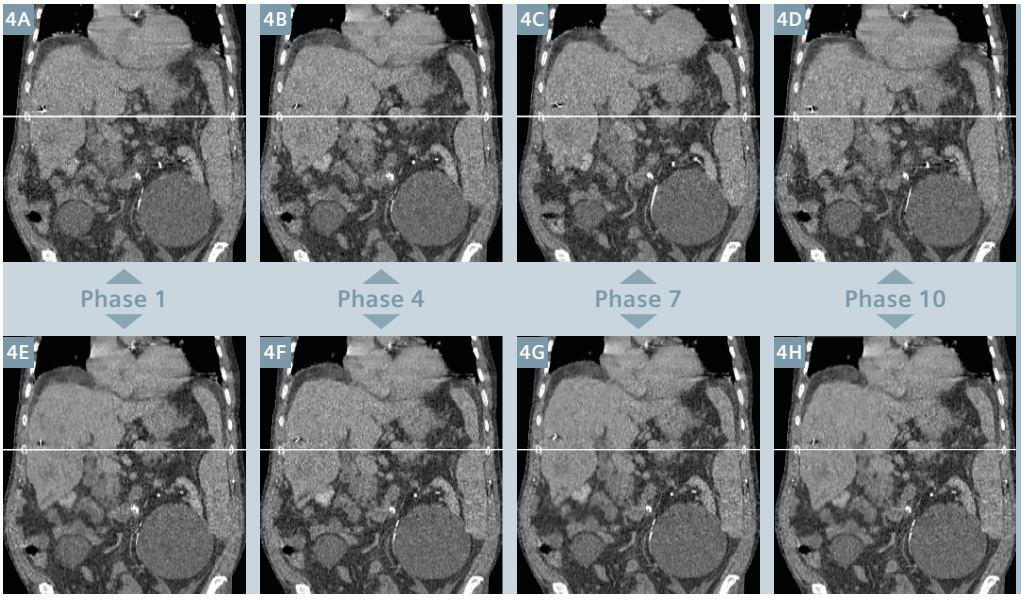

4 Comparison of different breathing phases of 4D-CT **(4A–D)** and 4D-CT (MRI) image sets **(4E–H)** simulated from the 4D-MRI motion library and a reference CT [4].

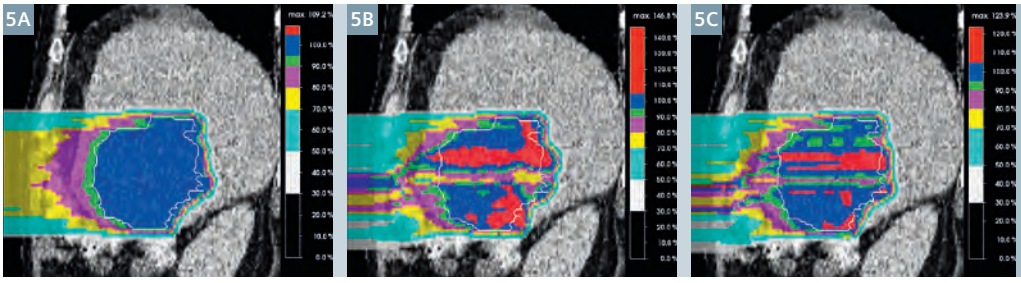

5 4D dose calculation results for different scanned proton tracking techniques based on 4D-CT (MRI) [5, 6].

Summary

4D-MRI, combined with CT data to produce 4D-CT (MRI) data sets, is a powerful new technique for imaging and modeling motion for radiotherapy applications. It allows for accurate modeling of motion variability, an important limitation of current 4D-CT techniques, and will allow in the future for the acquisition of patient specific motion libraries for advanced motion mitigation techniques such as tracking and re-tracking [5, 6].

References

1 von Siebenthal M, Székely G, Gamper U, Boesiger P, Lomax A, Cattin P., 4D MR imaging of respiratory organ motion and its variability., Phys Med Biol. 2007 Mar 21;52(6):1547-64. Epub 2007 Feb 16.

2 PhD Thesis, von Siebenthal, M. 2008, http://www.vision.ee.ethz.ch/~organmot/chapter_publications.shtml

3 Celicanin Z, Bieri O, Preiswerk F, Cattin P, Scheffler K, Santini F., Simultaneous acquisition of image and navigator slices using CAIPIRINHA for 4D MRI., Magn Reson Med. 2014 Feb 24. doi: 10.1002/mrm.25134. [Epub ahead of print].

4 Boye D, Lomax T, Knopf A., Mapping motion from 4D-MRI to 3D-CT for use in 4D dose calculations: a technical feasibility study. Med Phys. 2013 Jun;40(6):061702. doi: 10.1118/1.4801914.

5 Zhang Y., Knopf A, Tanner C, Boye D, Lomax AJ., Deformable motion reconstruction for scanned proton beam therapy using on-line x-ray imaging., Phys Med Biol. 2013 Dec 21;58(24):8621-45. doi: 10.1088/0031-9155/58/24/8621. Epub 2013 Nov 21.

6 Zhang Y, Knopf A, Tanner C, Lomax AJ., Online image guided tumour tracking with scanned proton beams: a comprehensive simulation study., Phys Med Biol. 2014 Nov 24;59(24):7793-7817. doi:10.1088/0031-9155/59/24/7793.

Contact

Kinga Barbara Bernatowicz
Paul Scherrer Institute
5323 Villigen PSI
Switzerland
kinga.bernatowicz@psi.ch

Siemens Healthcare Publications

Our publications offer the latest information and background for every healthcare field. From the hospital director to the radiological assistant – here, you can quickly find information relevant to your needs.

Medical Solutions
Innovations and trends in healthcare. The magazine is designed especially for members of hospital management, administration personnel, and heads of medical departments.

SOMATOM Sessions
Everything from the world of computed tomography.

AXIOM Innovations
Everything from the world of interventional radiology, cardiology, and surgery.

MAGNETOM Flash
Everything from the world of magnetic resonance imaging.

MReadings – Imprint

Publisher:
Siemens Healthcare GmbH
Magnetic Resonance,
Karl-Schall-Straße 6, D-91052 Erlangen,
Germany

Editor-in-chief:
Antje Hellwich
(antje.hellwich@siemens.com)

Editorial Board:
Elena Nioutsikou; Heidrun Endt, M.D.;
Martin Requardt, Ph.D.; Zoltan Vermes;
Peter Kreisler, Ph.D.

Production:
Norbert Moser,
Siemens Healthcare GmbH

Layout:
Agentur Baumgärtner,
Friedrichstraße 4, D-90762 Fürth, Germany

Printer:
G. Peschke Druckerei GmbH,
Taxetstrasse 4,
D-85599 Parsdorf b. Munich,
Germany

Note in accordance with § 33 Para.1 of the German Federal Data Protection Law: Despatch is made using an address file which is maintained with the aid of an automated data processing system.

The statements and views of the authors in the individual contributions do not necessarily reflect the opinion of the publisher.

The information presented in these articles is for illustration only and is not intended to be relied upon by the reader for instruction as to the practice of medicine. Any health care practitioner reading this information is reminded that they must use their own learning, training and expertise in dealing with their individual patients. This material does not substitute for that duty and is not intended by Siemens Healthcare to be used for any purpose in that regard. The drugs and doses mentioned herein are consistent with the approval labeling for uses and/or indications of the drug. The treating physician bears the sole responsibility for the diagnosis and treatment of patients, including drugs and doses prescribed in connection with such use. The Operating Instructions must always be strictly followed when operating the MR system. The sources for the technical data are the corresponding data sheets. Results may vary.

Partial reproduction in printed form of individual contributions is permitted, provided the customary bibliographical data such as author's name and title of the contribution as well as year, issue number and pages of MAGNETOM Flash or MReadings are named, but the editors request that two copies be sent to them. The written consent of the authors and publisher is required for the complete reprinting of an article.

We welcome your questions and comments about the editorial content of MAGNETOM Flash or MReadings. Please contact us at magnetomworld.med@siemens.com.

Manuscripts as well as suggestions, proposals and information are always welcome; they are carefully examined and submitted to the editorial board for attention. MAGNETOM Flash or MReadings is not responsible for loss, damage, or any other injury to unsolicited manuscripts or other materials. We reserve the right to edit for clarity, accuracy, and space. Include your name, address, and phone number and send to the editors, address above.

On account of certain regional limitations of sales rights and service availability, we cannot guarantee that all products included in this brochure are available through the Siemens sales organization worldwide. Availability and packaging may vary by country and is subject to change without prior notice. Some/All of the features and products described herein may not be available in the United States.

The information in this document contains general technical descriptions of specifications and options as well as standard and optional features which do not always have to be present in individual cases, and which may not be commercially available in all countries. Due to regulatory reasons their future availability cannot be guaranteed. Please contact your local Siemens organization for further details.

Siemens reserves the right to modify the design, packaging, specifications, and options described herein without prior notice. Please contact your local Siemens sales representative for the most current information.

Note: Any technical data contained in this document may vary within defined tolerances. Original images always lose a certain amount of detail when reproduced.

*MAGNETOM 7T is still under development and not commercially available yet. Its future availability cannot be ensured. This research system is not cleared, approved or licensed in any jurisdiction for patient examinations. This research system is not labelled according to applicable medical device law and therefore may only be used for volunteer or patient examinations in the context of clinical studies according to applicable law.

Not for distribution in the US

Siemens Healthcare Headquarters
Siemens Healthcare GmbH
Henkestr. 127
91052 Erlangen
Germany
Phone: +49 9131 84-0
siemens.com/healthcare

Order No. A91MR-1100-85C-7600 | Printed in Germany | CC MR 3868 05160.5 |

siemens.com/magnetom-world-rt